THERMO-ENVIRONMENTAL ANALYSIS OF A NOVEL SOLAR AND BIOMASS-BASED MULTI-GENERATION SYSTEM EQUIPPED WITH NANOFLUID-BASED COMPOUND PARABOLIC COLLECTORS

Alla Ali IBRAHIM

2021
Ph.D. THESIS
MECHANICAL ENGINEERING

Thesis Advisor
Prof. Dr. Muhammet KAYFECİ

THERMO-ENVIRONMENTAL ANALYSIS OF A NOVEL SOLAR AND BIOMASS-BASED MULTI-GENERATION SYSTEM EQUIPPED WITH NANOFLUID-BASED COMPOUND PARABOLIC COLLECTORS

Alla Ali IBRAHIM

T.C.
Karabuk University
Institute of Graduate Programs
Department of Mechanical Engineering
Prepared as
Ph.D. Thesis

Thesis Advisor
Prof.Dr. Muhammet KAYFECİ

KARABUK
November 2021

I certify that in my opinion the thesis submitted by Alla Ali IBRAHIM titled "THERMO-ENVIRONMENTAL ANALYSIS OF A NOVEL SOLAR AND BIOMASS-BASED MULTI-GENERATION SYSTEM EQUIPPED WITH NANOFLUID-BASED COMPOUND PARABOLIC COLLECTORS" is fully adequate in scope and in quality as a thesis for the degree of Doctorate of Philosophy.

Prof.Dr. Muhammet KAYFECİ   ....
Thesis Advisor, Department of Energy Systems Engineering

This thesis is accepted by the examining committee with a unanimous vote in the Department of Energy Systems Engineering as a Ph.D thesis. November 9, 2021

Examining Committee Members (Institutions)   Signature

Chairman   : Prof.Dr. Fevzi BEDİR (GTU)   ....

Member   : Prof.Dr. Ali KEÇEBAŞ (MSKU)   ....

Member   : Prof.Dr. Kamil ARSLAN (KBU)   ....

Member   : Assoc.Prof.Dr. Engin GEDIK (KBU)   ....

Member   : Prof.Dr. Muhammet KAYFECİ (KBU)   ....

The degree of Doctor of Philosophy by the thesis submitted is approved by the Administrative Board of the Graduate School of Natural and Applied Sciences, Karabük University.

Prof. Dr. Hasan SOLMAZ   ....
Director of the Institute of Graduate Programs

"I declare that all the information within this thesis has been gathered and presented in accordance with academic regulations and ethical principles and I have according to the requirements of these regulations and principles cited all those which do not originate in this work as well."

Alla Ali IBRAHIM

ABSTRACT

Ph.D. Thesis

THERMO-ENVIRONMENTAL ANALYSIS OF A NOVEL SOLAR AND BIOMASS-BASED MULTI-GENERATION SYSTEM EQUIPPED WITH NANOFLUID-BASED COMPOUND PARABOLIC COLLECTORS

Alla Ali IBRAHIM

Karabük University
Institute of Graduate Programs
Department of Mechanical Engineering

Thesis Advisor:
Prof. Dr. Muhammet KAYFECİ
November 2021, 99 Pages

In recent decades, the supply of various types of energy has become the predominant application of distributed generation systems. The depletion of fossil fuels, rising electricity prices, climate change and a significant increase in energy demand are the main reasons for this trend. Solar, geothermal, wind and biomass energy technologies are among the emerging sciences due to their availability, low cost, and environmental impact during operation.

The current thesis proposes a novel multi-generation system, which is integrated with compound parabolic collectors and a biomass combustor. Besides thermodynamic and environmental analyzing the comprehensive system in a steady state, the feasibility of using nanofluids as an absorption fluid in the solar cycle and its effect on the overall performance of the mentioned system was studied.

The multi-generation system is generally designed for generating electricity, cooling/heating, freshwater, drying, hot water, and hydrogen with the help of six subsystems, including a double stage refrigeration system, an organic Rankine cycle, a steam Rankine cycle, a dryer, a proton exchange membrane electrolyzer, and a multistage flash distillation system. Two types of nanoparticles (Graphene, Silver), which have various high-quality properties when used within the ethylene glycol, were chosen as heat transfer fluids in the solar cycle. The performance parameters of the base case thermodynamic analysis and some of the variable parameters were calculated and their effect on system performance was determined.

According to the results, the system performance actually improved when nanofluids were used as working fluids in the solar collector. It was found that the graphene nanoparticles were the most effective. The overall energy/exergy efficiencies were recorded for the multi-generation system, respectively, 34.72% and 20.73% when a base fluid was used. The overall efficiencies increased to 35.6% and 21.15% when graphene-ethylene glycol nanofluid was used. The highest exergy destruction rates of 15.42 MW and 9.14 MW were obtained for the steam and organic Rankine cycle subsystems, respectively. The freshwater production by the desalination subsystem was 37.93 kg/s and hydrogen production by PEM electrolyzer was 44.77 kg/h. The environmental impact assessment gave a strong impetus to switch to multi-generational systems as CO_2 emissions decreased from 1123 kg/MWh using the single-generation system to 364 kg/MWh using the multi-generation system. According to the analyses, spike in solar irradiation, ambient temperature, output temperature of biomass combustor, nanofluids' concentration, ORC working fluid, air-biomass flow rate, and inlet pressure of both Rankine cycles turbines positively affected the overall system performance.

Key Words : Compound parabolic collector, Biomass, Nanofluid, Multigeneration system.

Science Code : 91408

ÖZET

Doktora Tezi

NANOAKIŞKANLI BİLEŞİK PARABOLİK KOLLEKTÖR İÇEREN GÜNEŞ VE BİYOKÜTLE DESTEKLİ MULTİ JENERASYON SİSTEMİN TERMODİNAMİK VE ÇEVRESEL ANALİZİ

Alla Ali IBRAHIM

Karabük Üniversitesi
Lisansüstü Eğitim Enstitüsü
Makina Mühendisliği Bölümü

Tez Danışmanı:
Prof. Dr. Muhammet KAYFECİ
Kasım 2021, 99 Sayfa

Son yıllarda çeşitli enerji türlerinin temini dağıtılmış üretim sistemlerinin baskın uygulaması haline gelmiştir. Fosil yakıtların tükenmesi, artan elektrik fiyatları, iklim değişikliği ve enerji talebindeki önemli artış bu eğilimin ana nedenlerindendir. Güneş, jeotermal, rüzgar ve biyokütle enerjisi teknolojileri kullanılabilirlikleri, düşük maliyetleri ve işletme sırasındaki çevresel etkileri nedeniyle ortaya çıkan bilimler arasındadır.

Bu tez çalışması, bileşik parabolik kollektörler ve bir biyokütle yakıcı ile entegre edilmiş multi jenerasyon yeni bir sistem önermektedir. Sistemin kararlı durumda termodinamik ve çevresel analizinin yanı sıra nanoakışkanların güneş enerjisi çevriminde absorpsiyon sıvısı olarak kullanılmasının uygulanabilirliği ve sistemin genel performansı üzerindeki etkisi incelenmiştir.

Tasarlanan multi jenerasyon sistemi; elektrik, soğutma/ısıtma, tatlı su, kurutma, sıcak su ve hidrojen üretmek için; çift kademeli soğutma sistemi, organik Rankine çevrimi (ORC), buhar Rankine çevrimi, kurutucu, proton değişim membran elektrolizörü ve çok aşamalı bir flaş damıtma sisteminden oluşmaktadır. Güneş enerjisi çevriminde, ısı transfer akışkanı olarak etilen glikol içerisinde kullanıldığında üstün özelliklere sahip olan iki tip nanopartikül (Grafen ve Gümüş) seçilmiştir. Sistem performansı üzerine temel termodinamik analizi ve bazı değişken parametrelerinin etkisi belirlenmiştir.

Sonuçlara göre, güneş kollektöründe çalışma sıvıları olarak nanoakışkanlar kullanıldığında sistem performansı arttırdığı ve burada grafen nanoparçacıklarının en etkili olduğu bulunmuştur. Multi jenerasyon sisteminde baz akışkan kullanıldığında genel enerji/ekserji verimlilikleri sırasıyla %34.72 ve %20.73 olarak bulunmuştur. Grafen-etilen glikol nanoakışkan kullanıldığında genel verimlilik %35.6 ve %21.15'e yükselmiştir. En yüksek ekserji yıkımı sırasıyla 15,42 MW ve 9,14 MW ile buhar ve organik Rankine çevrimi alt sistemleri için elde edilmiştir. Damıtma ile tatlı su üretimi 37.93 kg/s ve PEM elektrolizörü tarafından hidrojen üretimi 44.77 kg/s'dir. Tek jenerasyon sistemi kullanıldığında CO_2 emisyonları 1123 kg/MWh'den, multi jenerasyon sistemi kullanıldığında 364 kg/MWh'e düştüğü için çevresel etki değerlendirmesi multi jenerasyon sistemlere geçiş için güçlü bir ivme kazandırmıştır. Analizlere göre güneş ışınımı, ortam sıcaklığı, biyokütle yanma odasının çıkış sıcaklığı, nanoakışkanların konsantrasyonu, ORC çalışma sıvısı, hava-biyokütle akış hızı ve her iki Rankine çevrimi türbininin giriş basıncı genel sistem performansını olumlu yönde etkilemiştir.

Anahtar Kelimeler : Bileşik parabolik toplayıcı, Biyokütle, Nanoakışkan, Multijenerasyon sistemi.

Bilim Kodu : 91408

ACKNOWLEDGEMENT

First and foremost, I feel always indebted to ALLAH, the most kind and most merciful, who gave me the ability and strength to complete this work.

I cannot find the words to express my gratitude to my supervisor, Prof.Dr. Muhammet KAYFECİ for the valuable knowledge that I learned from him throughout the study period in addition to his impressive supervision. I also thank him for his continuous support and appreciate his efforts, which he has made to bring me to this stage.

I would like to thank the examining committee members for their recommendations and detailed review.

My deep thanks to my father, my all family members and I dedicate this work to my dear mother's soul, that woman who taught me to trust in Allah, to believe in hard work and that so much could be done with little.

Also my deep thanks to my dear wife who was my best support throughout the study period.

I express my thanks and gratitude to the Libyan ministry of education, which gave me this opportunity to study the Ph.D. I would like to thank my second country (Turkey), its government and the people for their kind treatment and welcoming gestures throughout the study period. I thank the staff at the Karabuk University.

CONTENTS

LIST OF FIGURES

LIST OF TABLES

SYMBOLS AND ABBREVIATION INDEX

NOMENCLATURES

A : Area (m^2)

C_p : Specific heat capacity (kJ/kg.K)

COP : Coefficient of performance

Ex : Specific exergy (kJ/ kg)

Ex_{ph} : Physical exergy (W)

$\dot{E}x$: Exergy rate (kW)

$\dot{E}x_D$: Exergy destruction (W)

F_R : Heat removal factor

G_t : Total solar irradiation (W/m^2)

h : Specific enthalpy (kJ/kg)

HHV : Higher heating value (MJ/kg)

LHV : Lower heating value (MJ/kg)

J_0 : Exchange current density (A/m^2)

k : Thermal conductivity (W/m.K)

$\dot{m}$: Mass flow rate (kg/s)

P_0 : Reference pressure (kPa)

$\dot{Q}$: Heat transfer rate (kW)

$\dot{Q}_{eva}$: Evaporator heat Load (kW)

$\dot{Q}_{gen}$: Generator heat Load (kW)

$\dot{Q}_{abs}$: Absorber heat load (kW)

$\dot{Q}_{con}$: Condenser heat load (kW)

S : Absorbed radiation (W/m^2)

s : Specific entropy (kJ/kg.K)

S_{gen} : Entropy generation (kJ/K)

SST : Daily sunbathing time (h)

T_0 : Reference temperature (ºC, K)

U_L : Heat loss coefficient (W/m^2.K)

V : Velocity (m/s)

V_0 : Reversible potential

$V_{act,a}$: Activation over-potential of the anode (V)

$V_{act,c}$: Activation overpotential of the cathode (V)

V_{ohm} : Ohmic overpotential (V)

$\dot{W}$: Power (kW)

$\dot{W}_P$: Pump power (kW)

$\dot{W}_{net}$: Net power (kW)

$\dot{W}_T$: Turbine power (kW)

GREEK LETTERS

η : Energy Efficiency (%)

ρ : Density (kg/m³)

ψ : Exergy efficiency (%)

μ : Viscosity (kg/m.s)

τ : Transmissivity

φ : Nanoparticle volume concentration

α : Symmetrical factor

SUBSCRIPTS

abs   : Absorber

amb   : Ambient

bf   : Base fluid

con   : Condenser

des   : Destruction

en   : Energy

eva   : Evaporator

ex   : Exergy

gen   : Generator

in   : Inlet

p   : Pump

PEM   : Proton exchange membrane

tur   : Turbine

np   : Nanoparticle

nf   : Nanofluid

ACRONYMS

CCHP   : Combined Cooling, Heating and Power

CPC   : Compound parabolic collector

CSP   : Concentrated solar power

CFWH   : Closed feed water heater

DEAC   : Double effect absorption cycle

EG   : Ethylene glycol

EXV   : Expansion valve

ETC   : Evacuated Tube Collector

FPC   : Flat Plate Collector

HEX   : Heat exchanger

HPT   : High pressure turbine

HTG   : High temperature generator

HTHEX   : High temperature heat exchanger

IEA   : International Energy Agency

LiBr-H_2O : Lithium Bromide solution

LPT   : Low pressure turbine

LTHEX   : Low temperature heat exchanger

MSF   : Multi-stage flash distillation

ORC   : Organic Rankine cycle

OFWH   : Open feed water heater

PEM   : Proton exchange membrane

PDR   : Parabolic Dish Reflector

PTC   : Parabolic Trough Collector

SRC   : Steam Rankine cycle

CHAPTER 1

INTRODUCTION

1.1. OVERVIEW

There is a rise in the overall demand for energy for most countries to maintain the socio-economic development and improve the public health and economic well-being. To meet the basic human needs and to carry on with production, all societies need energy. There are about eight billion people on Earth and population growth is in turn increasing the demand for energy, which affects the adequacy of energy resources. Since 1850s, the global fossil fuel use (oil, coal, and gas) exceeded the energy supply, which resulted in excessive emissions of carbon dioxide[1, 2].

According to the 2020 Annual Report of the International Energy Agency (IEA), global energy production reached 14,421 Mtoe in 2018 - an increase of 3.2% over 2017. This increase was mostly with regard to fossil fuels, such as natural gas, oil, and coal, which increased together by >370 Mtoe in 2018. Additionally, all of the renewables as well as nuclear also showed an increase of 60 and 19 Mtoe, respectively. It was seen that fossil fuels comprised >81% of the production in 2018, which was the same as that in 2017. Figure 1.1 illustrates the fuel-based primary total energy supply (TES) for 1971 and 2018 [3].

The global TES recorded from 1971 to 2018 showed an increase from 5,519 to 14,282 Mtoe (by 2.6 times). Moreover, its structure also changed. Oil showed a decline from 1971 to 2010, with a TES from 44% to 32%, respectively. It has remained stable since then, and was still the dominant source of fuel in 2018. Natural gas maintained the third position, having grown from 16% to 23% from 1971 to 2018, respectively.

1

Coal power generation was still quite prevalent in 2018, accounting for 38% of the global production of electricity. This share continued to decline in 2018 after it rebounded a slight amount in 2017, which interrupted four consecutive years of decline. Renewables rank second in the mix of electricity, as they have since 2013, and reached nearly 26% of the electricity mix in 2018. Where the solar energy has progressed from providing less than 0.01% of global electricity in 2008 to more than 2% in 2018. Several scenarios predict that solar will supply over 20% of global electricity by 2040. Figure 1.2 demonstrates the world's electricity production by fuel between 1971 and 2018 [4].
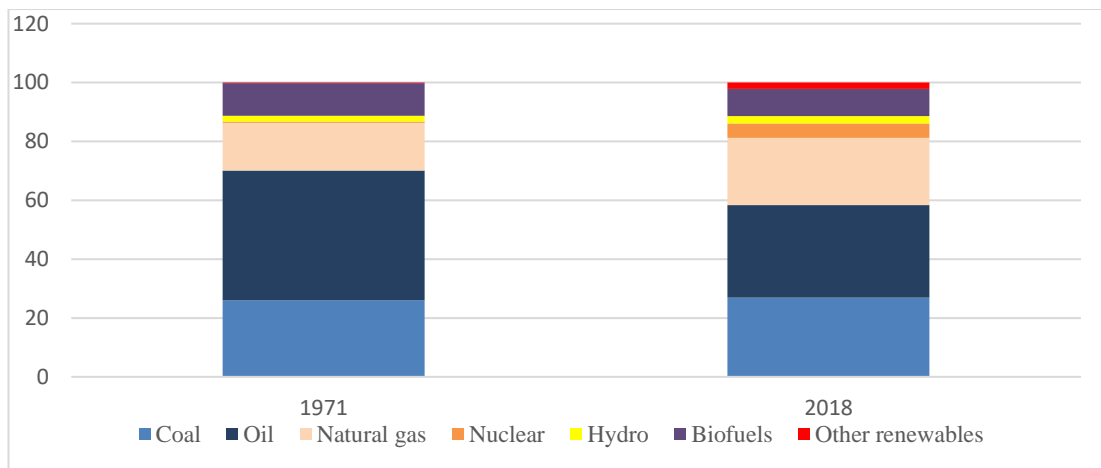
Figure 1.1. Primary fuel-based PES, 1971 and 2018.
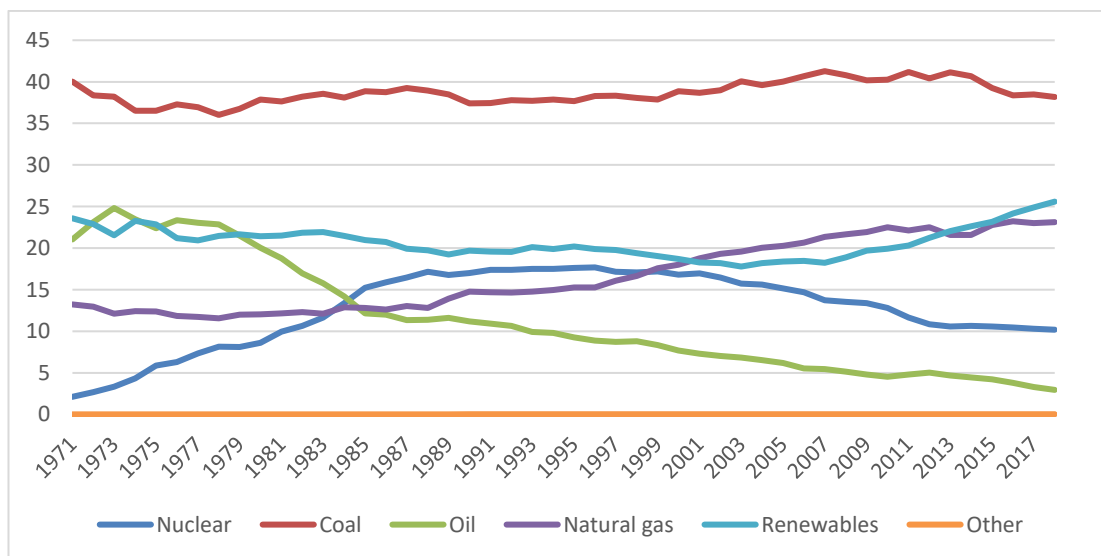
Figure 1.2. World fuel-based electricity generation mix, 1971-2018.

Recent data confirms that increasing fossil fuel consumption has led to global increase in greenhouse gas emissions and creates other serious environmental challenges. It is generally proved that CO_2 is a considerable cause of global warming. Over the past 20 years, the combustion of fossil fuels has accounted for about three quarters of carbon dioxide emissions from human activities. The remainder of this increase is mainly due to land use changes, especially deforestation. Fossil fuel power plants are the main source of CO_2 emissions, accounting for around 32% of the total CO_2 emissions. The second CO_2 emission source is cooling and heating, which makes up approximately 33% of the total CO_2 emissions. Therefore, around 65% of total CO_2 emissions come from electricity generation, cooling and heating, which are related directly to human energy needs [5].

To mitigate the climate challenge, addressing the problem of depleting fossil fuels and to meet the significant increase in demand for energy, it requires the transition of global energy systems to use clean energy. As energy sources that emit greenhouse gases are replaced by cleaner sources such as wind, solar, biomass combustion, geothermal and hydropower, which called the renewable energy. Renewable energy sources are a reasonable choice because they have a large number of reliable sources of supply and they are not harmful to the environment [6,7]. Most renewable energy solutions, including solar, wind, hydro, and biomass, have abundant supplies in almost every country, and unlike petroleum, they are the least affected by international issues.

Conventional power plants generally have very low efficiency. Therefore, heating and cooling systems must be integrated with existing plants can improve the efficiency of an entire plant. When this additional step is implemented, this is called trigeneration. This involves combined cooling, heating, and power (CCHP) generation [8]. Combining solar and trigeneration systems has been found to be an ideal combination when a rich and efficient source of renewable energy is used [9]. With regard to this, it is necessary for tri-generation energy systems to become better suited to the energy market. Tri-generation uses waste and/or other forms of heat from power plants in order to improve its overall thermal performance, typically using free energy that is available from energy loss. The waste heat from the main engine in a trigeneration system drives the heating and cooling devices by the temperature rises. The gain heat

can then be made use of for domestic hot water supply, space heating, or the production of steam to be used for processes heating. Moreover, this heat can additionally be made use of for cooling as the power source for an absorption chiller. Recently, there have been a number of studies of a trigeneration, possibly due to its benefits and possibility to widely use in residential buildings, airports, shopping malls, hotels, hospitals, food and chemical industries [10, 11]. Figure 1.3 shows the four main parts of a trigeneration energy system.
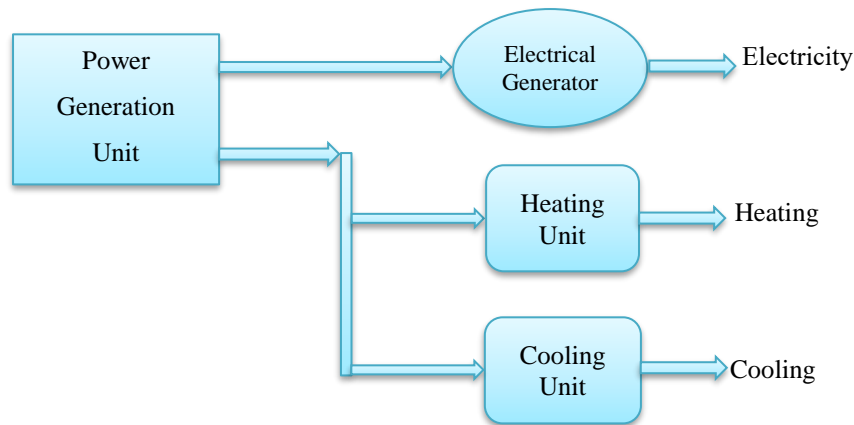
Figure 1.3. Typical configuration of a trigeneration energy system.

As the figure illustrates, a single main unit can produce heat, cool and electricity at the same time. Recently, researchers expanded the capabilities of trigeneration by using a single main unit in the production of more products, including hydrogen, fresh water and hot water, by utilizing a system called multigeneration. A huge contribution can be gain using the multigeneration system as a result of its high efficiency, low operation cost, as well as low emissions per unit of energy [12, 13].

Combining solar and multigeneration systems has been found to be an ideal combination when a rich and efficient source of renewable energy is used. For some reasons, the solar systems' efficiencies have not reached the desired operational level; so, they need further improvement. Solar energy conversion systems (SECSs) solve the problem of low thermal and optical performance via the use of nanofluids, which are used as a working fluids in solar thermal systems (STSs). This is considered an innovative approach for improving thermal performance as well as making the system more sustainable. Nanofluids are a new class of modern heat transfer fluids that are

designed for the dispersal of nanoparticles that are <100 nanometers in the conventional heat transfer fluids [14–18]. Nanofluids have shown improved thermal properties when they are compared to base fluids, so it can enhance the STSs' heat transfer properties.

1.2. MULTIGENERATION SYSTEMS

The researchers have developed trigeneration systems, and used the same system to produce more purposes, including hydrogen, hot water, drying, and drinkable water. A system that can produce more than three various forms of energy is called a multi-generation energy system. Systems such as this should be taken into consideration for use in residential areas, airports, manufacturing and a number of other places where many useful output forms are required. It is important to note that the location as well as requirements of such an application are key factors in its designing. As an example, in a situation in which there is a need for hot water, any system must prioritize this requirement. Multi-generation systems are considered as an adequate solution to the problem of global warming, which is one of this century's greatest challenges.

Multigeneration systems have many advantages, such as increased efficiency of power plants, reduced loss and waste heat, reduced operating costs, low greenhouse gas emissions, shorter transmission lines, better use of resources and more power generation options. These advantages motivated designers and researchers to develop energy systems for several generations. The improvement of efficiency is generally the most significant factor in the implementation of multigenerational energy systems. Before selecting multigeneration plant, additional evaluations, such as estimates of the initial operating and capital costs, are required to ensure that the construction and performance of the system is efficient and economical [19].

Figure 1.4 representative a typical multigeneration energy system to produce heating, cooling, power, fresh water, hydrogen and hot water and that works based on only solar energy [20]. Other configurations, such as those combining renewable energy sources with traditional energy sources, are also a possibility. As a clear in figure the electrolyzer is used to produce hydrogen, which, as it happens, is powered via a small

amount of the electricity that is generated via a concentrating solar collector. The hot water first enters into the electrolyzer and then undergoes an electrochemical reaction, breaking down the molecules into both oxygen and hydrogen. The heating system is made up of two basic parts. The first is used in the production of hot water, and the other is used for heating. The heat that is rejected from the storage system enters into the absorption cooling system for the production of cooling energy as well as air conditioning. Some of the heat that is produced via the solar concentrator is also used in the operation of the desalination system, whereas some of the electricity drives the pumps.
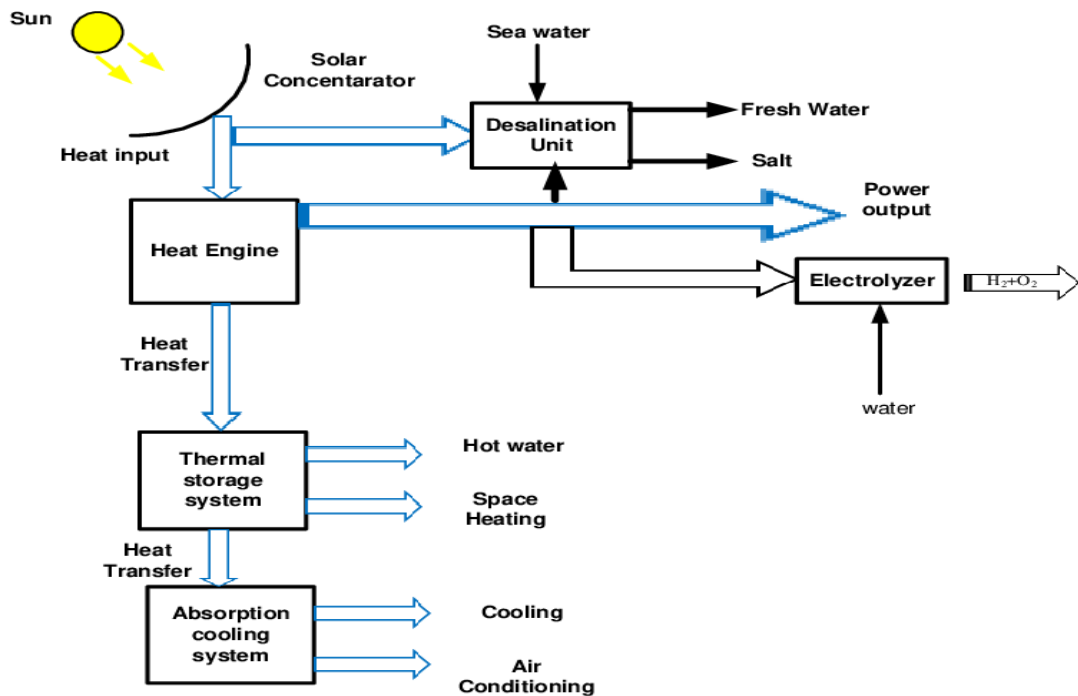
Figure 1.4. A typical multigeneration energy system.

However, unlike conventional energy sources, solar energy is usually non-continuous and unstable and solar radiation can also vary greatly over days or even hours. It is quite clear that using a single renewable energy source is not enough to support a continuous power supply system. To overcome the above disadvantages, multigeneration processes in hybrid solar power plants to produce many useful outputs is developed and improved as shown in Figure 1.5. Hybrid solar system can be considered as a next generation energy production technology that can overcome the problem of the discontinuity of solar energy [21].

1.3. RENEWABLE ENERGY RESOURCES

Generating renewable energy, including solar energy, as well as biomass, geothermal, or wind energy has rapidly increased during the last decades because of reducing renewable energy technology costs, increased energy demand, changes in fossil fuel prices, and other factors, which encourage the renewable energy usage. Recently, more and more attention has been paid to integrated renewable energy systems, as hybridization systems can be efficiently implemented to provide highly efficient and reliable electricity to end users, as opposed to standalone renewable sources.

1.3.1. Solar Energy

The energy of future generations is solar energy, not only because it does not pollute the environment, but also because the sun is inexhaustible, it provides abundant and stable energy. Since the sun is actually a thermonuclear reactor, the researchers estimate the solar heat on the solar surface to be around 5,700 K.

Researchers use specific equipment specifically designed to convert sun radiation into heat. They are called solar collectors. They are installed on sunny surfaces and continue to absorb solar energy in the daytime and when the weather is good. Receiving solar energy results in an increase in the absorption plate temperature and this energy conveys into the energy storage fluid. Basically, there are two basic types of solar energy collectors, which comprise stationary and concentrating type collectors or non-concentrating type collectors, as shown in Figure 1.6 [22]. They can also be classified according to the form of heat transfer fluid that is used, such as water, air, nanofluid, or heat transfer oil, and whether or not they are exposed or covered.

1.3.1.1. Non-concentrating Collectors

These type of collectors are fixed in position and do not track the sun. There are three main types of collectors in this group.
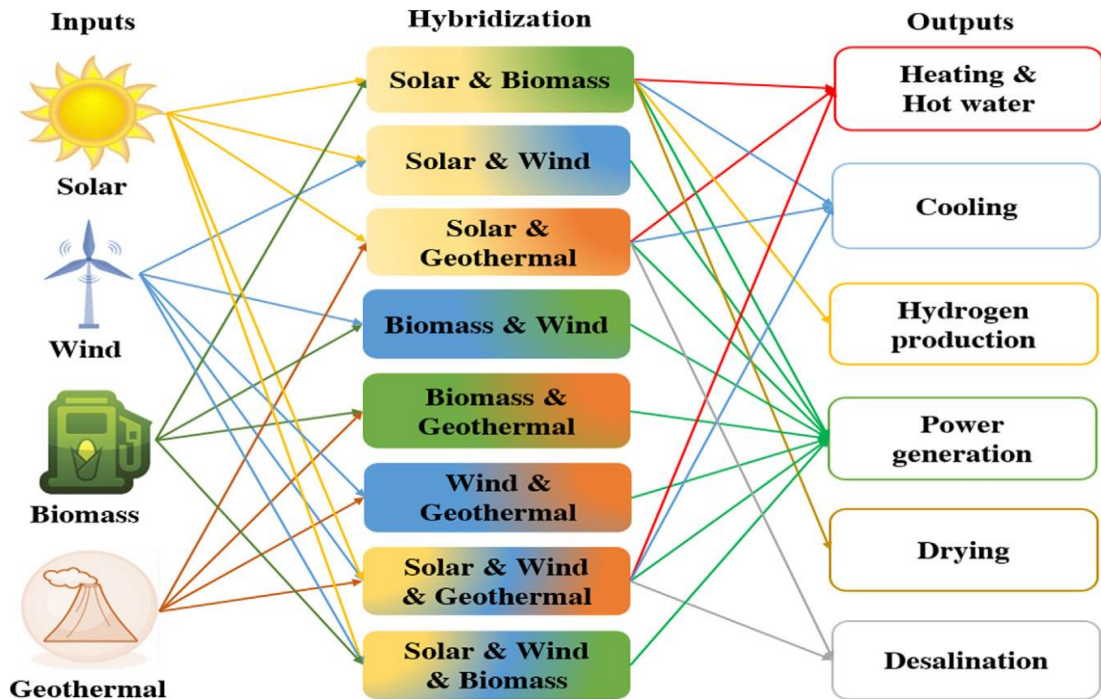
Figure 1.5. Route toward hybrid renewable energy utilization.

Compound Parabolic Collector (CPC)

Compound parabolic collectors collect both direct and indirect forms of solar radiation without the need for any tracking system. These concentrators are non-imaging types. They have the ability to reflect to the incident radiation absorber within a wide limit. The need to move the collector to adjust the changes in the solar orientation can thus be reduced via the use of a trough that has two parabolic sections that face each other. Compared with flat plate collectors, the optical performance of CPC collectors is lower as a result of scattering loss in reflection, but they can perform better at higher temperatures [23].

Flat-Plate Collector (FPC)

Flat plate collectors are available in a wide array of materials and designs. These are used in the heating of fluids like air and water. Their main goal is the collection of as much solar energy as is possible at the lowest possible total cost. FPCs have advantages such as being cheap to install, collecting both diffuse and beam radiation, and being consistently in a fixed position, so there is no need for sun monitoring [24].

8
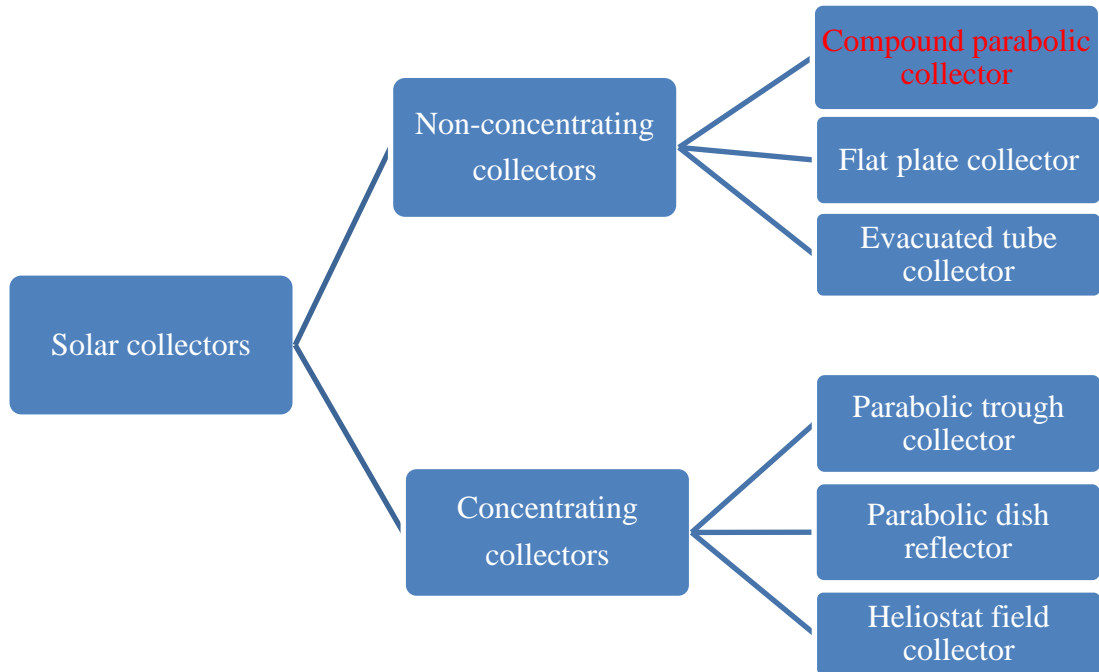
Figure 1.6. Classification of solar thermal collectors.

Evacuated Tube Collector (ETC)

This type of collector uses a series of evacuated pipes to heat the fluid. The evacuated space is used to capture solar energy and minimize radiation loss to the surroundings. The absorber consists of metal tubes which act as absorbent plates in the flat-plate collector type. The heat collected by the absorber is transferred into the fluid. The temperature of the inner tube can reach 150 °C due to the very high properties of evacuation insolation. Therefore, tube collectors that have been evacuated may be more efficient when compared to flat plate collectors, even in cold weather [25].

1.3.1.2. Concentrating Solar Collectors (CSC)

In concentrating type collectors, the solar energy is first optically concentrated and is then transferred into heat. The concentration can be achieved by using mirrors or lenses to reflect or refract solar radiation [26]. The collector collects a large volume of direct radiation within a small zone. High thermodynamic efficiency can be achieved by heating the working fluid to a high temperature. This category comprises three basic kinds of collectors.

Parabolic Trough Collector (PTC)

Parabolic trough collectors are constructed via folding of a sheet of some reflective material into a parabolic shape. Then a black-colored metal tube is lain along the receiver's focal line, which is then covered with a glass tube so as to reduce the heat loss. When the parabolic is facing the sun, the parallel rays that fall on the reflector are then reflected into the receiver tube. Then, the concentrated radiation finds its way into the receiver tube will heat the liquid that is circulating through it, which then converts the solar radiation into heat that can be used. To obtain good efficiency with high temperatures, it is necessary to have a high-performance solar collector. A PTC is quite effective at producing heat at temperatures as high as 400 °C [27].

Parabolic Dishes Reflector (PDR)

A parabolic dish reflector (PDR) is a point-focus collector, which is able to concentrate the solar irradiation collected onto a receiver that is located at a focal point located directly above the center of the dish. The receiver is able to absorb the radiated solar energy and then convert this energy into thermal energy within the working fluid. This thermal energy is then converted into electrical energy or directed to a central energy conversion system [28].

Heliostat Field Collector (HFC)

In the case of very high radiant energy input, a number of heliostats or plane mirrors can be made use of to reflect the collected incident direct solar radiation onto a common target, which is known as the heliostat field or a central receiver collector. By using the heliostat's mirror segments, which are slightly concave, a large volume of heat can thus be directed into the steam generator cavity to generate steam that has a high temperature and high pressure. This concentrated heat energy, which has now been absorbed by the receiver, is then transferred into the circulating fluid. This can then be stored and later used to generate energy [29].

1.3.2. Geothermal Energy

Inside the earth there is thermal energy that comes from physical processes that take place on earth's interior and the internal structure of our planet. This kind of energy is a good source of renewable energy due its clean and sustainable. Most of the Earth's core, which is called molten lava, has high temperatures that have persisted for thousands of years. Currently, there is a significant amount of thermal energy in the crust of the earth. The accessibility to that thermal energy varies from place to place. In some areas it is reachable, while in others it is deep underground. Heat propagates from the core of the earth to its surface by a gradient of 30 °C/km. This movement can hardly be noticed, but the temperature of rocks is known to increase with depth [30].

1.3.3. Biomass

The term "biomass" encompasses a vast range of materials, all of which can be made use of as fuel or as raw materials, and their common denominator is that they all originated from recent organisms. This definition explicitly does not include traditional fossil fuels. These fossil fuels are also sourced from plant, such as coal, or animal, such as oil and natural gas, sources, but it took millions of years to transform into their present form. Biomass sources include hay, wood wastes, agricultural residues, paper waste, sawdust, hay, food waste, animal waste, aquatic plants, as well as energy crops that are grown for their biomass as shown in figure 1.7 [31].
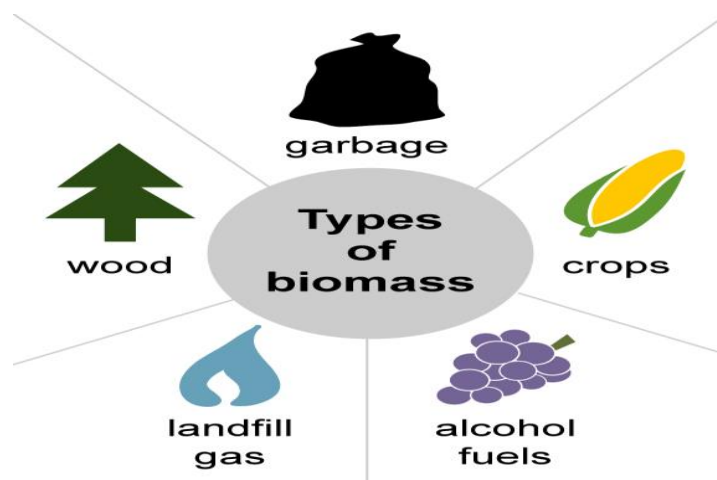
Figure 1.7. The main types of biomass.

Biomass is still a significant fuel in the majority of countries and is especially used for cooking and heating in countries that are still developing. In a number of developed countries, there is increasing growth in the use of biomass fuels for transportation and the generation of electricity, in order to decrease the amount of carbon dioxide emissions from the use of fossil fuels. In 2020, it was reported that, in the USA, biomass provided almost five quadrillion British thermal units (Btu) and approximately 5% total primary energy use [32]. Biomass comprises stored chemical energy that was absorbed from the sun. Plant biomass is produced through photosynthesis. This biomass can be burned directly in order to produce heat or it can be converted into renewable liquid and/or gaseous fuels as a result of various processes.

There are also several biomass conversion technologies available that can be used to obtain many products, such as electricity, heat, biofuels, charcoal and chemicals, amongst others. That fact makes biomass an important solution for increasing the integration of endogenous and renewable energy sources into smart energy systems. Using thermochemical and biochemical conversion methods, biomass can also be converted into energy. Moreover, thermochemical technologies include combustion, gasification and pyrolysis. Biomass combustion is currently the most used and most mature conversion technology. Biomass combustion is today the most developed and most used conversion technology.

1.3.4. Wind Energy

Wind power is an economical and renewable solution for electricity production. Wind power can significantly reduce the environmental impact that is associated with electricity production from fossil fuels, such as coal, natural gas, and oil. Wind turbines allow for the harnessing of wind power that can then be turned it into useful energy. As the wind is blowing, the blades of the wind turbine spin in a clockwise direction, and capture energy that is made by the wind. After this, the wind turbine's main shaft, which is connected via a nacelle to the gearbox, starts to spin. Next, this collected energy is sent by the gearbox to the generator, which is then converted into electricity. This new wind electricity is then transferred to a transformer, in which the voltage

levels are adjusted so that they match those of the grid. It is noticed that the wind speed is different on varying altitudes, and in many countries, its power is insufficient for assuring consistent power supply. Researchers find that whenever wind power penetration within the wind generator rises, the whole operation and supply of power gets affected. For stabilizing the power system and assuring consistent power supply, comprehensive planning is needed to deal with variations. For power generation, planning and capacity adjustments, accurate wind speed and direction forecasts are required [33].

1.4. NANUFLUIDS

For decades, growing engineering industries have been interested with rapid heat transfer. Researchers are constantly working to improve heat transfer rates and thermal conductivity for heat transfer fluid (HTF). A new type of HTF is engineered which is called nanofluid. This phrase was first used in 1995 by Choi, at the Argonne National Laboratory, in the USA. It is accepted that nanofluids are considered to be the next generation of heat transfer fluids. They offer exciting potential as a result of the increase in their heat transfer efficiency when compared to conventional fluids. Nanofluids are prepared by dispersing a nanoparticles smaller than 100 nanometers that are made by converting nanotubes of oxides, metals, carbon, and carbides into conventional type heat transfer fluids, including those such as water, hydrocarbons ethylene glycol, and fluorocarbons, which can be used with or without stabilizing agents [34].

The most common nanoparticles are Al_2O_3, CuO, Cu, Al, Fe, TiO_2 and SiO_2 [34]. It is generally observed that metals have thermal conductivity that is higher than all types of fluids. As an example, copper's thermal conductivity of is approximately 700 times higher than that of any fluid at room temperature. The thermal conductivity of nanoparticles increased on account of various physical factors such as Brownian motion of particles in the fluid, size of nanoparticles, concentration and grouping of nanoparticles in the base fluid. In addition, nanoparticles have excellent radiation absorption properties [35].

These nanofluids have advantages such as greater stability when compared to the fluids that contain fine or millimeter-sized particles, and their thermal conductivity is higher than that of the base fluids. Nanofluid properties are useful in extracting more energy from solar collectors, nuclear and geothermal power plants, enhancing their efficiencies. Several studies on the use of some types of nanofluids that are used as the working fluids in solar collector systems will be published in the literature, in particular some theoretical studies and interesting new experimental results [36].

1.5. PEM ELECTROLYSER

Water electrolysis is considered to be among the simplest methods to be used in the production of hydrogen. In the electrochemical process, electricity is used for the splitting the hydrogen and oxygen into their gaseous phase. This technique produces clean energy without pollution emission. A simple vision of water electrolysis process in the production of hydrogen via electrolysis is given in Figure 1.7. The electrolyzers can be categorized into three basic types, which include alkaline water electrolyzer (AE), proton exchange membrane electrolyzer (PEM), and high temperature electrolyzer [37].

PEM water electrolysis provides an interesting alternative to conventional AE. The advantages of PEM are environmental cleanliness, high hydrogen gas purity, small size and mass, low energy consumption, control of electrical power differences, high proton conductivity, ease of handling and maintenance and high safety level [38].

PEM electrolytes use black platinum, ruthenium, iridium and rhodium electrode catalysts and Nafion membrane. Water is introduced and separated into protons and hydrogen. Then the protons pass through the membrane, and then once there, they recombine and become hydrogen once again. PEM electrolytes can be connected to power stations, wind turbines and Rankine organic circuits (ORCs) [39].
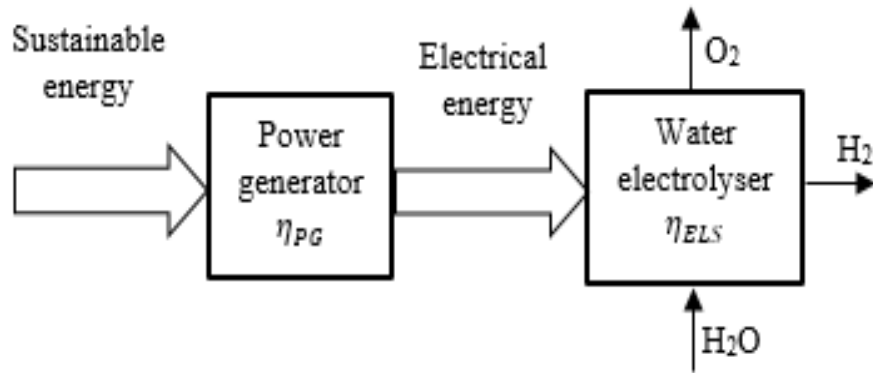
Figure 1.8. Water electrolyzer.

1.6. DESALINATION TECHNOLOGIES

The earth has around 1.4×10^9 km^3 of water covers about 70% of the planet's surface area; the percentage of salt water is 97.5%. The amount of fresh water resources is almost constant and the world population has increased very rapidly during the recent period. At present, more than 40% of the world's population suffers from a serious water shortage. All of this makes seawater desalination a major competitor for providing a sustainable source of fresh water to many countries around the world [40].

The industrial desalination process comprises the separation of nearly salt-free freshwater from marine or brackish water, where the salts are concentrated in the discharged brine stream. There are a number of desalination technologies (DTs), and some of these have undergone large-scale full-development, whereas others remain on a pilot scale for the purpose of demonstration or are at laboratory scale for the purpose of research and development. Figure 1.8 presents the most commonly used DTs [41].

Multistage flash distillation (MSF) is among the most commonly used water DTs and it accounts for 34% of the world's seawater desalination. MSF was designed on the basis of heating the fluid at a specific pressure, followed by flashing it at a much reduced pressure so as to form a vapor. The vapor is then collected and also condensed giving pure water. The pressure difference between the subsequent stages comprises the main factor that affects the production of the steam in each of the stages. This brine, which is highly concentrated, is drained at the very last stage [42].

15
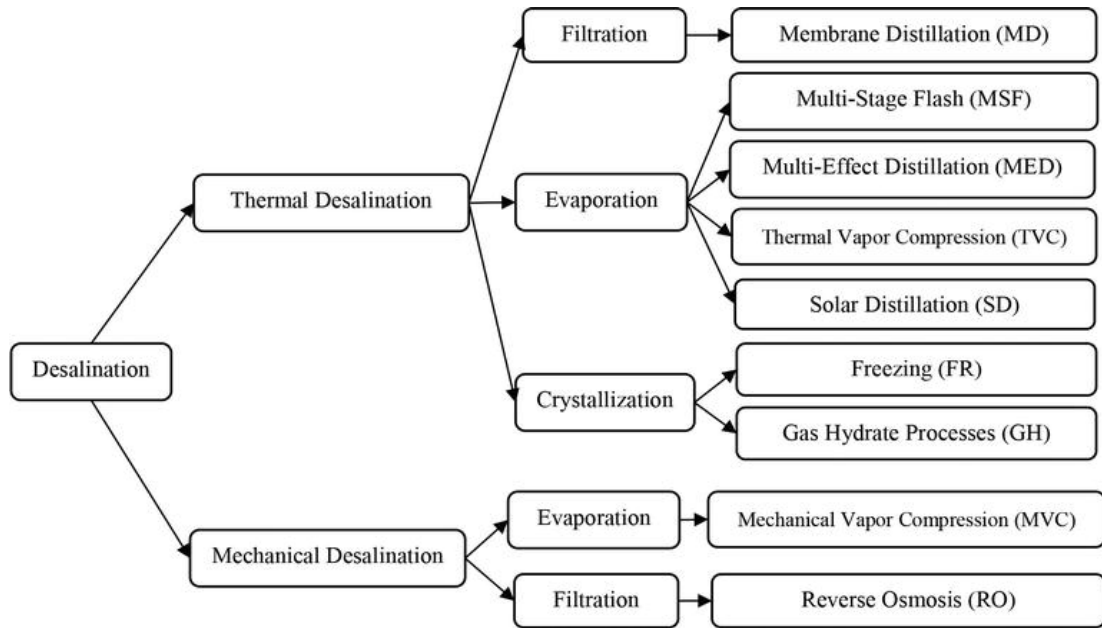
Figure 1.9. The most contemporary water DTs.

1.7. MOTIVATION AND OBJECTIVES

1.7.1. Motivation

Solar energy is recognized as not only renewable but also environment friendly. Hence, it is treated as a most sustainable and most powerful source. The common agreement is that the most important renewable fossil fuel replacement is solar energy. Combining multigeneration and solar systems has been found to be an ideal combination when a rich and efficient source of renewable energy is used. However, the use of solar energy does come with some challenges as a result of its volatile nature depending on the daytime and location. Like fluctuation in their potential which is a problem and need potential solutions. The fact that solar radiation is unavailable during night time and the problem with regard to the low optical and thermal performance of SECSs considered as major drawbacks for multi-generation systems powered by solar system. Therefore, the application of hybrid biomass-solar systems as an energy source of multi-generation system and the use of nanofluids as the working fluid in solar collector systems can tackle this issues.

1.7.2. Objectives

The objective of this dissertation was to comprehensively model, and then analyze and optimize a novel multigeneration energy system based on a hybrid solar-biomass that has not been previously considered in the literature. Another important goal herein was the use of two types of nanoparticles in a base fluid (ethylene glycol) to enhance the performance of the solar collectors and to assess their impact on the overall system performance. The exact objectives of the current research were as given below:

1. To design and analyze a novel hybrid system that is based on solar and biomass, in order to provide a number of useful products, including hydrogen, electricity, drying effect, fresh and hot water, and cooling/heating.
2. To evaluate the effect of using two different nanofluids (graphene and silver within ethylene glycol) as heat transfer fluids in the solar cycle on overall system performance.
3. To conduct an EIA of the system by calculating the carbon dioxide emissions of the system and determining the sustainability index.
4. To calculate mass flowrate, pressure, enthalpy, temperature, exergy, and entropy for all states in the multigeneration system.
5. To estimate useful outputs of the system, including energy and exergy efficiencies, and determine the exergy destruction value for each subsystem and check the possible improvements.
6. To conduct a parametric study in order to determine the effects of parameters such as ambient temperature, solar irradiation, output temperature of biomass combustor, types of nanofluids and their volume concentration on performance of the system.

1.8. THESIS STRUCTURE

This research is presented in six chapters. The first chapter reviews the energy challenges the world is facing and the solutions available so far. Different renewable energy resources are also commented and focus on solar energy systems and using nanofluids as a new and innovative approach for the improvement of their thermal

performance and making systems more sustainable. An overview of the most important sub-systems is provided and the justification and objectives of the thesis are presented.

Chapter 2 contains the most critical and recent studies on multigeneration technologies based on solar, biomass and hybrid systems. Furthermore, presents a comprehensive review of the available literature on the feasibility of solving the low thermal efficiency problem facing SECSs that use nanofluids as the working fluids in STSs. In the third part of the thesis, a detailed explanation of the proposed system is introduced. The system utilizes hybrid solar-biomass energy resources to power six subsystems.

The 4th chapter first deals with the description of the basic concept of thermodynamic analysis and also the equilibrium equations are presented. Then, the mathematical-based model of the integrated system is formulated in detail. The environmental impact of the multi-generational system was finally assessed.

Chapter 5 presents and discusses the results obtained of the numerical analysis that was conducted on the system proposed herein using the mathematical-based models that were presented in chapter 4. The effectiveness of nanofluids used in the solar cycle was also compared to the performance of the integrated system. Finally, some variable parameters were tested separately in order to determine what impact they had on the multigenerational system performance. The final chapter presents the conclusions of the thesis and future recommendations.

CHAPTER 2

LITERATURE REVIEW

2.1. INTRODUCTION

In a multi-generation system, it is important to select a prime mover that meets the energy requirements of the system. In the current chapter, an attempt is made to review important recent research on the main and sub-systems used in the current study and cover the most recent studies related to the application of solar, biomass, and solar-biomass as an energy source for multi-generation systems. It also throws light on recently conducted research on using a nanofluid as the working fluid in different types of solar collector systems.

2.2. SOLAR ENERGY BASED MULTI-GENERATION

Multi-generation systems of that provide useful outputs have been spreading rapidly across the world because they are able to provide a number of benefits, including a reduction in operating costs, an increase in efficiency, and a reduction in environmental impact. The concentrated solar power (CSP) is a viable option among solar energy technologies and it provides an ideal alternative to fossil fuels. There are some studies in literature dealing with the use of solar energy as the primary source of energy in multi-generation systems [43].

Yuksel et al [44] developed and presented a novel integrated multigeneration plant. This system consists of the solar tower as a main source of energy with thermal energy storage tanks, Rankine cycle, organic Rankine cycle, absorption cooling cycle, PEM electolyzer and drying process. Their results revealed that the overall energy efficiency of the system was 54.15% and the overall exergy efficiency was 51.28%. In addition, an increase in solar radiation from 300 to 1100 W / m2 increased the energy and exergy

efficiencies by 16.27% and 23.22%, respectively. The hydrogen production rate also increased by about 15% in the same range.

Ozturk and Dincer [45] designed a solar-based multi-generation energy production system that produced a different forms of useful outputs, such as electricity, heating, cooling, hydrogen and hot water. The researchers found that the multigeneration system's exergy efficiency was about 57.4%, which is more than when the subsystems are used separately. They also found that the parabolic dish collector exhibited the highest exergy destruction rate when compared to the other system components as a result of the high temperature difference that existed between the collector and the working fluid.

Thermodynamic performance of multigeneration which produced potable water, hydrogen, power, and heating-cooling based on solar energy was investigated by Yilmaz [46]. The system comprised a Rankine cycle, an organic Rankine cycle, a Brayton cycle, a flash desalination system, an absorption cooling and heating system and a PEM electrolyzer. The overall system energy was 78.93% and the overall exergy efficiencies was 47.56%.

Siddiqui and Dincer [47] presented and analyzed solar energy system integrated with a solid oxide fuel cell and an ammonia fuel cell that produce four types of output. Their study reported that the overall energy efficiency of the multigeneration system was 39.1% and the overall exergy efficiency was 38.7%. Thus, an increase of 19.7% and 17.8% in both efficiencies was achieved.

Yilmaz et al. [48] investigated parabolic solar dish collector based multigeneration system for the production of power, hydrogen, cooling and heating. The molten salt was considered for sensible thermal energy storage. Their study reported that the energy efficiency of the system was 48.19% and the exergy efficiency was 43.57%.

El-Emam and Dincer [49] presented a novel integrated polygeneration system driven via the use of solar power. That system consisting of parabolic trough collector that was integrated with an organic Rankine cycle, an absorption cooling system, a

desalination unit, and an electrolyzer. Their system was thermodynamically analyzed, and they also analyzed its overall performance. They estimated the average cost different operating points. Their study reported that the maximum exergy efficiency was 39% and the minimum exergy efficiency was 21.7%. It was also achieved at a cost rate of $309.56/hour and $241.7/hour, respectively.

Ahmadi et al. [50] examined the thermodynamic simulation of a flat plate solar collector integrated with a PEM electrolysis and an ocean thermal energy conversion system. They concluded that the exergy destruction of the ocean thermal energy conversion cycle decreases with increasing solar radiation. Moreover, the exergy efficiency of the ocean thermal energy conversion cycle can reach 22%.

A parabolic trough collector based multi-generation system for hydrogen, electricity, heat water, heating and cooling is suggested by Ozturk [51]. He studied the exergy analysis to calculate the total number of losses, as well as their causes and their locations by computing the irreversibility that existed in each of the subsystems, as well as in the entire system. According to the results, the parabolic trough solar collector has the highest rate of exergy destruction among other components of the proposed system. In addition to that, it had the lowest exergy efficiency, at a rate of 17%.

Al-Ali and Dincer [52] suggested a multigeneration system that was based on the use of solar and geothermal energy. The researchers concluded that in the event that there was any shifting of the system, from single-generation to multi-generation, the energy efficiency of the overall system can be increased by 61.6% and exergy efficiency can be increased by 10.4%.

Almahdi et al. [53], in their study, developed and presented a solar-based multi-generation system that was used for the production of hydrogen. The system consisted of three ORCs, in addition to two absorption systems, as well as a heat pump, and a PEM electrolyzer. The overall energy efficiency of the system was 20.7% and the overall exergy efficiency was 13.7%. The system was also capable of producing 18.8 liters/sec of hydrogen.

21

Hassoun and Dincer [54] evaluated the efficiency of a multigeneration system that was powered via the use of an organic Rankine cycle, which utilized solar energy as the primary source of energy. They developed the system so as to meet the basic requirements of large residential complexes, including fresh and hot water, electricity, and cooling and heating. Their study reported that the system's overall exergy efficiency was 44.67%, which showed an increase to 58.8% following the application of multi-objective optimization.

2.3. BIOMASS BASED MULTI-GENERATION

It is known that fossil fuels release very deadly pollutants, which have been proven to be extremely harmful to both human health and the environment. Therefore, implementing alternative sources of energy like solar, geothermal, wind, hydroelectric, and biomass energy is very important for the future. Moreover, biomass very quickly became one of the most commonly used alternative sources of energy because of its sustainability and the fact that it causes no harm to the environment. Today, many of the power plants around the world that are biomass-powered plants.

Thermodynamic analysis of a biomass-based trigeneration system that used an organic Rankine cycle was studied by Al-Sulaiman et al. [55]. Four different generations were compared: single generation, cogeneration and trigeneration. They investigated the performance of the system under a variety of parameters. They have achieved the highest energy and exergy efficiency by using trigeneration. Overall, the energy efficiency increased by 75% and the exergy efficiency increased by 17% with their trigeneration system.

Ahmadi et al. [56] examined a multigeneration system that was based on the combustion of biomass. In their study, the useful products provided by their system included electricity, hot water, cooling, heating, and hydrogen production. In this study, an environmental impact analysis was conducted. Their analysis results proved that the greenhouse gas emissions from their multigeneration system were lower than that determined for the co-generation of the power and heat.

Safari and Dincer [57] designed a multigeneration system that is operated with the biogas produced from digestion process. Thermodynamic analyses of an integrated system for supposed system are studied in this paper. The main outputs of this system are power, heat, fresh water and hydrogen, and there is some heat recovery in the system to improve efficiency. The production rates for the useful outputs provided by their system were freshwater: 0.94 kg/s, power: 1102 kW, hydrogen: 0.347 kg/h, and hot water: 1.82 kg/s, under base conditions. In addition, the developed system achieved overall energy efficiency was 63.6% and the exergy efficiency was 40%.

Casas Ledón et al. [58] presented an exergoenvironmental analysis on a combined cycle that was integrated with biomass gasification that uses municipal solid waste as a biomass fuel. They noticed that the environmental impact for the system that they examined was 13.5 mPts/kWh where it was significantly lower than what was determined for the conventional natural gas energy system, which was 22–26 mPts/kWh.

Al-Sulaiman et al. [59] proposed a biomass combustor based trigeneration system, which consists of an organic Rankine Cycle, an Absorption Refrigeration system and heat exchanger. The main useful production are electricity, cooling load and heating load. Four different situations were studied and analyzed to conduct an examination of the impact that some parameters had on the performance of the system. The results proved that the use of a biomass combustion-based trigeneration system improved the system's exergy efficiency by 16%. It was also found that the carbon dioxide emissions of the trigeneration case are significantly reduced.

Exergetic as well as environmental analyses were done on the biomass gasification based combined cycle by Gholamian et al. [60]. Paper and wood were used as the biomass fuels. The results outlined that the cycle efficiency with using the wood as biomass fuel was 2.5% higher than the efficiency with using paper. On the other hand, the emission value using paper was 0.8% lower than when wood is used.

Boyaghchi et al. [61] designed and developed a biomass gasification process based multigeneration system that consisted of a dual-organic Rankine cycle, as well as an

ejector refrigeration loop, and also a proton exchange membrane electrolyzer for the production of the refrigeration effect, heating load, power, syngas, and hydrogen. Their system was also subjected to exergy, exergo-environmental, and exergo-economic analyses. Their results demonstrated that the cost of the hydrogen improved by 49.18% and the environmental impact/unit of exergy improved by 34.58%.

2.4. HYBRID SOLAR AND BIOMASS BASED MULTI-GENERATION

Since solar energy is a discontinuous source of energy, it is essential to employ another energy source or an energy storage medium to recover the energy demands on an ongoing basis. There are limited studies that consider solar energy and biomass as the main source of energy for a multi-generational system. Khalid et al. [62] designed and analyzed a biomass- and solar-based integrated system that was used to produce a variety of outputs. They found that the energy and exergy efficiency improve with incorporation of two energy sources.

Shahid et al. [63] evaluated thermodynamic efficiency of solar and biomass-based multi-generation systems. Moreover, they also analyzed exergy destructions of each subsystem. Their results showed overall energy efficiency improvement of 18.9% and exergy efficiency improvement of 28.0%. The steam Rankine cycle sub-system showed the highest exergy destruction rate (32 MW).

Wang and Yang [64] evaluated the thermodynamic studies on combined multi-generation systems powered by solar and biomass, which integrated subsystems for cooling, power generation, and heating. Their results showed overall energetic efficiency of 57.9% and exergy efficiency 16.1%.

Sarkis and Zare [65] carried out the thermodynamic examination of three different but novel configurations of hybrid solar-biomass. Gaseous substances were emitted after biomass combustion, which were used in the operations of both the gas turbines and the Rankin cycle of System 1 and 2, respectively. They found that the exergy and energy efficiencies of a standard plant are 40.68 % and 47.52%, for System 1 are 39.25% and 45.06%, and for System 2 are 36.91% and 40.12%, respectively.

Hashemian and Noorpoor [66] introduced a new biomass-based and solar multi-generation system design and conducted its thermodynamic assessment. They found that the system can generate 137.3 MW cooling rate, 26.3 MW power, 21.4 MW heating rate, 3927m3/h fresh water, and 72 kg/h hydrogen.

Karellas and Braimakis [67] proposed a trigeneration system based biomass and solar energy. Their system was analyzed during both the summer and the winter from an economic viewpoints. The researchers found that the net electric efficiency is 2.38%, while the savings in power consumption about 12%.

Ghasemi et al. [68] proposed and also analyzed an inventive multi-generation energy system based on parabolic trough collector and biomass combustion using thermodynamic and multi-purpose optimization. Multigeneration system consists of a Rankine cycle for supplying electricity, a double effect absorption chiller for heating and cooling, a multi-effect desalination system for desalination of sea water and a Linde-Hampson cycle for natural gas liquefaction. The results showed that the system could potentially generate 16.11 kW of electricity, 28.94 kW of heating power, 23.41 kW of cooling power, 8.8 kg/h of fresh water, and 0.02 m3/h of liquefied natural gas with energy efficiency and exergy efficiency by 46.8%. 11.2%, respectively.

Bai et al. [69] evaluated a polygeneration system based on biomass gasification using solar energy through dynamic simulation. The proposed system is generally designed for producing power and methanol. The overall energy efficiency was approximately 51.89% and the exergy efficiency was approximately 51.23%. Standard cost of methanol was 361.88 $/ton.

Cao et al [70] proposed a novel solar and gas turbine-based multi-generation system. The solar gas turbine cycle consists of a PTC and biomass burner. The multi-generation process using biomass and solar power showed 92.11% and 60.05% performances in terms of energy and exergy, respectively. Besides, they concluded that the electrical power, heating rate, cooling rate, and the freshwater flow rate were 106.5 kW, 0.7703 kW, 56.01 kW, and 35.74 kg/h, respectively.

To use renewable energy effectively, Bai et al. [71] conducted an analysis of the performance of a new solar-biomass based poly-generation plant. The researchers found that this energy system uses biomass sources and renewable energy sources efficiently.

Sahoo et al. [72] evaluated and optimized the performance of hybrid solar-biomass system in polygeneration process for cooling, power, heating and desalination. The effect of various operating parameters was determined. The results outlined that primary energy savings of solar-biomass based polygeneration system to 50.5 %. The energy yield from this system has increased to 78.12% when a comparison was made with a basic power plant.

Liu et al. [73] evaluated energy and exergy performance of a hybrid solar-biomass system in two varies situations. In the first, they performed biomass gasification by a solar collector, while the combined cycle was fueled with gasifier gas for power generation. In the other, when the biomass gasification was performed separately, concentrated solar energy was utilized to heat the air that was compressed at the Bryton cycle. It was shown by their results that, for the first case, the energy efficiency was more than that for the second case by 5.4%.

Pantaleo et al. [74] conducted a technoeconomic evaluation for a novel hybrid solar-biomass plant arrangement. They regained the exhaust gases heat of the gas turbine that externally powered by thermal energy storage tank. They also incorporated heat from the parabolic-trough collector in which molten salts were used as the heat transfer medium. They found that by using the integration of concentrated solar energy, the electricity production and cost of solar-based electricity increased, so, for the proposed system, the overall energy efficiency would be higher.

Ishaq and Dincer [74] proposed, analyzed and evaluated a solar energy- and biomass-based multi-generation system through energy and exergy approaches. The system that they proposed comprised a solar heliostat, a gas turbine cycle, copper-chlorine cycle, reheat Rankine cycle and absorption cooling system for for produce the multiple useful outputs. The integrated system was then simulated via the use of Aspen Plus, whereas

analysis of the subsystems was conducted via the use of engineering equation solver software. The proposed multigeneration system provides electric power of 8.3 MW and produce 118.9 g/s of hydrogen. The overall energy and exergy efficiencies of their system were determined to be 29.9% and 31.5%, respectoively.

2.5. NANOFLUIDS BASED SOLAR COLLECTORS

The solar systems' efficiencies have not reached the desired operational level; so, they need further improvement. Researchers have solved the problem of low thermal efficiency faced in SECSs using nano-fluids as operating fluids in solar-thermal systems. Nanofluids have shown improved thermal properties when they were compared to base fluids; so they can enhance the STSs' heat transfer properties.

To date, limited studies are available on using solar energy as a main energy source when nanofluids are used as working fluids. Boyaghchi et al. [75] proposed a multigeneration solar and geothermal system using water/CuO nanofluid to transfer heat. They compared four working fluids, including R134a, R1234ze, R1234yf, and R423A in the organic Rankine cycle. Results proved that R134a is a superior working fluid for ORCs. Additionally, the utilization of a nanofluid as a medium of heat transfer rather than pure water was declared effective because it increased the system's thermal and energy efficiencies.

Nasrin et al. [76] designed the cooling system of a PV module by improving a new heat exchanger and evaluated PVT performance using a water/MWCNT nanofluid in terms of thermal energy efficiency and output power. The overall performance and thermal efficiency for the PVT system operating with a water/MWCNT nanofluid exceeded the performance and thermal efficiency of the water in numerical and experimental results.

Verma et al. [77] conducted an assessment of a flat plate solar collector using varying types of nanofluids, SiO_2/water, TiO_2/water, Al_2O_3/water, CuO/water, graphene/water, and MWCNTs/water. Experimental results had shown that the increase of exergy,

energy efficiency and maximum reduction in the entropy using MWCNTs is the highest, followed by graphene.

Toghyani et al. [78] utilized certain types of nanofluid in a parabolic trough solar system to operate the Rankine cycle. It was determined that nanoparticle dispersion into the thermal oil was able to improve the system's exergetic efficiency by 3% with TiO_2, 6% with CuO, 11% with SiO_2, and 9% with Al_2O_3.

Abid et al. [79] comparatively and thermodynamically analyzed a parabolic trough solar thermal power plant using two different nanofluids (Al_2O_3, Fe_2O_3) and two different types of thermal fluids, Glycerol and Therminol 66. They noticed that a nanofluid improves the solar thermal plant's net power.

Tzivanidis and Bellos [80] evaluated an absorption chiller system powered by solar collectors and consisting of flat plate collectors based on nanofluids. $LiBr/H_2O$ was the working fluid in the absorption chiller while the solar system was run using water/CuO nanofluid. The researchers found that using nanofluids in a solar collector can improve the system's daily exergetic performance by 3.99% and refrigeration production by 0.84%.

The effects of using nanofluids in a parabolic trough collector (PTC) and a solar dish collector (SDC) on the multi-generation system was studied in the research of Abid et al. [81] who found that the PTC systems produced more electricity than SDC systems. They were able to achieve exergy efficiency of 23.8% and 23.25% with the PTSC system and SDC system, respectively.

Faizal et al. [82] tested the effect of using metal oxides, including SiO_2, Al_2O_3, CuO, and TiO_2 nanoparticles with water on the power generation and cost of a solar collector for obtaining the targeted product temperature. According to the results, low specific heat and high density of nanoparticles leads to improved thermal efficiency while the CuO nanofluid shows higher value as compared to other nanofluids.

A comparative analysis performed by Ibrahim and Kayfeci [83] to analyze the thermodynamics of a trigeneration system that used graphene as well as ferrofluid nanoparticles shows that the system efficiency enhanced when 0.1%-0.6% volumetric fraction of nanofluids was used. The researchers found that the performance of graphene nanoparticles was better when a comparison was made with that of ferrofluid nanoparticles.

Lu et al. [84] conducted experiments on the CuO-water nanofluid to investigate its thermal performance in the CPC. They reported the greatest heat transfer coefficient as almost 30% with a nanofluid at 1.2% mass concentration. In another experimental study [85], the same researchers revealed that the improvement in the CPC thermal efficiency was almost 12.7% when the same nanofluid was used. Since the literature on nanofluid use in a CPC is limited, further investigations should be conducted in order to be able to assess the CPC performance using different nanofluid types.

Alsaady et al. [86] examined the effects of ferrofluid on the efficiency of a parabolic trough collector. It was determined that using ferrofluids in solar collectors provided some environmental benefits, as well as improvements in the heat transfer, in addition to reductions in the heat transfer area required. A study presented by Khosravi et al. [87] showed an excellent performance of the optical thermal conversion of solar collectors under very specific conditions via the use of magnetic nanofluids (MNFs). Their results proved that MNFs would absorb solar radiation very well and improve solar collector efficiency.

Previous papers in the literature show that the performances of multiple production systems depend on their design; therefore, increasing system efficiency by choosing different designs is as important as using latest technologies in the researches. The current multi-generation system is practical and feasible, because it uses modern technologies and existing systems. In this study, we developed and analyzed a novel multi-generation system, which uses biomass and solar energy. To the best of our knowledge and after conducting a comprehensive literature review, we can claim that there is no previous study, in which, researchers used compound parabolic collector to collect the solar irradiation for the multi-generation system, in addition to using

graphene and silver nanoparticles within the base fluid. Besides analyzing and assessing the overall system according to several criteria, a comparative study was conducted to analyze two different nanofluids as heat transfer fluids in the solar cycle for evaluating their effect on the overall performance. We calculated useful outputs of the system, including energy and exergy efficiencies, and determined the exergy destruction value for each subsystem, checked the possible improvements, and studied the effect of significant parameters.

CHAPTER 3

SYSTEMS DESCRIPTION

The multi-generation systems offer a promising application, as already mentioned in literature. The application of hybrid biomass-solar systems as an energy source of multi-generation system is an interesting option, and it is currently an important goal for the researchers. Therefore, the studied multigeneration energy system is based on this prime mover. Figure 3 shows the suggested multi-generation system. It is evident that the integrated system benefits from both solar and biomass systems as two independent sources of energy. This combined plant includes:

1. A compound parabolic collector (CPC).
2. Hot and cold energy storage tanks.
3. Reheat–Regenerative steam Rankine cycle (SRC).
4. Biomass combustor.
5. Broton exchange membrane electrolyzer (PEM).
6. Organic Rankine cycle (ORC)
7. Multi-stage flash distillation (MSF)
8. Dryer process.
9. Double-effect absorption cycle (DEAC).

Two types of nanoparticles, including graphene and silver (Ag) were chosen as working fluids, and they were used in Ethylene glycol (EG) as a base fluid in the solar system. These nanofluids possess excellent and diverse physical properties that help to provide the thermal energy needed to contribute to drive the subsystems.

It is clear in the system schematic that solar radiation falls on the solar system and it is concentrated by a CPC. The heat transfer fluid enters the CPC to receive solar energy and leaves the solar collectors at a comparatively high temperature.
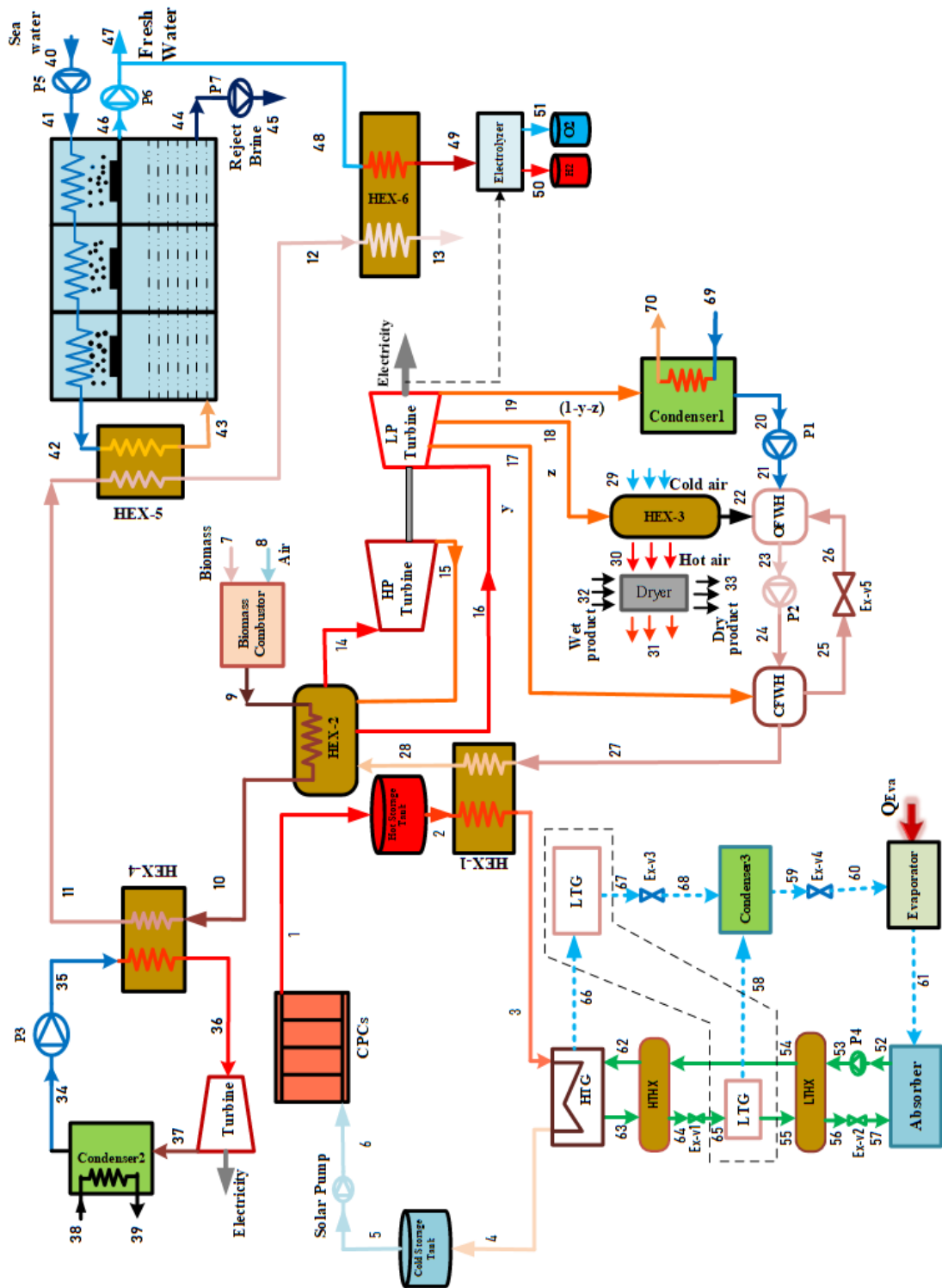
Figure 3.1. Schematic of biomass and solar energy driven multigeneration system.

After leaving the hot energy storage tank, this hot fluid flows in the first heat exchanger (HEX-1) to exchange heat with water that comes from a closed-feed water heater in the SRC and leaves the HEX-1 at a relatively lower temperature.

The residual heat in the absorption fluid is used to heat the LiBr/H_2O solution in the high temperature generator (HTG) of a DEAC. The pump returns the relatively low-temperature fluid that comes from the cold energy storage tank to the CPC to increase its temperature, and the cycle begins again. The steam produced by the HEX-1 outlet has high-quality energy that is usable again to improve the system efficiency.

To complement the energy requirements of the entire plant and provide more feasible inputs to the system, biomass combustion is incorporated into the system where air and biomass are mixed in a biomass combustor to produce thermal energy and provide extremely hot steam. The steam Rankine cycle is run using the produced hot steam, and it is utilized in HEX-2 for heating up a medium-temperature fluid that comes from HEX-1. For more effective energy recovery, high pressure and low pressure turbines are combined in an SRC that has an appropriate temperature range. The high-temperature steam leaves the HEX-2 (used as a boiler for the SRC) is used to generate electricity by sending it to a high-pressure turbine (HPT), and later, it is passed back to HEX-2 for reheating. When the steam is reheated at low pressure, it is sent to a low-pressure turbine (LPT) for generating electricity.

The regeneration process takes place in the SRC through bleeding the steam from the LPT at various points. The steam is used to warm the feedwater by a regenerator, or a feedwater heater (FWH). Single-stage reheating, process heater (HEX-3), closed feed water heater (CFWH), and open feed water heater (OFWH) are used in SRC because of their benefits, perhaps the most important of which is raising the cycle efficiency and thus improving the overall efficiency of the system. Extra heat (state 18) is shifted to HEX-3, where it is used in the drying subsystem for drying the wet products.

Since the absorption fluid that leaves HEX-1 still has energy, it is reused to power the DEAC, which uses wasted heat. DEAC combines a couple of single-effect absorption-cooling systems. This system has two generators, which are available in different

designs. For this research, we used Lithium Bromide solution (LiBr-H_2O) as a working fluid because water acts as a refrigerant while LiBr acts as an absorber. In this cycle, dilute lithium bromide solution first flows to the HTG, while the concentrated lithium bromide solution passes through a solution expansion valve before it enters the LTG. The refrigerant vapor condenses in the condenser and reaches the cooling temperature. Then, chilled water gets into the evaporator to provide a cooling load. The weak H_2O-LiBr solution enters the absorber and absorbs the vapor coming from the evaporator by releasing heat to the environment.

The ORC is integrated into the system to further utilize biomass energy and generate more power. A main benefit of this cycle is converting low- and medium-temperature heat sources into electricity. Isobutane is used as the working fluid in ORC. To take advantage of the waste heat of the condenser, it was used to obtain hot water.

The requirements for MFS reheating are fulfilled by using the steam, which is generated from the biomass combustor when it leaves HEX-3. The remaining part of the heat is utilized for warming up the water before it enters the PEM. MSF performs thermal desalination that passes hot brine from several vacuum stages. Where each consecutive stage operates in gradually low pressures. The sea water is heated under high pressure at first and then is sent into the successive flash chambers. A standard MSF system consists of 24 instillation stages in a series configuration. During these stages, the brine evaporates, which is called "flashing". When the flashed vapors condense on the preheating tubes' surfaces, it simultaneously produces distillates and transfers heat to the incoming feed water, which is supplied through the tubes. The rejected brine comes out of the desalination system at a 178.1 kg/s mass flow rate and discharges the fresh water at a 21.89 kg/s flow rate. Some freshwater, which is obtained through the MSF, is transferred to the electrolyzer for producing hydrogen.

Some proportion of the generated electricity is utilized in the electrolyzer to produce hydrogen via water splitting by electrochemical reactions into hydrogen and oxygen, which are shifted to storage tanks. Hydrogen's reputation as a promising alternative as a fuel with carbon free and an excellent carrier of energy makes it a desirable useful output.

CHAPTER 4

ANALYSIS AND ASSESSMENT

4.1. INTRODUCTION

After describing the proposed system design and providing a detailed explanation of its working mechanism in the previous chapter, this chapter outlines the mathematical models and analyses carried out in this thesis. General formulas for thermodynamic analysis are presented. The specific focus has been given to the first and second laws of thermodynamic analysis. Finally, the thermodynamic analyses for the system are performed.

4.2. THERMODYNAMIC PRINCIPLES

The conversion of heat-work energy must be within the specified limits in the laws of thermodynamics. The first and second laws of thermodynamics are described the behaviors of thermodynamic systems depending on their type. Moreover, the third law of thermodynamics represents the state of thermodynamic equilibrium.

By viewing the system as a control volume, four balance equations types must be considered; Mass balance, energy balance, entropy balance and exergy balance. These equations can be properly solved by writing the equations for each component in the subsystems.

4.2.1. Mass Balance Equation

According to the principle of conservation of mass, the general balance equation for conservation of mass can be written as:

$$\sum \dot{m}_{in} - \sum \dot{m}_{out} = \frac{dm_{cv}}{dt} \tag{4.1}$$

Where $\dot{m}_{in}$ and $\dot{m}_{out}$ are the inlet and outlet mass flow rate, while m_{cv} represents the mass of the control volume and t is the time.

4.2.2. Energy Balance Equation

Based on the thermodynamic first law, the general energy-balance equation can be written as:

$$\sum \dot{m}_{in} \left(h_{in} + \frac{v_{in}^2}{2} + gZ_{in} \right) - \sum \dot{m}_{out} \left(h_{out} + \frac{v_{out}^2}{2} + gZ_{out} \right) + \sum \dot{Q} - \sum \dot{W}$$
$$= \frac{dE_{cv}}{dt} \tag{4.2}$$

In steady-state conditions (ignoring kinetic and potential energy), the energy balance equation can be formulated as:

$$\sum \dot{m}_{in} \, h_{in} - \sum \dot{m}_{out} \, h_{out} + \sum \dot{Q} - \sum \dot{W} = 0 \tag{4.3}$$

Where h is specific enthalpy, v is velocity, g is gravitational acceleration, Z is the elevation, $\dot{Q}$ is heat transfer rate and $\dot{W}$ is work rate.

4.2.3. Exergy Balance Equation

Exergy is defined as the maximum useful work that can be produced by balanced system with its surrounding. Exergy cannot be conserved due to irreversibility which leads to exergy destruction and entropy generation. The total exergy includes physical, kinetic, chemical, and potential energy, and can be formulated as:

$$Ex_{total} = Ex_{ph} + Ex_{ch} + Ex_{ke} + Ex_{pe} \tag{4.4}$$

Physical and chemical exergy are common types, while kinetic and potential exergy are supposed here to be neglected, since velocities are relatively low and elevation changes are slight [88].

To formulate an exergy balance equation, work, heat and mass must be included in the equation due to the fact that the transformation of a system can occur in three forms: mass, work and heat.

$$\sum \dot{E}x_{in} - \sum \dot{E}x_{out} + \sum \dot{Q}\left(1 - \frac{T_{amb}}{T}\right) - \sum \dot{W} = \dot{E}x_d \qquad (4.5)$$

Where x *is the* mass fraction of the LiBr in the solution, h the specific enthalpy and $\dot{E}_D$ the exergy destruction. The specific exergy is given by the following expression:

$$\dot{E}x = \dot{m}\left((h - h_{out}) - T_{amb}(s - s_{out})\right) \qquad (4.6)$$

4.2.4. Definition of Efficiency

To evaluate any system or process, we must introduce the term "efficiency". The efficiency associated with all types of heat conversion systems is defined as "total net work per total heat input". Energy efficiency is fundamentally based on the thermodynamic first-law. For energy systems where the inputs and outputs are expressed as one of an energy forms, energy efficiency is described as:

$$\eta_{en} = \frac{\dot{E}_{useful}}{\dot{E}_{input}} \qquad (4.7)$$

To make a perfect expression of efficiency, exergy must be used to define it. Assuming the process is reversible, efficiency is defined as an "exergetic view as the ratio of the exergy associated with the product to exergy associated to the fuel."

$$\psi = \frac{\dot{E}x_{Product}}{\dot{E}x_{Fuel}} = 1 - \frac{Ex_{d,t}}{Ex_{Fuel}} \qquad (4.8)$$

Where $Ex_{d,t}$ is the total exergy destruction and $\dot{Ex}_{useful}$ is the useful product exergy, which is the sum of the exergy destruction within the system and the exergy destruction by the surrounding environment.

4.3. MODELING OF THE MULTIGENERATION SYSTEM

The current section presents the mathematical model of our proposed multi-generation system. All the equations of thermodynamic equilibrium pertaining to energy, mass, and exergy are mentioned for all the integrated system components. The equations have been solved by Engineering Equation Solver (EES) software [89].

Before moving on to the mathematical model, we present the general assumptions that are consistent throughout the integrated system analysis. They are listed below:

1. All system parts operate under steady-state conditions
2. Reference pressure and temperature are 101.3kPa and 25°C.
3. We neglected all kinetic and potential changes to the entire system
4. Pressure and heat losses are not taken into account in flow channels.
5. Pump and turbine isentropic efficiency is assumed as 0.85.
6. The sulfur, chlorine and ash contents are trivial and thus ignored in the biomass energy calculations.
7. At the entrance to the MSF, the seawater has a 25°C constant temperature.
8. Heat loss at each desalination stage is ignored.
9. At every desalination stage, there is equal temperature increase of the preheated feed water.
10. The temperature of the hot brine equally reduces at each desalination stage.

For facilitate thermodynamic modeling, the multigenerational system presented in Figure 3.1 was divided into eight main parts: a compound parabolic collector (CPC), biomass combustor, proton exchange membrane electrolyzer (PEM), steam Rankine cycle (SRC), organic Rankine cycle (ORC), multi-stage flash distillation (MSF), dryer process, and the double-effect absorption cycle (DEAC). Then the efficiency of the overall system and the EIA are calculated.

4.3.1. Compound parabolic collector

It is a non-imaging form of concentrator that has the ability to focus light on a small absorber surface. It is designed as a fixed solar collector to achieve cost-effectiveness with relatively higher temperature, Figure 4.1 shows different CPC configurations. The nanofluid, which passes through the collectors, absorbs heat from solar energy and it is directly fed to other integrated subsystems for power generation. The detail parameters and operating conditions considered in the present study for the CPC are given in Table 4.1.
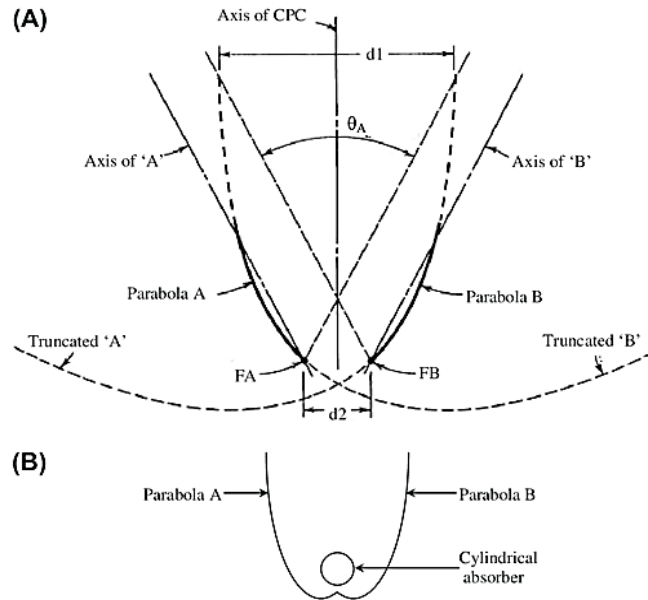
Figure 4.1. a) The geometry of conventional CPC, b) Schematic of CPC with cylindrical absorber.

The CPC analysis in this section is based on the equations presented by Kalogirou [90]. The CPC's energy efficiency can be computed using the given formula:

$$\eta_{CPC} = \frac{Q_u}{A_a\,G_t} \tag{4.9}$$

Where (η_{CPC}) is the thermal efficiency of a CPC, Q_u is the useful energy, G_t is the total incident radiation and (A_a) is the aperture plane. The useful energy provided by a CPC is calculated as follows:

$$Q_u = F_R \left[S\, A_a - A_r\, U_L\, (T_{in} - T_{amb}) \right] \tag{4.10}$$

The absorbed radiation (S) is obtained from:

$$S = G_t\, \tau_{cover}\, \tau_{CPC}\, \alpha_r\, \gamma \tag{4.11}$$

Where τ_{cover} is the transmissivity of the cover glass, α_r is the receiver absorptivity, CPC effective transmissivity is $\tau_{CPC} = \rho^n$, ρ is the specular reflectivity of the CPC walls and the diffusion radiation correction factor, and n represents the average number of reflections.

$$\gamma = 1 - \left(1 - \frac{1}{C} \right) \frac{G_D}{G_t} \tag{4.12}$$

Where the factor (γ) represents the diffused radiation wastage outside the acceptance angle of the CPC at concentration C, and C is the concentration ratio of collector $C = 1/sin\,\theta$. The G_D/G_t ratio varies from about 0.11 on a clear sunny day to about 0.23 on a foggy day.

F_R is the heat removal factor, given by:

$$F_R = \frac{\dot{m}_{nf}\, Cp_{nf}}{A_c\, U_L} \left[1 - \exp\left(-\frac{U_L\, \dot{F}\, A_c}{\dot{m}_{nf}\, Cp_{nf}} \right) \right] \tag{4.13}$$

The receiver area $A_r = A_a/C$. The collector efficiency factor $\dot{F}$ is given by:

$$\dot{F} = \frac{\dfrac{1}{U_L}}{\dfrac{1}{U_L} + \dfrac{D_{r,0}}{h_{fi}\, D_{r,i}} + \left(\dfrac{D_{r,0}}{2.\, k_r} \ln \dfrac{D_{r,0}}{D_{r,i}} \right)} \tag{4.14}$$

Where r is the receiver tube, $D_{r,0}$ is the outside diameter, $D_{r,i}$ the inside diameter, k_r the thermal conductivity and U_L the overall heat loss coefficient. The convective heat transfer coefficient inside the receiver tube calculated thus:

$$h_{fi} = \frac{N_u\ k_{nf}}{D_{r,i}}$$ (4.15)

Where k_{nf} is the thermal conductivity of nanofluid, and N_u is the Nusselt number of the flow inside the receiver tube. For turbulent flow (Re > 2300) as the flow in this analysis,

$$N_u = 0.023(R_e)^{0.8}(Pr)^{0.4}$$ (4.16)

Where;

$$R_e = \text{Reynolds number} = \frac{\rho_{nf}\ V\ D_{r,i}}{\mu_{nf}}$$ (4.17)

$$P_r = \text{Prandtle number} = \frac{C_{p,nf}\ \mu_{nf}}{K_{nf}}$$ (4.18)

The overall collector heat loss coefficient is obtained thus:

$$U_L = \left[\frac{A_r}{A_g\ (h_w + h_{r,c-a})} + \frac{1}{h_{r,r-c}}\right]^{-1}$$ (4.19)

Where A_g and A_r are respectively the outer area of the glass cover and the receiver. The radiation heat transfer coefficient for the glass cover to the ambient is calculated thus:

$$h_{r,ca} = \varepsilon_g\ \sigma\ (T_g + T_{amb})(T_g^2 + T_{amb}^2)$$ (4.20)

For glass cover, the radiation heat transfer coefficient to the surrounding is calculated as follows:

$$h_{r,cr} = \frac{\sigma\ (T_r^2 + T_g^2)(T_r + T_g)}{\frac{1}{\epsilon_r} + \frac{A_r}{A_g}\left[\frac{1}{\varepsilon_g} - 1\right]}$$ (4.21)

41

To determine accurately the thermal emissivity (ϵ_r) and thermal conductivity of the receiver tube, it is made a function of the surface temperature (in Kelvin):

$$\epsilon_r = 0.000327 \, T_r - 0.065971 \tag{4.22}$$

$$k_r = 0.0153 \, T_r + 14.775 \tag{4.23}$$

Also, the convective heat transfer coefficient can be measured by:

$$h_w = \frac{N_u \, k_{nf}}{D_{c,o}} \tag{4.24}$$

Where σ is the Stefan-Boltzmann constant, T_r is the receiver temperature and T_g is the glass cover temperature. The temperature (T_g) will be assumed initially, followed by the assumption being verified using the following equation:

$$T_g = \frac{A_r \, h_{r,r-c} \, T_r + A_g \left(h_w + h_{r,c-a} \right) T_{amb}}{A_r \, h_{r,r-c} + A_g \left(h_w + h_{r,c-a} \right)} \tag{4.25}$$

For the wind loss coefficient, the Nusselt number can be obtained using the following equation, which applies to turbulent flow ($1000 < \mathrm{Re} < 50{,}000$), as is the case of this analysis.

$$N_u = 0.3 \, R_e^{0.6} \tag{4.26}$$

This useful energy can also be calculated from:

$$Q_u = \dot{m}_{htf} \, Cp_{nf} \left(T_{out} - T_{in} \right) \tag{4.27}$$

Here $T_{out} \ and \ T_{in}$ are respectively the outlet and inlet temperature of the solar collectors, $\dot{m}_{htf}$ is the mass flow rate of heat transfer fluid inside the receiver, and Cp_{htf} is the specific heat of the heat transfer fluid.

The inlet exergy can be calculated by:

$$\dot{E}x_{solar,in} = Q_{sol}\left(1 - \frac{4}{3}\left(\frac{T_{amb}}{T_{sun}}\right) + \frac{1}{3}\left(\frac{T_{amb}}{T_{sun}}\right)^4\right)$$
(4.28)

For N number of solar collectors, the total solar irradiation will be:

$$Q_{sol,total} = A_a \, G_t \, N$$
(4.29)

And the heat transfer loss rate is obtained:

$$\dot{Q}_{loss} = \dot{Q}_{tot} - \dot{Q}_u$$
(4.30)

Finally, the heat stored in hot and cold thermal storage tanks can be calculated using the enthalpy of the heat transfer fluid and solar sunbathing time (SST) [91]:

$$\dot{Q}_{ST} = \dot{m}_{htf}\left(1 - \frac{SST}{24}\right)(SST)(h_{htf})(3600)$$
(4.31)

Here SST depends on the season and clouds and h_{HTF} is the enthalpy of HTF at the collector outlet. The SST of this study was considered to be 11.71 hours [91], which resulted in the choice of energy storage for a permanent operation at night.

Table 4.1. CPC parameters and operating conditions.

Parameter	Symbol	Value [unit]
Ambient pressure	P_{amb}	101.3 kPa
Ambient temperature	T_{amb}	25 °C
Solar beam irradiation	G_t	960 W/m^2
Diffuse radiation	G_D	150 W/m^2
Sun temperature	T_{sun}	5770 K
Number of collectors	N	4
Collector length	L	1 m
Specular reflectivity	ρ	0.9
Cover transmittance	τ_{cover}	0.75
Receiver tube inner diameter	$D_{r,i}$	60 mm

Glass cover outer diameter	$D_{c,o}$	120 mm	
Receiver tube outer diameter	$D_{r,0}$	75 mm	
Wind speed	V	1-5 m/s	
Acceptance half angle	θ	40°	
Daily sunbathing time	SST	4-14 *hours*	
Reflections average number	n	0.77	
Stefan-Boltzmann constant	σ	$5.67 \times 10^{-8}\,W/m^2.K^4$	

Nanofluids properties

The nanofluids of our study include graphene/Ethylene glycol, and silver/Ethylene glycol. A main reason for selecting these nanoparticles is their excellent and varied physical properties, which are higher in comparison with base fluids. The thermodynamic properties of Ethylene glycol were obtained using EES software. Table 4.2 shows thermodynamic properties of nanoparticles. The thermal properties of the nanofluids examined can be calculated from the characteristics of the base fluid and the nanoparticles at the bulk temperature. In the following modeling, the subscript "bf" is used for the base fluid (Ethylene glycol), the subscript "np" for the nanoparticle (graphene, silver), while the subscript "nf" for the nanofluids. The volumetric concentration (φ) is equal to 6% in the present study.

Table 4.2. Thermal properties of selected nanoparticles and the base fluid at 293 K.

Properties	Density (kg/m³)	Specific heat (J/kg K)	Thermal conductivity (W/m K)	Dynamic viscosity (Pa.s)
Graphene	2160	710	5000	-
Silver	10500	235	429	-
Ethylene glycol	1126	2345	0.256	21×10^{-3}

The density of the nanofluid (ρ_{nf}) is calculated according to the Pak and Cho formula [92]:

$$\rho_{nf} = \emptyset\,\rho_{np} + (1-\emptyset)\,\rho_{bf} \tag{4.32}$$

The nanofluid specific heat ($C_{p,nf}$) is calculated according to Xuan and Roetzel model [93]:

$$C_{p,nf} = \frac{\emptyset\left(\rho_{np}\, C_{p,np}\right) + (1 - \emptyset)\left(\rho_{bf}\, C_{p,bf}\right)}{\rho_{nf}} \qquad (4.33)$$

The thermal conductivity of the examined nanofluid (k_{nf}) can be determined according to the suggested model by Yu and Choi [94]:

$$k_{nf} = k_f\, \frac{k_{np} + 2\,k_{bf} + 2\left(k_{np} - k_{bf}\right)(1 + \beta)^3\,\emptyset}{k_{np} + 2\,k_{bf} - \left(k_{np} - k_{bf}\right)(1 + \beta)^3\,\emptyset} \qquad (4.34)$$

The nanofluid viscosity (μ_{nf}) is estimated by the Batchelor model [95]:

$$\mu_{nf} = \mu_{bf}\,(1 + 2.5\,\emptyset + 6.5\,\emptyset^2) \qquad (4.35)$$

The parameter β indicates the ratio between the thickness of the nanolayer and the initial radius of the particle. Typically, this parameter is specified to be 0.1 [96]. It is essential to state that the thermal properties are calculated at the mean temperature of the nanofluid ($T_{m,nf}$), which can be calculated with the following equation:

$$T_{m,nf} = \frac{T_{out} + T_{in}}{2} \qquad (4.36)$$

4.3.2. Biomass Combustion

As shown in Figure 3.1, both air and biomass respectively enter the biomass combustor at points 7 and 8. Table 4.3 shows the biomass (pine sawdust) composition examined in this study. The chemical formula for complete biomass combustion with air is as follows:

$$C_x\, H_y\, O_z + \omega H_2O + \lambda(O_2 + 3.76N_2) \rightarrow aCO_2 + bH_2O + cN_2 \qquad (4.37)$$
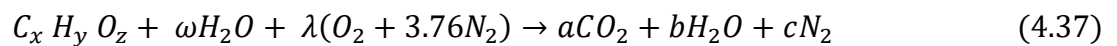
Where ω represents the fuel's moisture content. For biomass fuel, the molar mass flow rate is as follows:

$$\dot{n}_{biomass} = \frac{\dot{m}_{biomass}}{M_{C_x H_y O_z}} \tag{4.38}$$

Where $M_{C_x H_y O_z}$ represents the molar mass of biomass. The coefficients in Eq. (4.37) are determined by considering an elemental balance. The resulting expressions for the coefficients are determined with element balances:

$$a = x \tag{4.39}$$

$$b = \frac{y + 2\omega}{2} \tag{4.40}$$

$$c = \frac{79}{21}\lambda \tag{4.41}$$

$$\lambda = \frac{2a + b - \omega - z}{2} \tag{4.42}$$

The energy balance of the control volume around the biomass combustor is carried out to calculate the exhaust gas temperature as follows.

$$\bar{h}_{C_x H_y O_z,8} + \omega \bar{h}_{H_2O,7} + \lambda \bar{h}_{O_2,7} + 3.76\lambda \bar{h}_{N_2,7} = a\bar{h}_{CO_2,9} + b\bar{h}_{H_2O,9} + c\bar{h}_{N_2,9} \tag{4.43}$$

Where, $\bar{h}_{C_x H_y O_z,8}$ is the biomass fuel enthalpy and defined as [97]:

$$\bar{h}_{C_x H_y O_z,8} = \overline{x\bar{h}}_{CO_2,8} + \left(\frac{y}{2}\right)\bar{h}_{H_2O(l),7} + \overline{LHV}_{\text{moisture}} M_{C_x H_y O_z} \tag{4.44}$$

Here, lower heating value (LHV) of the biomass depends on the ultimate elemental composite and the moisture content in the biomass.

$$\overline{LHV} \left(\frac{MJ}{kg}\right) = \overline{HHV} \,(1 - \omega) - (2.44\omega)\big(8.396(1 - \omega)\big) \qquad (4.45)$$

Where, $\overline{HHV}$ represents the higher heating value of the selected biomass.

$$\overline{HHV} \left(\frac{MJ}{kg}\right) = 35.160C + 116.225H - 11.090O + 6.280N + 10.465S \qquad (4.46)$$

Here C, O, H, N and S show the elemental mass fractions in the selected biomass. The energy supplied to an integrated system comes from solar system and biomass combustor. The biomass energy depends on the fuel type and its mass flow rate.

$$\dot{Q}_{Biomass} = \dot{m}_f \, \overline{LHV} \left(\frac{MJ}{kg}\right) \qquad (4.47)$$

The exergy of heat supplied by a biomass combustor can be calculated as follows:

$$\dot{EX}_{Biomass} = \left(1 - \frac{T_0}{T_9}\right) \dot{Q}_{Biomass} \qquad (4.48)$$

Table 4.3. Pine sawdust biomass composition.

Description	Value (%)
Moisture content with respect to weight	10
Elemental analysis (dry basis by weight)	
Carbon (C)	50.54
Oxygen (O)	41.11
Hydrogen (H)	7.08
Sulfur (S)	0.57

4.3.3. Steam Rankine Cycle (SRC)

Table 4.4 shows the thermodynamic balance equations for the SRC components. The amount of power generated by the high and low pressure turbines are calculated from equations (4.49) and (4.50), respectively.

$$\dot{W}_{HPT} = \dot{m}_{SRC} \left(h_{14} - h_{15}\right) \tag{4.49}$$

$$\dot{W}_{LPT} = \dot{m}_{SRC} \left(h_{16} - y\,h_{17} - z\,h_{18} - (1 - y - z)\,h_{19}\right) \tag{4.50}$$

The net power used by the pumps in the steam Rankine cycle is:

$$\dot{W}_{P,s,net} = \dot{W}_{P1} + \dot{W}_{P2} \tag{4.51}$$

$$\dot{W}_{P,s,net} = \dot{m}_{SRC} \left((1 - y - z)(h_{21} - h_{20}) + (h_{24} - h_{23})\right) \tag{4.52}$$

The net power that can be obtained from the cycle is expressed as

$$\dot{W}_{net,SRC} = \dot{W}_{HPT} + \dot{W}_{LPT} - \dot{W}_{P,s,net} \tag{4.53}$$

The rate of energy input to the Rankine cycle is denoted by:

$$\dot{Q}_{SRC,in} = \dot{m}_9 \left(h_9 - h_{10}\right) + \dot{m}_{27} \left(h_{28} - h_{27}\right) \tag{4.54}$$

A closed feed water heater (CFWH) and an open feed water heater (OFWH) are used to preheat the steam that passes through the cycle. They reduce irreversibilities in the system and increase the efficiency of the power cycle.

The energy balance equation for the OFWH is expressed as:

$$(1 - y - z)h_{21} + zh_{22} + yh_{26} = h_{23} \tag{4.55}$$

The energy balance equation for the CFWH is expressed as:

$$yh_{17} + h_{24} = yh_{25} + h_{27} \tag{4.56}$$

Where y, z represent the mass fraction of the steam bled from the LPT at both 17 and 18 points. The extra heat of steam at point 18 is used for drying process.
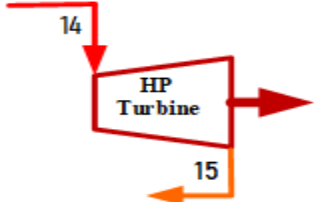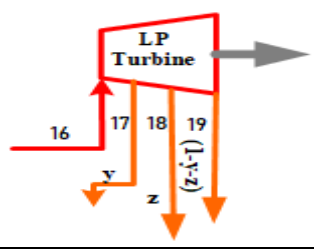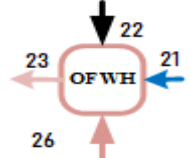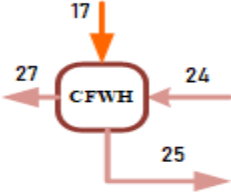The energy efficiency of the steam Rankine cycle is obtained by:
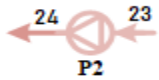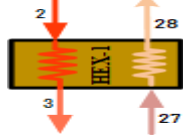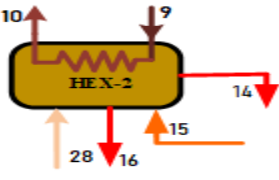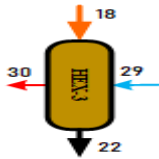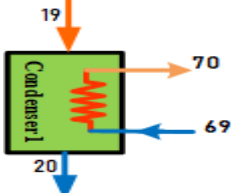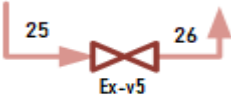
$$\eta_{SRC} = \frac{\dot{W}_{net,SRC}}{\dot{Q}_{SRC,in}} \tag{4.57}$$

The exergy efficiency of the steam Rankine cycle is obtained by:

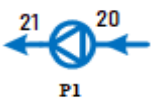$$\psi_{SRC} = \frac{\dot{W}_{net,SRC}}{\dot{Ex}_{SRC,in}} \tag{4.58}$$

Table 4.4. Thermodynamic balance equations of SRC components.

Component	Energy Balance Equation	Exergy Balance Equation
HPT	$\dot{m}_{14}\, h_{14} = \dot{m}_{15}\, h_{15} + \dot{W}_{HPT}$	$\dot{m}_{14}\, ex_{14} = \dot{m}_{15}\, ex_{15} + \dot{W}_{HPT}$ $+ \dot{Ex}_{D,HPT}$
LPT	$\dot{m}_{16}\, h_{16} = \dot{m}_{17}\, h_{17} + \dot{m}_{18}\, h_{18}$ $+ \dot{m}_{19}\, h_{19} + \dot{W}_{LPT}$	$\dot{m}_{16}\, ex_{16} = \dot{m}_{17}\, ex_{17} + \dot{m}_{18}\, ex_{18}$ $+ \dot{m}_{19}\, ex_{19} + \dot{W}_{LPT} + \dot{Ex}_{D,LPT}$
OFWH	$\dot{m}_{21}\, h_{21} + \dot{m}_{22}\, h_{22}$ $+ \dot{m}_{26}\, h_{26} = \dot{m}_{23}\, h_{23}$	$\dot{m}_{21}\, ex_{21} + \dot{m}_{22}\, ex_{22} +$ $\dot{m}_{26}\, ex_{26} = \dot{m}_{23}\, ex_{23} +$ $\dot{Ex}_{D,OFWH}$

CFWH 	$\dot{m}_{17}\,h_{17} + \dot{m}_{24}\,h_{24} =$ $\dot{m}_{25}\,h_{25} + \dot{m}_{27}\,h_{27}$	$\dot{m}_{17}\,ex_{17} + \dot{m}_{24}\,ex_{24} =$ $\dot{m}_{25}\,ex_{25} + \dot{m}_{27}\,ex_{27} +$ $\dot{E}x_{D,CFWH}$
Pump-1 	$\dot{m}_{20}\,h_{20} + \dot{W}_{P\_I} = \dot{m}_{21}\,h_{21}$	$\dot{m}_{20}\,ex_{20} + \dot{W}_{P_I} =$ $\dot{m}_{21}\,ex_{21} + \dot{E}x_{D_{P\_I}}$
Pump-2 	$\dot{m}_{23}\,h_{23} + \dot{W}_{P\_II} = \dot{m}_{24}\,h_{24}$	$\dot{m}_{23}\,ex_{23} + \dot{W}_{P_{II}} =$ $\dot{m}_{24}\,ex_{24} + \dot{E}x_{D_{P\_II}}$
HEX-1 	$\dot{m}_{2}\,h_{2} + \dot{m}_{27}\,h_{27} =$ $\dot{m}_{3}\,h_{3} + \dot{m}_{28}\,h_{28} + \dot{Q}_{HEX1}$	$\dot{m}_{2}\,ex_{2} + \dot{m}_{27}\,ex_{27} =$ $\dot{m}_{3}\,ex_{3} + \dot{m}_{28}\,ex_{28}$ $+\dot{Q}_{HEX1}\left(1 - \dfrac{T_{amb}}{T_{HEX1}}\right) + \dot{E}x_{D_{HEX1}}$
HEX-2 	$\dot{m}_{9}\,h_{9} + \dot{m}_{28}\,h_{28} + \dot{m}_{15}\,h_{15}$ $= \dot{m}_{10}\,h_{10} + \dot{m}_{14}\,h_{14}$ $+ \dot{m}_{16}\,h_{16} + \dot{Q}_{HEX2}$	$\dot{m}_{9}\,ex_{9} + \dot{m}_{28}\,ex_{28} + \dot{m}_{15}\,ex_{15}$ $=$ $\dot{m}_{10}\,ex_{10} + \dot{m}_{14}\,ex_{14} +$ $\dot{m}_{16}\,e\dot{x}_{16} + \dot{Q}_{HEX2}\left(1 - \dfrac{T_{amb}}{T_{HEX2}}\right)$ $+ \dot{E}x_{D_{HEX2}}$
HEX-3 	$\dot{m}_{18}\,h_{18} + \dot{m}_{29}\,h_{29} =$ $\dot{m}_{19}\,h_{19} + \dot{m}_{30}\,h_{30} + \dot{Q}_{HEX3}$	$\dot{m}_{18}\,ex_{18} + \dot{m}_{29}\,ex_{29} =$ $\dot{m}_{22}\,ex_{22} + \dot{m}_{30}\,ex_{30}$ $+ \dot{Q}_{HEX3}\left(1 - \dfrac{T_{amb}}{T_{HEX3}}\right)$ $+ \dot{E}x_{D_{HEX3}}$
Condenser-1 	$\dot{m}_{19}\,h_{19} = \dot{m}_{20}\,h_{20} + \dot{Q}_{C1}$	$\dot{m}_{19}\,ex_{19} =$ $\dot{m}_{20}\,ex_{20} + \dot{Q}_{C1}\left(1 - \dfrac{T_{amb}}{T_{C1}}\right)$ $+ \dot{E}x_{D_{C1}}$
Expansion Valve-5 	$\dot{m}_{25}\,h_{25} = \dot{m}_{26}\,h_{26}$	$\dot{m}_{25}\,ex_{25} = \dot{m}_{26}\,ex_{26} +$ $\dot{E}x_{D,EXV5}$

4.3.4. Drying Process

The drying process means that relatively small amounts of water are removed from the solid to reduce the residual liquid content to an acceptable low value. For exergy and energy analysis of drying process in this study, the thermodynamic Dincer and Sahin model was applied [98]. Figure 4.2 shows the drying system with input and output terms.
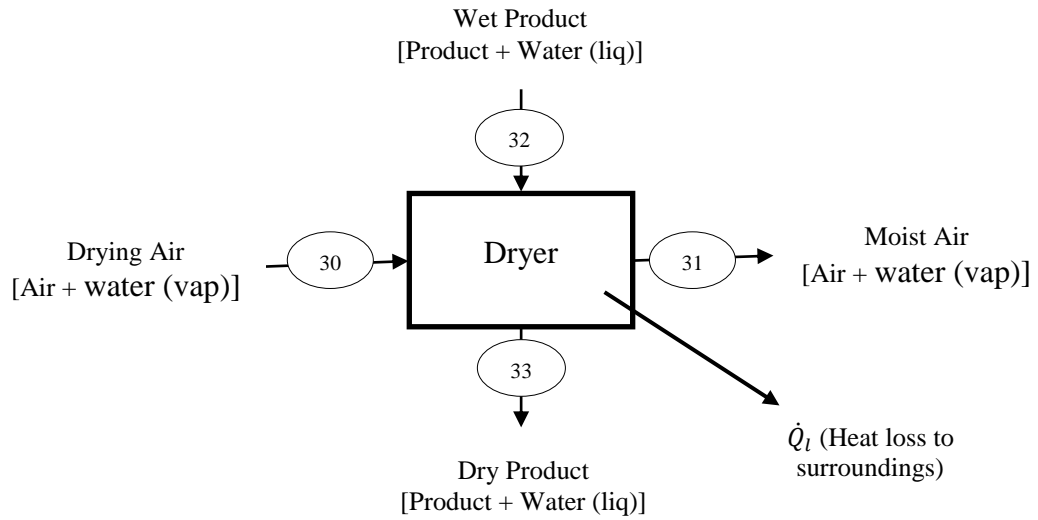
Figure 4.2. Illustration of drying process with input and output terms.

The energy balance equation can be written for the drying system as the following:

$$\dot{m}_{a30} h_{30} + \dot{m}_{p32} h_{p32} + \dot{m}_{w32} h_{w32}$$
$$= \dot{m}_{a31} h_{31} + \dot{m}_{p33} h_{p33} + \dot{m}_{w33} h_{w33} + \dot{Q}_{Drying} \qquad (4.59)$$

Where a represents the air and p represents the product. Similar to an energy balance, the exergy balance equation for the drying system can be written as:

$$\dot{m}_{a30} ex_{30} + \dot{m}_{p32} ex_{p32} + \dot{m}_{w32} ex_{w32} =$$
$$\dot{m}_{a31} ex_{31} + \dot{m}_{p33} ex_{p33} + \dot{m}_{w33} ex_{w33} + \dot{Q}_{Drying} \left(1 - \frac{T_{amb}}{T_{dry}} \right) + \dot{Ex}_{D_{Dryer}} \qquad (4.60)$$

The specific exergy for the moist products can be expressed as:

$$ex_p = \left[h_p(T,P) - h_p(T_0,P_0) \right] - T_0 \left[s_p(T,P) - s_p(T_0,P_0) \right] \tag{4.61}$$

And the specific exergy for water content can be written as:

$$
\begin{aligned}
ex_W = {}& \left[h_f(T) - h_g(T_0) \right] - v_f \left[P - P_g(T) \right] - T_0 \left[s_f(T) - s_g(T_0) \right] \\
& + T_0 R_V \ln \left[\frac{P_g(T_0)}{x_V^0 \, P_0} \right]
\end{aligned}
\tag{4.62}
$$

The specific exergy for state 30 can be expressed as:

$$
\begin{aligned}
ex_{30} = {}& \left[(C_p)_a + \omega_{30}(C_p)_V \right] (T_{30} - T_0) - \\
& T_0 \left\{ \begin{array}{l} \left[(C_p)_a + \omega_{30}(C_p)_V \right] ln\left(\frac{T_{30}}{T_0} \right) \\ -(R_a - \omega_{30}R_V) ln\left(\frac{P_{30}}{P_0} \right) \end{array} \right\} + \\
& T_0 \left\{ \begin{array}{l} (R_a - \omega_{30}R_V) ln\left(\frac{1+1.6078\omega^0}{1+1.6078\omega_{30}} \right) \\ +1.6078\omega_{30}R_a ln\left(\frac{\omega_{30}}{\omega^0} \right) \end{array} \right\}
\end{aligned}
\tag{4.63}
$$

And the specific exergy for state 31 can be expressed as:

$$
\begin{aligned}
ex_{31} = {}& \left[(C_p)_a + \omega_{31}(C_p)_V \right] (T_{31} - T_0) - \\
& T_0 \left\{ \begin{array}{l} \left[(C_p)_a + \omega_{31}(C_p)_V \right] ln\left(\frac{T_{31}}{T_0} \right) \\ -(R_a - \omega_{31}R_V) ln\left(\frac{P_{31}}{P_0} \right) \end{array} \right\} + \\
& T_0 \left\{ \begin{array}{l} (R_a - \omega_{31}R_V) ln\left(\frac{1+1.6078\omega^0}{1+1.6078\omega_{31}} \right) \\ +1.6078\omega_{31}R_a ln\left(\frac{\omega_{31}}{\omega^0} \right) \end{array} \right\}
\end{aligned}
\tag{4.64}
$$

The energy efficiency of the drying process is the ratio of the energy used to evaporate the moisture in the product to the total energy of the drying air supplied to the system and can be expressed as:

$$\eta_{Dryer} = \frac{\dot{Q}_{Drying}}{\dot{m}_{29}\,(h_{30} - h_{29})} \tag{4.65}$$

The exergy efficiency of the drying process can be given as:

$$\psi_{Dryer} = \frac{\dot{Q}_{Drying}\left(1 - \frac{T_{amb}}{T_{dryer}}\right)}{\dot{m}_{29}\left(\dot{ex}_{30} - \dot{ex}_{29}\right)} \tag{4.66}$$

4.3.5. Organic Rankine Cycle (ORC)

The organic Rankine cycle is composed of four major components running with isobutene as the working fluid, where useful heat obtained from the biomass combustor is used to drive this power cycle generating electricity. Table 4.5 shows design and operating parameters for ORC. Table 4.6 shows the thermodynamic balance equations of ORC components.

Table 4.5. ORC assumptions and inputs parameters.

Parameter	Symbol	Value [unit]
mass flow rate	$\dot{m}_{34}$	50 kg/s
Turbine inlet pressure	P_{36}	12500 kPa
Pressure ratio	PR_{ORC}	50
Pump Isentropic efficiency	$\eta_{s,ORC}$	0.85
Turbine Isentropic efficiency	$\eta_{t,ORC}$	0.85

The net power that can be obtained from the cycle is expressed as

$$\dot{W}_{net,ORC} = \dot{W}_{T,ORC} - \dot{W}_{P,ORC} \tag{4.67}$$

Where the power that can be obtained from the cycle is defined as

$$\dot{W}_{T,ORC} = \dot{m}_{36}\,h_{36} - \dot{m}_{37}\,h_{37} \tag{4.68}$$

And the power consumed by pump is expressed as

$$\dot{W}_{P3} = \dot{m}_{35}\,h_{35} - \dot{m}_{34}\,h_{34} \tag{4.69}$$

Table 4.6. Thermodynamic balance equations of ORC components.

Component	Energy Balance Equation	Exergy Balance Equation
HEX-4	$\dot{m}_{10}\, h_{10} + \dot{m}_{35}\, h_{35} =$ $\dot{m}_{11}\, h_{11} + \dot{m}_{36}\, h_{36}$ $+ \dot{Q}_{HEX4}$	$\dot{m}_{10}\, ex_{10} + \dot{m}_{35}\, ex_{35} =$ $\dot{m}_{11}\, ex_{11} + \dot{m}_{36}\, ex_{36}$ $+ \dot{Q}_{HEX4}\left(1 - \dfrac{T_{amb}}{T_{HEX4}}\right) + \dot{Ex}_{D_{HEX4}}$
Turbine	$\dot{m}_{36}\, h_{36} = \dot{m}_{37}\, h_{37} +$ $\dot{W}_{T,ORC}$	$\dot{m}_{36}\, ex_{36} = \dot{m}_{37}\, ex_{37} + \dot{W}_{T,ORC}$ $+ \dot{Ex}_{D_{T,ORC}}$
Condenser-2	$\dot{m}_{37}\, h_{37} = \dot{m}_{34}\, h_{34}$ $+ \dot{Q}_{C2}$	$\dot{m}_{37}\, ex_{37} = \dot{m}_{34}\, ex_{34}$ $+ \dot{Q}_{C2}\left(1 - \dfrac{T_{amb}}{T_{C2}}\right) + \dot{Ex}_{D_{C2}}$
Pump-3	$\dot{m}_{34}\, h_{34} + \dot{W}_{P3}$ $= \dot{m}_{35}\, h_{35}$	$\dot{m}_{34}\, ex_{34} + \dot{W}_{P3} = \dot{m}_{35}\, ex_{35} +$ $\dot{Ex}_{D_{P3}}$

The energy efficiency of isobutene Rankine cycle is defined as:

$$\eta_{ORC} = \frac{\dot{W}_{net,ORC}}{\dot{m}_{10}\,(h_{10} - h_{11})} \qquad (4.70)$$

The exergy efficiency of isobutene Rankine cycle can be expressed as follows:

$$\psi_{ORC} = \frac{\dot{W}_{net,ORC}}{\dot{m}_{10}\,(ex_{10} - ex_{11})} \qquad (4.71)$$

4.3.6. PEM electrolyzer

The electrolyzer's mathematical modelling is significant to estimate the hydrogen production rate using electrolysis, and we have used the equations to investigate the electrolyzer, which are given in some previous studies [99, 100]. When electrolysis is initiated, both heat and electricity are supplied to the electrolyzer for splitting water as Figure 3.1 shows. For PEM electrolyzer, pure water is supplied using the desalinated water, which is provided by the MSF after heating in HEX-6 while the SRC turbines supply the electricity. The typical parameter values used in the PEM electrolyzer analysis are summarized in Table 4.7.

Table 4.7. Input parameters used in modeling of the PEM electrolyzer.

Parameters	Values
P_{H2}, P_{O2}	101.3 kPa
J_a^{ref}	1.7 x 10^5 A/m^2
J_c^{ref}	4.6 x 10^3 A/m^2
$E_{act,a}$	76 kJ/mole
$E_{act,c}$	18 kJ/mole
F	96,486 C/mole
HHV_{H_2}	146.96
λ_a	14
λ_c	10

The output flow rate of produced hydrogen and oxygen from electrolysis reaction can be computed as given below:

$$\dot{N}_{H_2} = \frac{J}{2F} \tag{4.72}$$

$$\dot{N}_{O_2} = \frac{J}{4F} \tag{4.73}$$

Where, F is the Faraday's constant and J is the current density. The PEM electrolyzer voltage can be expressed as follows:

$$V_{total} = V_0 + V_{act,a} + V_{act,c} + V_{ohm} \qquad (4.74)$$

Here, V_0 is the reversible potential, $V_{act,c}$ is the activation overpotential of the cathode, and $V_{act,a}$ is the activation over-potential of the anode. V_{ohm} represents the electrolyte ohmic over-potential and are obtained as:

$$V_0 = 1.229 - 8.5 * 10^{-4}(T_{PEM} - 298) \qquad (4.75)$$

$$V_{act,i} = \frac{RT}{F} sinh^{-1}\left(\frac{J}{2J_{0,i}}\right) \quad i = a, c \qquad (4.76)$$

$$V_{ohm} = JR_{PEM} \qquad (4.77)$$

Where V_{ohm} results from the resistance of the membrane to hydrogen ions traveling through it. The ionic resistance of the membrane depends on its temperature, thickness and the degree of humidification. The local ionic conductivity $\sigma(x)$ of the PEM is determined as:

$$\sigma_{PEM}[\lambda(x)] = (0.5139\lambda(x) - 0.326)exp\left[1268\left(\frac{1}{303} - \frac{1}{T}\right)\right] \qquad (4.78)$$

Where x is the location in the membrane measured from the cathode-membrane interface and $\lambda(x)$ is the water content at point x in the membrane.

$$\lambda(x) = \frac{\lambda_a - \lambda_c}{L} x + \lambda_c \qquad (4.79)$$

Where L is the membrane thickness; λ_a and λ_c are the water content at the anode and the cathode, respectively. Thus the total ohmic resistance can be defined as:

$$R_{PEM} = \int_0^d \frac{dx}{\sigma_{PEM}[\lambda(x)]} \qquad (4.80)$$

The electrode activation overpotential can be expressed by Butler-Volmer equation,

$$J = J_{0,i}\left[exp\left(\frac{\alpha z F V_{act,i}}{RT}\right) - exp\left(\frac{(1-\alpha)z F V_{act,i}}{RT}\right)\right] \qquad i = a, c \qquad (4.81)$$

Where subscripts a and c represent anode and cathode, respectively; α is the symmetrical factor; and z is the number of electrons involved per reaction. For water electrolysis, α and z are found to be 0.5 and 2, respectively. J_0 represents the exchange current density and can be defined as:

$$J_0 = J_i^{ref} exp\left(-\frac{E_{act,i}}{RT}\right) \qquad i = a, c \qquad (4.82)$$

Here, $E_{act,i}$ is the activation energy of the anode and cathode and J_i^{ref} is the pre-exponential factor. The activation overpotential of an electrode can be expressed as:

$$V_{act,i} = \frac{RT}{F}\ln\left[\frac{J}{2J_{0,i}} + \sqrt{\left(\frac{J}{2J_{0,i}}\right)^2 + 1}\right] \qquad i = a, c \qquad (4.83)$$

The energy balance equation of the PEM electrolyzer is;

$$\dot{m}_{49}\,h_{49} + \dot{W}_{PEME} = \dot{m}_{50}\,h_{50} + \dot{m}_{51}\,h_{51} \qquad (4.84)$$

The exergy balance equation of the PEM electrolyzer is;

$$\dot{m}_{49}\,ex_{49} + \dot{W}_{PEME} = \dot{m}_{50}\,ex_{50} + \dot{m}_{51}\,ex_{51} + \dot{Ex}_{D_{PEME}} \qquad (4.85)$$

Finally, the energy and exergy efficiencies of PEM electrolyzer can be determined by considering the higher heating value (HHV) of the hydrogen produced as the useful output [101]:

$$\eta_{PEM} = \frac{HHV_{H_2}/100}{V_{total}} \tag{4.86}$$

For exergy efficiency, the denominator in the energy efficiency does not change since the nominator is to be the standard chemical exergy of H_2, which corresponds to 83% of the HHV of H_2 and hence

$$\psi_{PEM} = 0.83\eta_{PEM} \tag{4.87}$$

4.3.7. Multi-Stage Flash Distillation (MSF)

MSF consists of a series of stages, ranging from 10 to 30 stage. In this thesis the MSF process of 24 stages is adopted. The MSF analysis in this study is based on the equations presented by El-Dessouky and Ettouney [102]. In Table 4.8, the input data for the MSF is given. The overall mass balance equation of MSF is given by:

$$\dot{m}_f = \dot{m}_d + \dot{m}_b \tag{4.88}$$

Where, f is feed, d is distillate b is brine. Total distillate flow rate can be obtained by

$$\dot{m}_d = \dot{m}_f(1 - (1 - y)^n) \tag{4.89}$$

Where y is the specific ratio of sensible heat and latent heat and can be gained by:

$$y = C_p * \Delta T / \lambda_{ave} \tag{4.90}$$

Where C_p is the specific heat capacity and λ_{ave} is the average latent heat calculated at the average temperature.

$$\lambda_{ave} = 2501.897 - 2.4071\,T_{ave} + 1.192X10^{-3}\,T_{ave}{}^2 - 1.586X10^{-5}\,T_{ave}{}^3 \tag{4.91}$$

$$T_{ave} = (T_o + T_n)/2 \tag{4.92}$$

58

The overall salt balance is given by:

$$\dot{m}_f * X_f = \dot{m}_b * X_b \tag{4.93}$$

Where X is the salt concentration in ppm. The temperature drop per stage (ΔT) is obtained from

$$\Delta T = (T_o - T_n)/n \tag{4.94}$$

Where n is the number of stages. Thus, the temperature of the stage (i) is determined by the following equation.

$$T_i = T_o - i\Delta T \qquad\qquad i = 1,2,3, \ldots .. n \tag{4.95}$$

The heating steam flow rate ($\dot{m}_s$) is obtained from

$$\dot{m}_s = \dot{m}_f C_p (T_0 - t_1)/\lambda_s \tag{4.96}$$

Where sea water temperature leaving the condenser of the first stage is defined by:

$$t_1 = T_f + n\,\Delta T \tag{4.97}$$

Also the steam latent heat (λ_s) can be calculated by using equation 4.71 at steam temperature T_s. The performance ratio for the system can be calculated by:

$$PR = \frac{\dot{m}_d}{\dot{m}_s} \tag{4.98}$$

The energy balance equation of the brine heater can be expressed as;

$$\dot{m}_{11} * h_{11} = \dot{m}_{12} h_{12} + \dot{Q}_{in,MSF} \tag{4.99}$$

The overall energy balance equation of the desalination system is;

$$\dot{m}_{41} * h_{41} + \dot{Q}_{in,MSF} = \dot{m}_{44} h_{44} + \dot{m}_{46} h_{46}$$ (4.100)

The overall exergy balance equation of the desalination system is;

$$\dot{m}_{41} * ex_{41} + \dot{Q}_{in,MSF} \left(1 - \frac{T_{amb}}{T_s}\right) = \dot{m}_{44} ex_{44} + \dot{m}_{46} ex_{46}$$ (4.101)

Table 4.8. Input parameters used in thermodynamic modeling of the MSF.

Parameter	Symbol	Value [unit]
Seawater Salinity	X_f	42000 ppm
Number of stages	n	24
Brine exit temperature	T_n	40 °C
Feed flow rate	$\dot{m}_f$	338.5 kg/s
Seawater temperature	T_f	25 °C
Heat capacity of liquid streams	C_p	4.18 kJ/kg °C

The energy efficiency of MSF is defined as:

$$\eta_{MSF} = \frac{\dot{m}_{46} h_{46}}{\dot{m}_{11} (h_{11} - h_{12})}$$ (4.102)

The exergy efficiency of MSF can be expressed as follows:
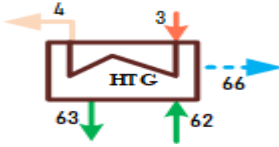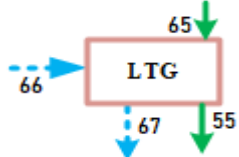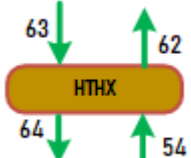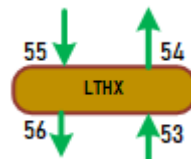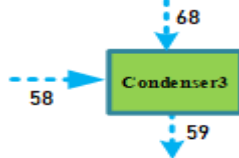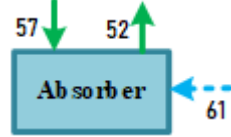
$$\psi_{MSF} = \frac{\dot{m}_{46} \dot{ex}_{46}}{\dot{m}_{11} (\dot{ex}_{11} - \dot{ex}_{12})}$$ (4.103)

4.3.8. Double-Effect Absorption Cycle (DEAC)

This subsystem contains of two generators, namely: high-temperature generator (HTG) and low-temperature generator (LTG), two heat exchangers: high temperature heat exchanger (HTHX) and low temperature heat exchanger (LTHX), a pump (P4), a condenser, an evaporator, an absorber and four expansion valves. LiBr is used as an

absorbent and H$_2$O is used as a refrigerant. Energy balances for components of DEAC subsystem can be illustrated in Table 4.9.

Table 4.9. Thermodynamic balance equations of DEAC components.

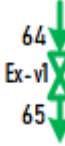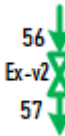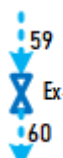| Component	Energy Balance Equation	Exergy Balance Equation
Pump-4	$\dot{m}_{52}\, h_{52} + \dot{W}_{P4} = \dot{m}_{53}\, h_{53}$	$\dot{m}_{52}\, ex_{52} + \dot{W}_{P4} = \dot{m}_{53}\, ex_{53} + \dot{E}x_{D_{P4}}$
HTG	$\dot{m}_3\, h_3 + \dot{m}_{62}\, h_{62} = \dot{m}_4\, h_4 + \dot{m}_{63}\, h_{63} + \dot{m}_{66}\, h_{66} + \dot{Q}_{HTG}$	$\dot{m}_3\, ex_3 + \dot{m}_{62}\, ex_{62} = \dot{m}_4\, ex_4 + \dot{m}_{63}\, ex_{63} + \dot{m}_{66}\, ex_{66} + \dot{Q}_{HTG}\left(1 - \dfrac{T_{amb}}{T_{HTG}}\right) + \dot{E}x_{HTG}$
LTG	$\dot{m}_{65}\, h_{65} + \dot{m}_{66}\, h_{66} = \dot{m}_{55}\, h_{55} + \dot{m}_{58}\, h_{58} + \dot{m}_{67}\, h_{67} + \dot{Q}_{LTG}$	$\dot{m}_{65}\, ex_{65} + \dot{m}_{66}\, ex_{66} = \dot{m}_{55}\, ex_{55} + \dot{m}_{58}\, ex_{58} + \dot{m}_{67}\, ex_{67} + \dot{E}x_{LTG}$
HTHX	$\dot{m}_{54}\, h_{54} + \dot{m}_{63}\, h_{63} = \dot{m}_{62}\, h_{62} + \dot{m}_{64}\, h_{64} + \dot{Q}_{HTHEX}$	$\dot{m}_{54}\, ex_{54} + \dot{m}_{63}\, ex_{63} = \dot{m}_{62}\, ex_{62} + \dot{m}_{64}\, ex_{64} + \dot{Q}_{HTHEX}\left(1 - \dfrac{T_{amb}}{T_{HTHEX}}\right) + \dot{E}x_{D_{HTHEX}}$
LTHX	$\dot{m}_{53}\, h_{53} + \dot{m}_{55}\, h_{55} = \dot{m}_{54}\, h_{54} + \dot{m}_{56}\, h_{56} + \dot{Q}_{LTHEX}$	$\dot{m}_{53}\, ex_{53} + \dot{m}_{55}\, ex_{55} = \dot{m}_{54}\, ex_{54} + \dot{m}_{56}\, ex_{56} + \dot{Q}_{LTHEX}\left(1 - \dfrac{T_{amb}}{T_{LTHEX}}\right) + \dot{E}x_{D_{LTHEX}}$
Condenser-3	$\dot{m}_{58}\, h_{58} + \dot{m}_{68}\, h_{68} = \dot{m}_{59}\, h_{59} + \dot{Q}_{C3}$	$\dot{m}_{58}\, ex_{58} + \dot{m}_{68}\, ex_{68} = \dot{m}_{59}\, ex_{59} + \dot{Q}_{C3}\left(1 - \dfrac{T_{amb}}{T_{C3}}\right) + \dot{E}x_{D_{C3}}$
Absorber	$\dot{m}_{52}\, h_{52} + \dot{m}_{61}\, h_{61} = \dot{m}_{57}\, h_{57} + \dot{Q}_{abs}$	$\dot{m}_{52}\, ex_{52} + \dot{m}_{61}\, ex_{61} = \dot{m}_{57}\, ex_{57} + \dot{Q}_{abs}\left(1 - \dfrac{T_{amb}}{T_{abs}}\right) + \dot{E}x_{D_{abs}}$

Component	Energy Balance	Exergy Balance
Evaporator 60 Q_{Eva} Evaporator 61	$\dot{m}_{60}\,h_{60} + \dot{Q}_{eva}$ $= \dot{m}_{61}\,h_{61}$	$\dot{m}_{60}\,ex_{60} + \dot{Q}_{eva}\left(1 - \dfrac{T_{amb}}{T_{eva}}\right)$ $= \dot{m}_{61}\,ex_{61}$ $+ \dot{E}x_{D_{eva}}$
Expansion Valve-1 64 Ex-v1 65	$\dot{m}_{64}\,h_{64} = \dot{m}_{65}\,h_{65}$	$\dot{m}_{64}\,ex_{64} = \dot{m}_{65}\,ex_{65} + \dot{E}x_{D,EXV1}$
Expansion Valve-2 56 Ex-v2 57	$\dot{m}_{56}\,h_{56} = \dot{m}_{57}\,h_{57}$	$\dot{m}_{56}\,ex_{56} = \dot{m}_{57}\,ex_{57} + \dot{E}x_{D,EXV2}$
Expansion Valve-3 67 Ex-v3 68	$\dot{m}_{67}\,h_{67} = \dot{m}_{68}\,h_{68}$	$\dot{m}_{67}\,ex_{67} = \dot{m}_{68}\,ex_{68} + \dot{E}x_{D,EXV3}$
Expansion Valve-4 59 Ex-v4 60	$\dot{m}_{59}\,h_{59} = \dot{m}_{60}\,h_{60}$	$\dot{m}_{59}\,ex_{59} = \dot{m}_{60}\,ex_{60} + \dot{E}x_{D,EXV4}$

The coefficient of performance for a DEAC is defined as the ratio of the cooling load provided by the chiller to the heat received by the HTG as:

$$COP_{DEAC} = \frac{\dot{Q}_{eva}}{\dot{m}_3\,(h_3 - h_4)} \tag{4.104}$$

The exergy coefficient of performance is the most common performance parameter of an absorption system and can be expressed as:

$$\psi_{DEAC} = \frac{\dot{Q}_{eva}\left(1 - \dfrac{T_{amb}}{T_{61}}\right)}{\dot{m}_3\,(ex_3 - ex_4)} \tag{4.105}$$

4.3.9. Overall System Efficiency

The energy efficiency is defined as the ratio of useful outputs that are obtained by the system (power, hydrogen, cooling, drying, fresh water, heating and/or hot water) to the energy input of the system. Therefore, energy efficiency of the multigeneration system is calculated thus:

$$\eta_{Overall} = \frac{\dot{W}_{Net} + \dot{Q}_{eva} + \dot{Q}_{Drying} + \dot{m}_{46}\, h_{46} + \dot{m}_{49}\, h_{49} + \dot{Q}_{heating}}{Q_{sol} + \dot{Q}_{Biomass}} \qquad (4.106)$$

The exergy efficiency of the system is the best performance indicator that takes into account the useful output and it is determined according to the following equation:

$$\psi_{Overall}$$
$$= \frac{\dot{W}_{Net} + \dot{EX}_{cooling} + \dot{EX}_{Drying} + \dot{m}_{46}\, \dot{ex}_{46} + \dot{m}_{50}\, \dot{ex}_{50} + \dot{m}_{38}\,(\dot{ex}_{39} - \dot{ex}_{38}) + \dot{m}_{69}\,(\dot{ex}_{70} - \dot{ex}_{69})}{\dot{Ex}_{sol,in} + \dot{EX}_{Biomass}}$$

$$(4.107)$$

Where;

$$\dot{W}_{Net} = \dot{W}_{T,Net} - \dot{W}_{P,Net} \qquad (4.108)$$

$$\dot{EX}_{cooling} = \dot{Q}_{eva}\left(1 - \frac{T_{amb}}{T_{61}}\right) \qquad (4.109)$$

$$\dot{EX}_{Drying} = \dot{Q}_{Drying}\left(1 - \frac{T_{amb}}{T_{dry}}\right) \qquad (4.110)$$

4.3.10. Environmental Impact Assessment (EIA)

The real advantages of multi-generation systems can only be considered positive if they also play a positive role in environmental impact. Therefore, the environmental impact of such multi-generation systems needs to be considered more comprehensively than the existing individual systems. Only after a comprehensive EIA can a fair decision be made about the sustainability and feasibility of any of these multi-generational systems. The main evaluation standard at this early stage is the

reduction of the environmental impact by decreasing carbon dioxide (CO_2) emissions ratio per energy unit produced by the system. For this purpose, the CO_2 emission of the whole system is calculated and compared with cases where the system was not multigeneration. In the first case, both the ORC and the SRC are used to generate electricity. In the second one, electricity and cooling load are considered at the same time. In the third case, trigeneration system is considered and, in the last, the whole system for multiple products is considered. The formulas for above cases can be expressed as follows:

$$\varepsilon_A = \frac{\dot{m}_{CO2}}{\dot{W}_{Net}} \tag{4.111}$$

$$\varepsilon_B = \frac{\dot{m}_{CO2}}{\dot{W}_{Net} + \dot{Q}_{eva}} \tag{4.112}$$

$$\varepsilon_C = \frac{\dot{m}_{CO2}}{\dot{W}_{Net} + \dot{Q}_{eva} + \dot{Q}_{heating}} \tag{4.113}$$

$$\varepsilon_D = \frac{\dot{m}_{CO2}}{\dot{W}_{Net} + \dot{Q}_{eva} + \dot{Q}_{Drying} + \dot{m}_{46} h_{46} + \dot{m}_{49} h_{49} + \dot{Q}_{heating}} \tag{4.116}$$

Where, $\dot{m}_{CO2} = \dot{m}_9 \, x_{CO2}$ \hfill (4.117)

It is important to use non-renewable sources more efficiently to reduce environmental damage and to improve environmental sustainability. Thus, society has the ability to limit the use of limited resources. The environmental sustainability index (ESI) is a measure of overall progress towards environmental sustainability. The index is used to link exergy to environmental impact and is considered as a measure of how the exergy efficiency affects sustainable development. It can be calculated by the following equation:

$$ESI = \frac{1}{1 - \psi} \tag{4.118}$$

CHAPTER 5

RESULTS AND DISCUSSION

5.1.   INTRODUCTION

The performances of multiple production systems depend on their design; therefore, increasing system efficiency by choosing different designs is as important as using latest technologies in the researches. The current multi-generation system is practical and feasible, because it uses modern technologies and existing systems. In this thesis, a novel multi-generation system, which uses biomass and solar energy are developed and analyzed. The current chapter describes the numerical analysis of examined system using the mathematical models, which are presented in the previous chapter. The results of thermodynamic modeling, energy, exergy and EIA are explained. The analyses were performed using the EES software under steady-state conditions. Besides analyzing and assessing the overall system according to several criteria, a comparative study was conducted to analyze two different nanofluids as absorption fluids in the solar cycle for evaluating their effects on the overall performance. The exergy destruction value for each subsystem are determined, checked the possible improvements, and studied the effect of significant parameters. The examined system produces hydrogen, electricity, drying effect, fresh and hot water, and cooling/heating.

5.2. SYSTEM MAIN RESULTS

For thermodynamic modeling of the system, the following conditions are considered: Ambient temperature 25 °C, ambient pressure 101.3 kPa, ORC and SRC turbine inlet pressure 12500 kPa, and Isobutane is the working fluid in the ORC while Ethylene glycol (EG) is the base fluid in solar cycle.

The solar direct normal irradiation intensity (G_t) is 0.96 kW/m^2, which is the monthly average daily maximum irradiation during the summer season that was obtained during an experimental work at the University of Karabuk. The mass flowrate, pressure, enthalpy, temperature, exergy, and entropy for all states in the multigeneration system were calculated and presented in Table 5.1.

Table 5.2 presents the key results of the thermodynamic evaluation for our proposed system. From the results, it can be seen that the mass flow rate inside the CPC is 0.01429 kg/sec and the outlet temperature is up to 170 °C. The net electricity generated by the system is about 14.85 MW, PEM electrolyzer needs 2.6 MW of electricity to produce about 44.77 kg/h of hydrogen. MSF system produces fresh water at a rate of 37.93 kg/s from 338.5 kg/s of sea water fed into it. The streams properties in desalination stages are listed in Table 5.3. Steam bleeds from the LPT of the SRC at 115°C to provide 0.568 MW of energy used during moisture removal of the product.

The CPC energy efficiency is 51.31% whereas the exergy efficiency is 14.76%. The energy and exergy COP's of the DEAC are 0.9922 and 24.27%, respectively. The energy efficiencies of the SRC and the ORC are 39.91% and 29.45%, respectively. Also, the exergy efficiencies of the SRC and the ORC are 78.96% and 40.2%, respectively. The multigeneration system has 34.72% and 20.73% energetic and exergetic efficiency, respectively. For a better understanding of system performance, the exergy efficiency and energy efficiency of each sub-system and for overall system are shown in Figure 5.1.

Table 5.1. Thermodynamic properties at each stage of the proposed system under basic design conditions.

St.	$\dot{m}$ (kg/s)	T (°C)	P (kPa)	h (kJ/kg)	ex (kJ/kg)	St.	$\dot{m}$ (kg/s)	T (°C)	P (kPa)	h (kJ/kg)	ex (kJ/kg)
0	-	25	101.3	104.8	-	37	50	114.9	500	760.8	86.44
1	0.01429	170	10000	485.2	0.8821	38	50	25	101.3	104.8	0
2	0.01429	170	10000	485.2	85.05	39	50	81.11	101.3	339.6	19.77
3	0.01429	155	2000	432.4	63.4	40	338.5	25	101.3	98.71	0
4	0.01429	95.02	2000	261.9	20.52	41	338.5	25	212.5	98.71	0
5	0.01429	95.02	2000	261.9	20.52	42	338.5	91	152.5	361.7	25.39
6	0.01429	100	10000	282.9	5.243	43	338.5	106	150	421.5	37.18
7	7.5	25	101.3	14299	17523	44	300.6	40	7.232	157	1.934

8	17.5	25	101.3	237.2	4729	45	300.6	40	108.5	157	1.934
9	25	625	1000	3599	1501	46	37.94	38	7.232	159.1	1.058
10	25	393.1	1000	3361	831	47	37.83	38.01	101.3	159.2	1.153
11	25	219.4	1000	1076	226.8	48	0.1119	38.01	101.3	159.2	1.153
12	25	154.2	1000	692.5	87.3	49	0.1119	78.06	101.3	352	67.65
13	25	150.9	1000	691	85.1	52	12.5	30	0.8136	68.32	12.7
14	10	530	12500	3423	1471	53	12.5	30	130.2	68.4	12.78
15	10	395.4	5000	3184	1213	54	12.5	53.29	130.2	116.8	15.19
16	10	530	5000	3504	1403	55	11.1	85.02	7.381	203.9	61.65
17	0.9583	247.4	500	2955	795.9	56	11.1	57.51	7.381	150.7	54.51
18	0.7826	115	100	2706	493.4	57	11.1	43.14	0.8136	150.7	54.51
19	8.259	45.82	10	2428	149.8	58	0.6536	77.51	7.381	2645	125.1
20	8.259	45.82	10	191.8	2.856	59	1.398	40	7.381	167.5	1.464
21	8.259	45.82	100	191.9	2.948	60	1.398	4	0.8136	167.5	-8.23
22	0.7826	69.99	100	2525	2245	61	1.398	4	0.8136	2508	-184.3
23	10	99.63	100	417.5	33.8	62	12.5	101.6	130.2	220.8	31.11
24	10	100.2	5000	423.5	39.09	63	11.76	155	130.2	339.1	77.29
25	0.9583	151.9	500	640.4	90.3	64	11.76	104.2	130.2	231.4	48.93
26	0.9583	99.63	100	640.4	78.51	65	11.76	104.2	7.381	231.4	48.93
27	10	152.4	5000	645.3	95.21	66	0.7448	155	130.2	2784	550.2
28	10	161.2	5000	683.4	106.9	67	0.7448	107.2	130.2	449.4	40.48
34	50	37.74	500	291.3	50.8	68	0.7448	40	7.381	449.4	15.1
35	50	45.62	12500	317.3	73.15	69	50	25	101.3	104.8	0
36	50	235.4	12500	888.5	231.6	70	50	42.16	101.3	289.5	12.55

Table 5.2. Thermodynamic assessment results for the multi-generation system.

Description	Value	Description	value
Outlet temperature of the CPC (°C)	170	Energy efficiency of PEM (%)	67.94
Mass flow rate inside the CPC (kg/s)	0.014	Exergy efficiency of PEM (%)	56.39
ORC Turbine (MW)	6.38	Energy efficiency of CPC (%)	51.3
HP Turbine (MW)	2.388	Exergy efficiency of CPC (%)	14.76
LP Turbine (MW)	10.04	Energy efficiency of Dryer (%)	79.85
PEM electrical requirement (MW)	2.6	Exergy efficiency of Dryer (%)	43.09
Net power production (MW)	14.85	Energy efficiency of MSF (%)	38.72
Energy efficiency of ORC (%)	29.45	Exergy efficiency of MSF (%)	8.233
Exergy efficiency of ORC (%)	40.2	Overall energy efficiency (%)	34.72

COP $_{DEAC}$	0.992	Overall exergy efficiency (%)	20.73
Exergy efficiency of DEAC (%)	24.77	Cooling rate of DEAC (MW)	3.273
Energy efficiency of SRC (%)	39.91	Drying heat (MW)	0.568
Exergy efficiency of SRC (%)	78.96	Heating load (MW)	20.97
Fresh water production rate (kg/s)	37.93	CO_2 emissions (kg/MWh)	364.5
Hydrogen production rate (kg/h)	44.77	Sustainability index	1.262

Table 5.3. The flows properties in the MSF distillation stages.

Stages	T_f °C	T_b °C	T_d °C	P_f kPa	P_b kPa	P_d kPa	h_f kJ/kg	h_b kJ/kg	h_d kJ/kg	$\dot{m}_f$	$\dot{m}_b$	$\dot{m}_d$	X_f
0		106		150				372.6					42000
1	90.98	103.2	103.2	152.5	113.7	113.7	361.5	361.5	2681	338.5	336.8	1.672	42208
2	88.23	100.5	100.5	155	103.2	103.2	350.4	350.4	2677	338.5	335.2	3.336	42418
3	85.48	97.73	97.73	157.5	93.5	93.5	339.4	339.4	2672	338.5	333.5	4.992	42629
4	82.73	94.98	94.98	160	84.6	84.6	328.3	328.3	2668	338.5	331.9	6.639	42840
5	79.98	92.23	92.23	162.5	76.42	76.42	317.2	317.2	2663	338.5	330.2	8.278	43053
6	77.23	89.49	89.49	165	68.91	68.91	306.2	306.2	2659	338.5	328.6	9.909	43267
7	74.49	86.74	86.74	167.5	62.02	62.02	295.1	295.1	2654	338.5	327	11.53	43481
8	71.74	83.99	83.99	170	55.71	55.71	284.1	284.1	2650	338.5	325.4	13.15	43697
9	68.99	81.24	81.24	172.5	49.95	49.95	273.1	273.1	2645	338.5	323.7	14.75	43914
10	66.24	78.49	78.49	175	44.69	44.69	262	262	2641	338.5	322.1	16.35	44132
11	63.49	75.74	75.74	177.5	39.9	39.9	251	251	2636	338.5	320.6	17.95	44351
12	60.74	72.99	72.99	180	35.54	35.54	240	240	2631	338.5	319	19.53	44571
13	57.99	70.24	70.24	182.5	31.58	31.58	229	229	2627	338.5	317.4	21.1	44793
14	55.24	67.49	67.49	185	27.99	27.99	218	218	2622	338.5	315.8	22.67	45015
15	52.49	64.74	64.74	187.5	24.75	24.75	207	207	2617	338.5	314.3	24.23	45239
16	49.74	61.99	61.99	190	21.82	21.82	196	196	2612	338.5	312.7	25.78	45463
17	46.99	59.24	59.24	192.5	19.18	19.18	185.1	185.1	2607	338.5	311.2	27.33	45689
18	44.24	56.5	56.5	195	16.81	16.81	174.1	174.1	2602	338.5	309.6	28.87	45916
19	41.5	53.75	53.75	197.5	14.69	14.69	163.2	163.2	2597	338.5	308.1	30.4	46144
20	38.75	51	51	200	12.79	12.79	152.3	152.3	2592	338.5	306.6	31.92	46373
21	36	48.25	48.25	202.5	11.12	11.12	141.3	141.3	2587	338.5	305.1	33.43	46603
22	33.25	45.5	45.5	205	9.638	9.638	130.4	130.4	2582	338.5	303.6	34.94	46834
23	30.5	42.75	42.75	207.5	8.346	8.346	119.6	119.6	2578	338.5	302.1	36.44	47067
24	27.75	40	40	210	7.232	7.232	108.7	108.7	2573	338.5	300.6	37.93	47300
25	25			212.5			97.8						

5.3. NANOFLUID EFFECT ON SYSTEM PERFORMANCE

As shown in table 5.4, comparisons are made between the use of two types of nanofluids and pure thermal oil as working fluids for the solar cycle, including graphene, silver and EG base fluid. It becomes clear that existence of nanoparticles in an absorption fluid positively affects the solar system in particular and the integrated system in general. The outlet temperature and mass flow rate increase within the CPC receiver tube because nanoparticles are added to the base fluid. The output temperature increased from 170 °C with EG to 197.6 °C with graphene-EG. Likewise, the mass flow and the convective heat transfer coefficient inside the solar collector increased using nanofluids. Both energy and exergy efficiencies were tested for a multigeneration system using different working fluids of the solar system, respectively, which were 34.72% and 20.73% with EG, 35.6% and 21.15% with graphene-EG, and with silver-EG were 35% and 20.86%.
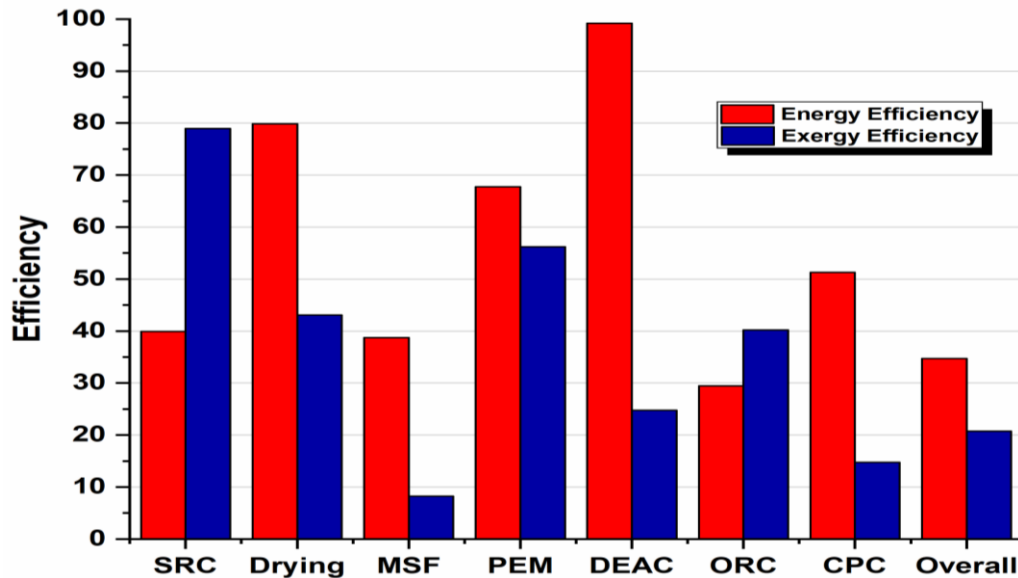

Figure 5.1. Bar chart for energy and exergy efficiencies of individual cycles.

It is clear that the effect of nanofluids is more pronounced on the solar cycle than on the entire system and that some of the cycles results do not change at all when the absorbing fluid used in the solar cycle is changed due to the fact that solar energy is not the only source of energy in our proposed system. In general, the results indicated that the system performance improved with nanoparticles and the effect of graphene

69

nanoparticles was better than that of the silver nanoparticles. This result is obtained because graphene-based nanofluid shows the highest thermal conductivity and relatively high specific heat, while silver shows the highest value of density.

Table 5.4. Thermodynamic assessment results of the multi-generation system with different heat transfer fluids in CPC.

Description	EG	Silver-EG	Graphene-EG
Outlet temperature of the CPC (°C)	170	178.3	197.2
Mass flow rate inside the CPC (kg/s)	0.0143	0.0932	0.0237
Convective heat transfer coefficient (W/m^2.K)	60.04	468.6	248.9
Net power production (MW)	14.85	14.95	15.14
Cooling rate of DEAC (MW)	3.27	3.51	4.04
Hot water production rate (MW)	20.97	21	21.07
Energy efficiency of Overall system (%)	34.72	35.02	35.7
Exergy efficiency of Overall system (%)	20.73	20.86	21.15

5.4. EXERGY ANALYSES RESULTS

The exergy destruction value and its percentage for each sub-system in the proposed system under basic operating conditions are shown in Figure 5.2. It is consider as an indication of whether the system is properly functioning or not. In other words, detection and reduction of the high exergy destruction source can improve the system performance. The greatest exergy destruction rate occurs in the SRC at approximately 15.5 MW (49.4%), which is followed by the ORC at more than 9 MW (29.3%). In contrast, the other subsystems have less values of exergy destruction. The MSF destroys 2.7 MW of exergy (8.66%), the DEAC destroys 2.48 MW of exergy (about 8%), the PEM destroys 1.13 MW of exergy (3.6%) and the dryer destroys 0.16 MW of exergy (0.5%). The main reason for this considerable exergy destruction is the large temperature difference in these subsystems components, especially in the SRC components as shown in Figure 5.3. Therefore, the SRC is deemed to be the most important cycle that requires careful design and selection. In addition, the results show that DEAC does not show considerable exergy destruction, in part because it does not use direct fuel energy, but rather steam produced by HTG.
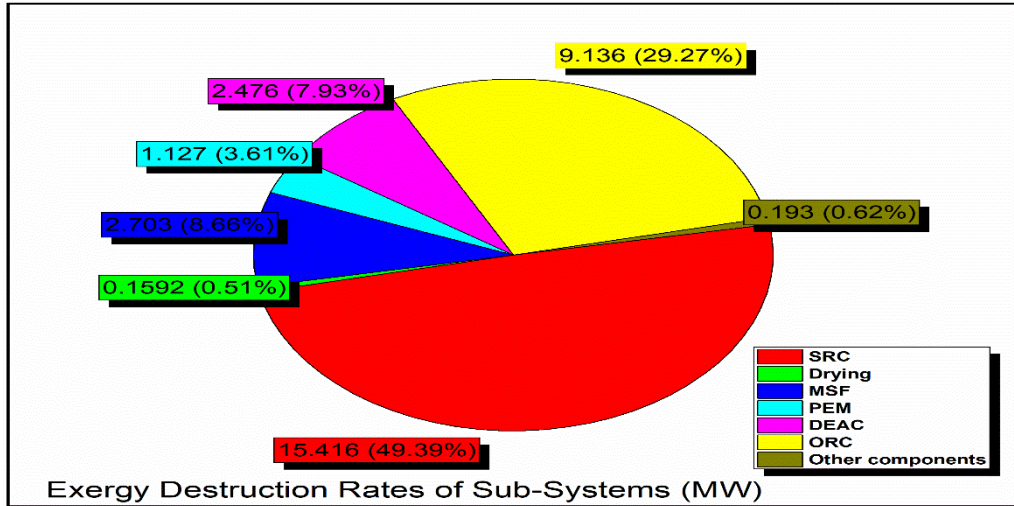
70

Figure 5.2. Exergy destruction pie diagram in the various subsystems of the system.

For further explanation, the exergy destruction of the main components of the subsystems is calculated as shown in Figure 5.3. This measurement is useful for prioritizing exergy losses in an intuitive manner. High pressure turbine in the SRC exhibits the largest exergy destruction at approximately 12 MW of exergy (40.65%), which is followed by the fourth heat exchanger at more than 5 MW (17.9%), while the ORC condenser and MSF cycle destroy equal exergy about 2.7 MW (9%). In contrast, the other components have lower destruction of exergy. The main reason for considerable exergy destruction in the SRC high pressure turbine is due to the temperature difference and pressure drop across the component. Therefore, it may be worthwhile to focus improvement efforts on this device.
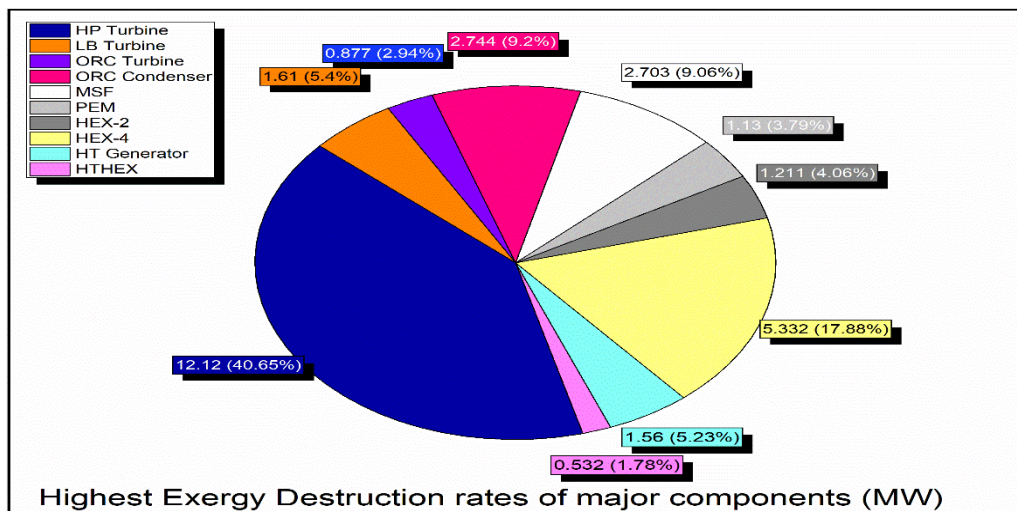

Figure 5.3. Exergy destruction rates of the major components of the system.

71

5.5. PARAMETRIC STUDY

To investigate the possibility of improving the system, the effects of certain variables on system performance were studied. The variation of solar irradiation, outlet temperature of biomass combustor, ambient temperature and nanoparticle volume concentration are considered as the key variables in the system performance to be examined.

5.5.1. Effect of Nanoparticles' Volume Concentration

The thermal properties of the studied nanofluids are shown in Figures 5.4 to 5.7. In these figures, the effect of nanoparticle volume concentration on: specific heat capacity (Figure 5.4), thermal conductivity (Figure 5.5), density (Figure 5.6) and dynamic viscosity (Figure 5.7) of nanofluid are illustrated. It is important to note that these thermal properties are given for the mean temperature ($T_{m,nf}$), which was obtained by equation (4.38).

It is obvious that increasing the concentration of nanoparticles increases the thermal conductivity, density and dynamic viscosity of the nanofluid, while its specific heat capacity decreases. This trend of specific heat capacity is due to the fact that the specific heat capacity of the base fluid (EG) is higher than that of the nanoparticles and vice versa for other thermal properties. It can also be observed that a graphene based nanofluid has the highest specific heat capacity and thermal conductivity while a silver has the highest density. Moreover, the dynamic viscosity is the same for both nanofluids.

It is important to note that nanofluids have higher thermal conductivity than pure thermal oil ($\varphi = 0\%$). This observation shows that the use of metallic nanoparticles within the base fluid increases the thermal conductivity and therefore increases the rate of heat transfer in the flow.
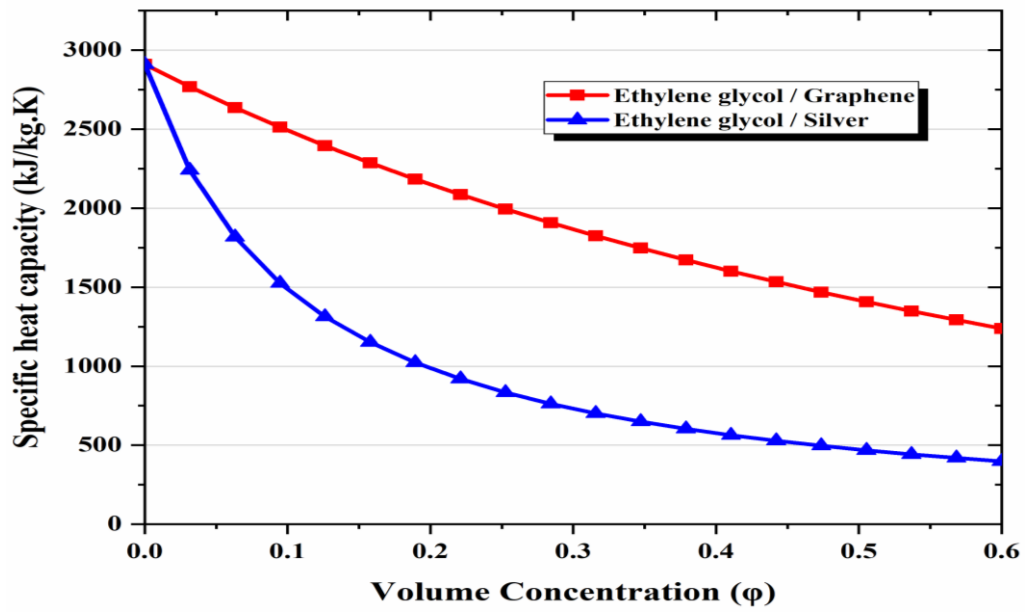
Figure 5.4. Effect of nanoparticle volume concentration on the specific heat capacity of nanofluids.
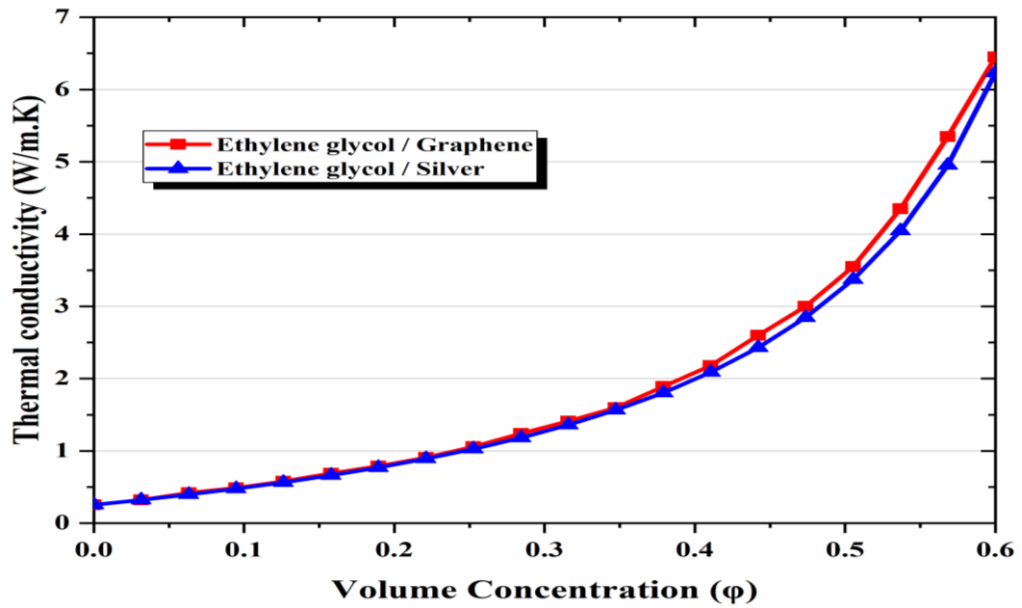

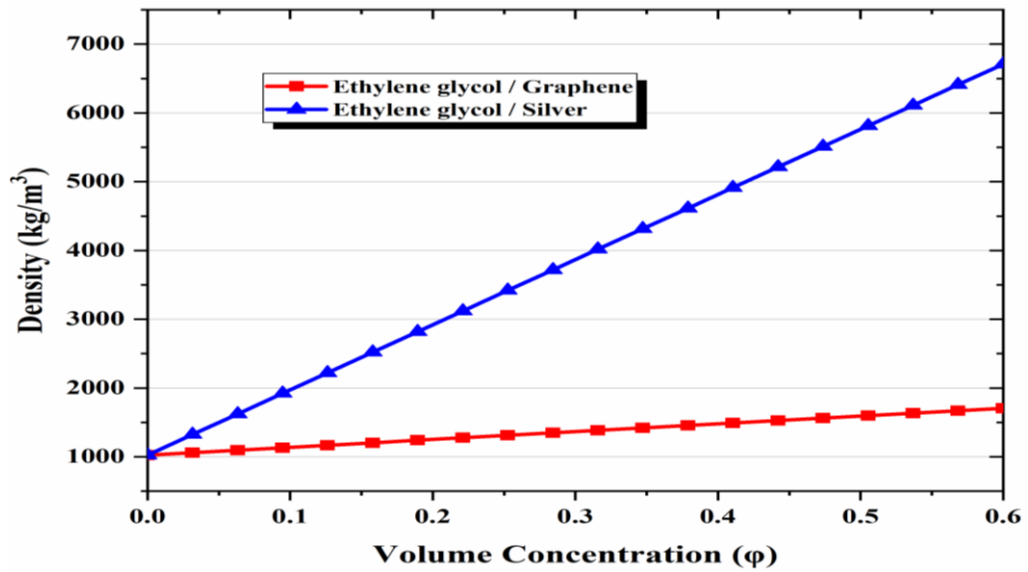Figure 5.5. Effect of nanoparticle volume concentration on the thermal conductivity of nanofluids.

Figure 5.6. Effect of nanoparticle volume concentration on the density of nanofluids.
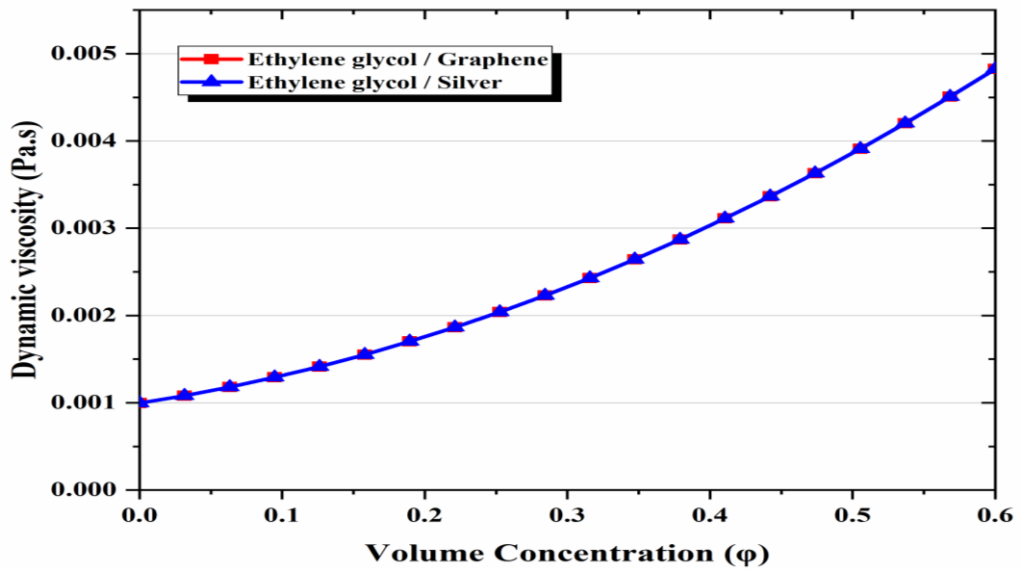

Figure 5.7. Effect of nanoparticle concentration on dynamic viscosity of nanofluids.

Subsequent to determining the results of the multi-generation system for basic operating parameters, we investigated the effect of using two nanofluid types (Graphene-EG, Silver-EG) on the overall system. The volume fraction ranged between 0% and 6%. Zero concentration means using base fluid. Figures 5.8, 5.9, 5.10 and 5.11 show curves, which exhibit similarities and they can be analyzed in comparison with each other. These figures indicate the collector outlet temperature, overall cooling load, overall heating load, net power production, overall energy efficiency and overall

exergy efficiency. It should be noted that in all cases, nanofluids improve all the indicators, and increase in their concentration also increases the values of indicators. Moreover, it is important to state that graphene-EG is the best nanofluid, and increase with it is significantly larger as compared to silver-EG, which shows relatively little improvement. This result is obtained because Graphene-based nanofluid shows the highest thermal conductivity and relatively high specific heat, while Silver shows the highest value of density.
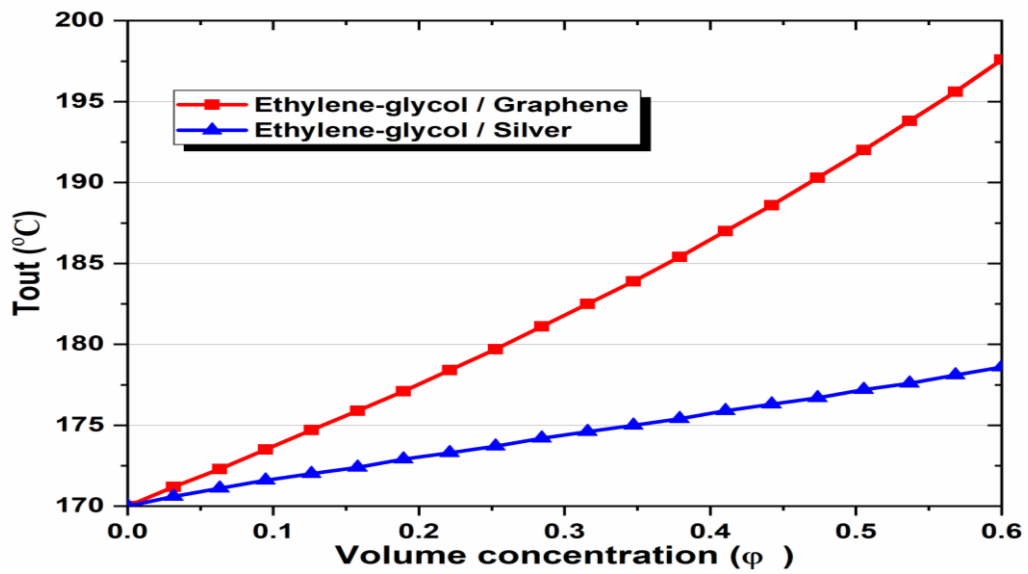

Figure 5.8. Effects of nanoparticle concentration on the outlet temperature of CPC.
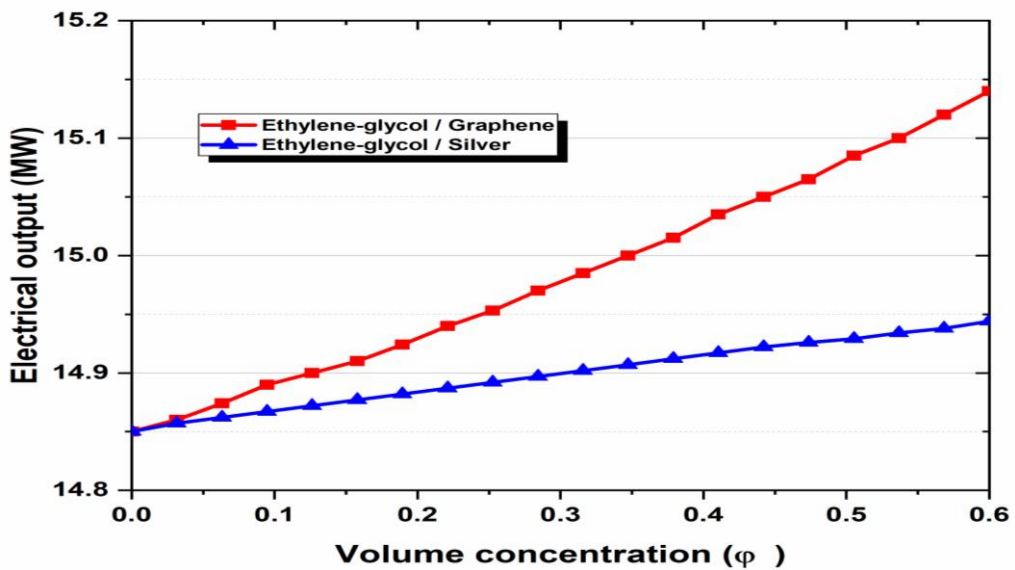

Figure 5.9. Effects of nanoparticle volume concentration on the net power generation.
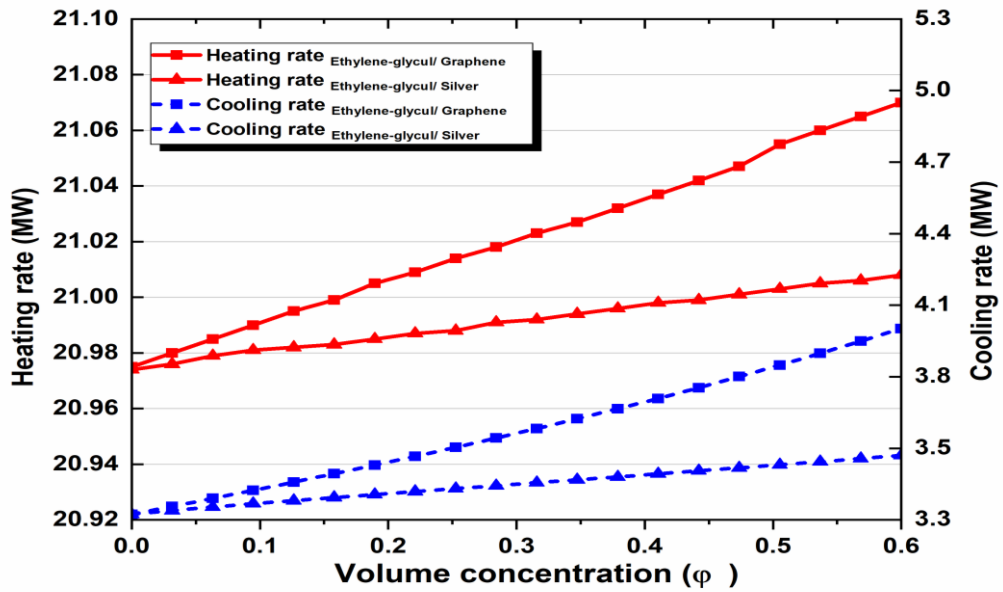
Figure 5.10. Effects of nanoparticle volume concentration on heating and cooling loads.
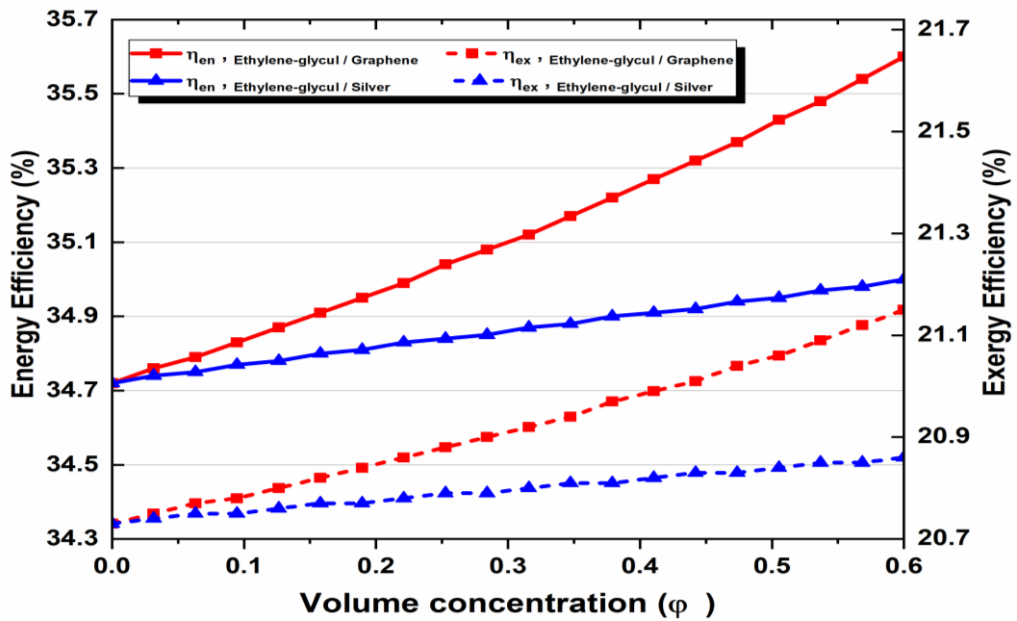

Figure 5.11. Effects of nanoparticle concentration on overall energy efficiency and overall exergy efficiency.

5.5.2. Effect of Solar Irradiation

Solar irradiation is one of the main energy sources of the proposed system and has a significant impact on its performance. Solar radiation varies greatly from region to

region and can vary throughout the day depending on the region's climate. Therefore, the crucial parameter when considering energy systems based on solar is the solar irradiation availability.
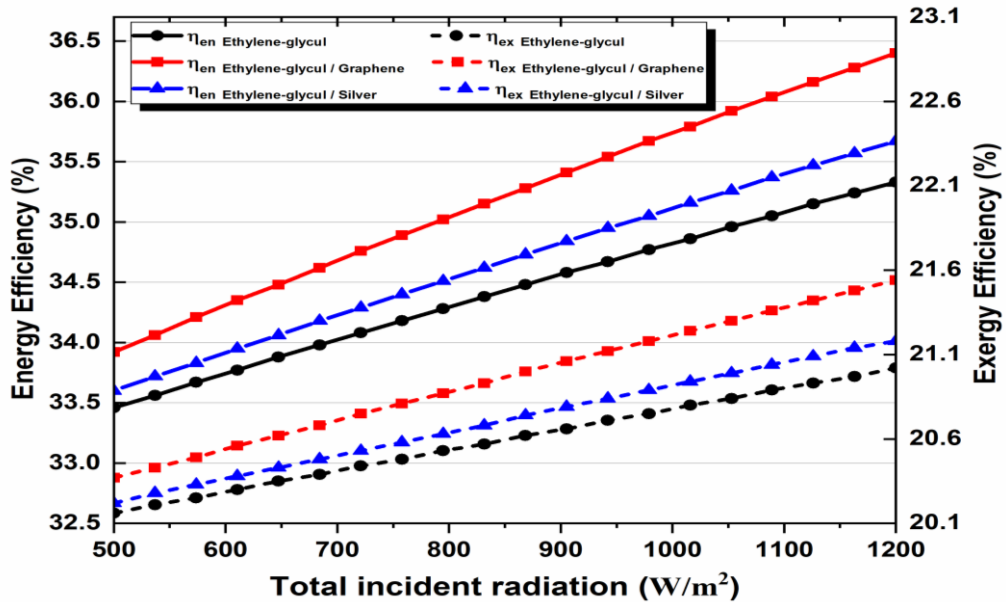

Figure 5.12. Effect of solar irradiation on the overall energy and exergy efficiencies.

Figure 5.12 shows a comparison between pure thermal oil and two different types of nanofluids, which shows the effect of the total incident radiation on a multi-generation system's exergy and energy efficiencies. It is obvious that both system efficiencies increase when solar radiation rises from 500 to 1200 W/m². We expected spike in overall efficiencies because higher solar irradiation results in greater heat transmission to the selected working fluid, which also increases temperature transfer to the subsystems; therefore, it results in higher system performance. Moreover, we can observe that the energy and exergy efficiencies improved with nanofluids and the effect of graphene nanoparticles was the best. This happens because graphene nanoparticles have relatively high specific heat capacity and thermal conductivity, which increases the energy absorption efficiency of the solar collector, and it assures a higher outlet temperature, as shown in Table 5.3. As a consequence, greater useful energy will be gained and the overall efficiency of the multigeneration system will increase more than the energy it will gain when other absorption fluids are applied.

Figure 5.13 illustrates how solar radiation affects cooling and heating rates for all the investigated working fluids in the solar system. Higher solar radiation results in a linear raise in cooling and heating. The curves for cooling and heating rates are shown in Figure 5.13, which are similar to the energy and exergy efficiency curves shown in Figure 5.12. It proves that a direct relationship exists between their values.
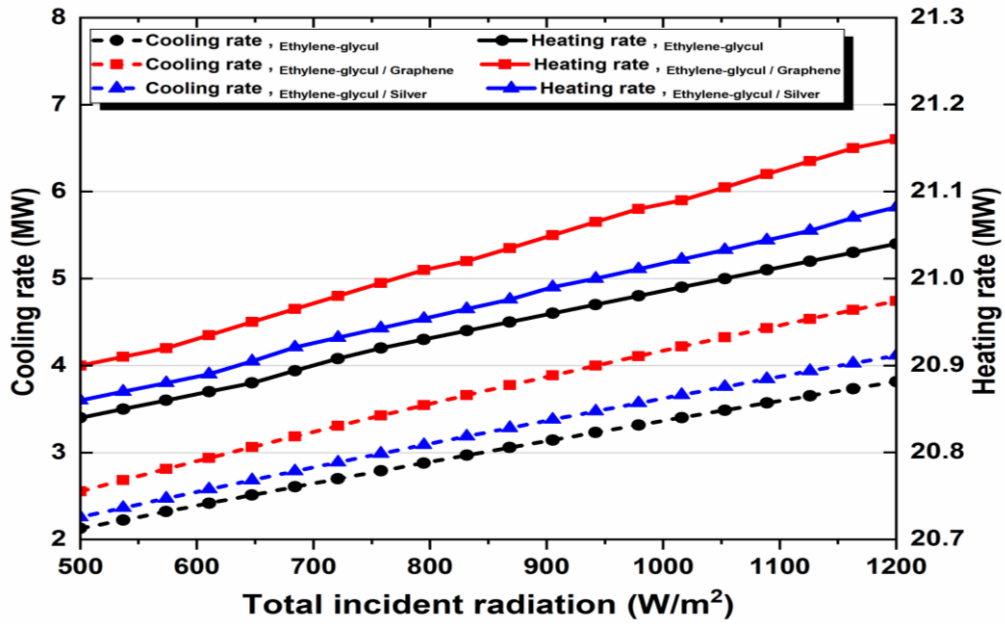

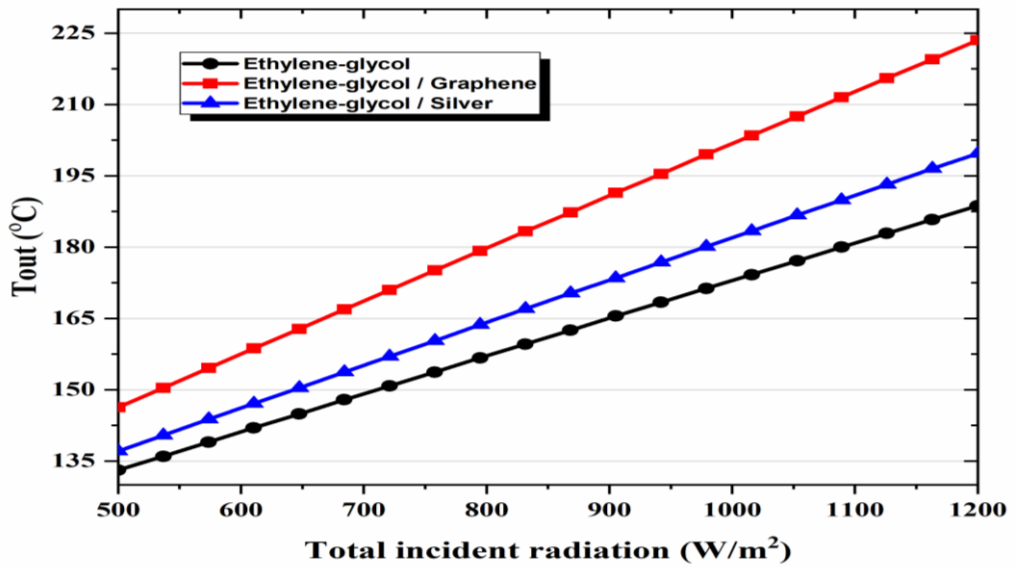Figure 5.13. Effect of solar irradiation on heating and cooling loads.

Figure 5.14. Effect of solar irradiation on the outlet temperature of solar collector.

In Figure 5.14, the effect of solar irradiation on the outlet temperature of the solar collectors is evaluated using three different absorbing fluids in solar cycle (EG, EG-Graphene, EG-Silver). It is found that the outlet temperature of the solar collectors increases with increases in solar irradiation. The highest values of the outlet temperature of the solar collectors are obtained using EG-Graphene as a working fluid in the solar cycle. This is due to the fact that the EG-Graphene nanofluid has relatively low specific heat capacity and a high density compared to other absorbent fluids. On the other hand, the lowest values are obtained using EG as a working fluid in the solar cycle, which supports the other results obtained that show the preference of nanofluids over the base fluids.

5.5.3. Effect of Ambient Temperature

Ambient temperature affects the exergy destruction rates; so, we studied the overall energy and exergy efficiencies for a detailed analysis of the subsystems and the overall system. In this study, ambient temperature ranged from 10 °C to 40 °C, and the effect of this increase on the subsystems' exergy destruction rates are shown in Figure 5.15. It is obvious that the SRC and ORC subsystems exhibited the top exergy destruction rates, which are followed by the MSF and DEAC subsystems, but both PEM and drying subsystems have the lowest rates.
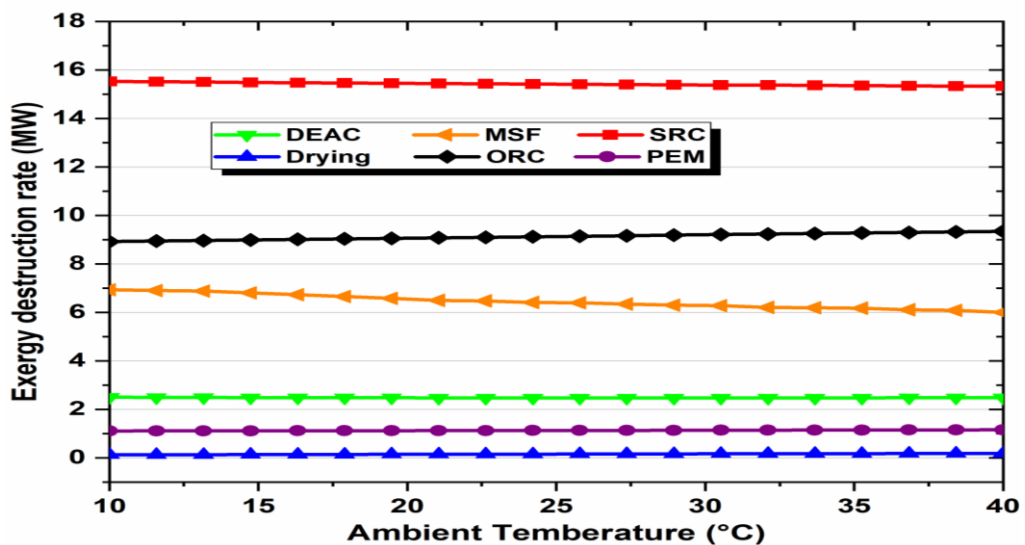

Figure 5.15. Effect of ambient temperature on the subsystems' exergy destruction rates.

The ambient temperature has effect on the multi-generation system's performance applying different working fluids, which has been shown in Figure 5.16. It is obvious that rising ambient temperature rises the overall exergy efficiency irrespective of the type of absorbent fluid, while showed inconsiderable impact on the system's overall energy efficiency; therefore, the overall energy efficiency remained almost constant despite increasing ambient temperature. In addition, when nanofluid types were compared, Graphene-EG has shown superior exergy efficiency. It can also be noted that when nanoparticles exist in the base fluid, it positively affects the multi-generation system performance.
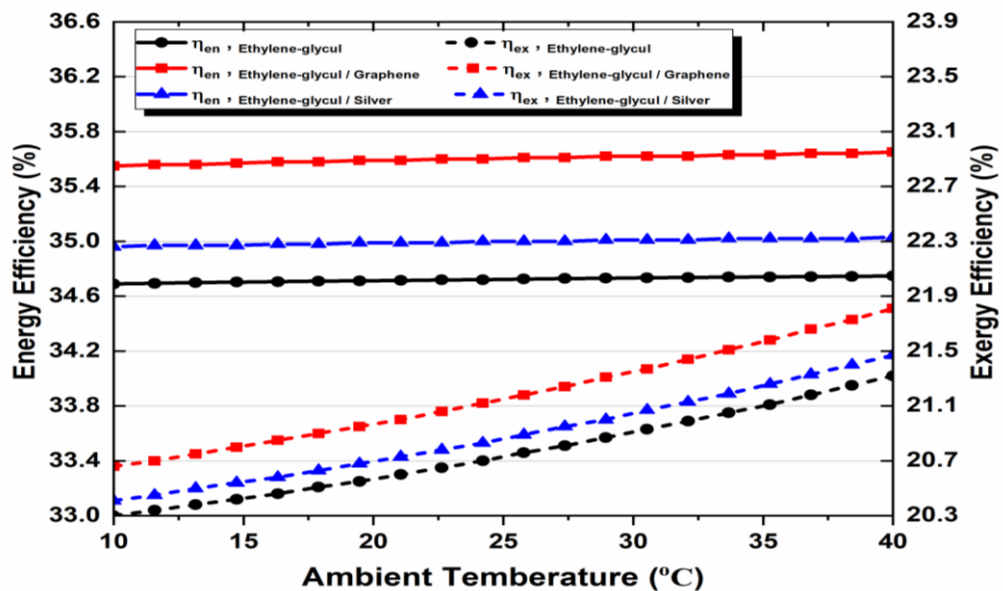
Figure 5.16. Effect of ambient temperature on the overall energy efficiency and overall exergy efficiency.

5.5.4. Effect of Outlet Temperature of Biomass Combustor

Biomass combustion is very important for the design of a multi-generation system as it is one of its energy sources. Its outlet temperature was studied and the effect of its change on system performance was analyzed as shown in figure 5.17. The outlet temperature remained within the range 600-800 °C.

It is clear that, when it increases, the overall energy efficiency and the overall exergy efficiency increase as well, which satisfies thermodynamic principles. In addition, it

was noticed that raising the output temperature of the biomass combustor and using nanofluids in the solar cycle improves the proposed system performance as compared to the performance of the basic fluid. It is also clear that the nanofluid behavior shown in Figure 5.17 matches the behavior, which has been depicted in the former figures. Graphene-based nanofluids showed the top performance enhancement, which was followed by Silver-based nanofluids, and the EG base fluid respectively.
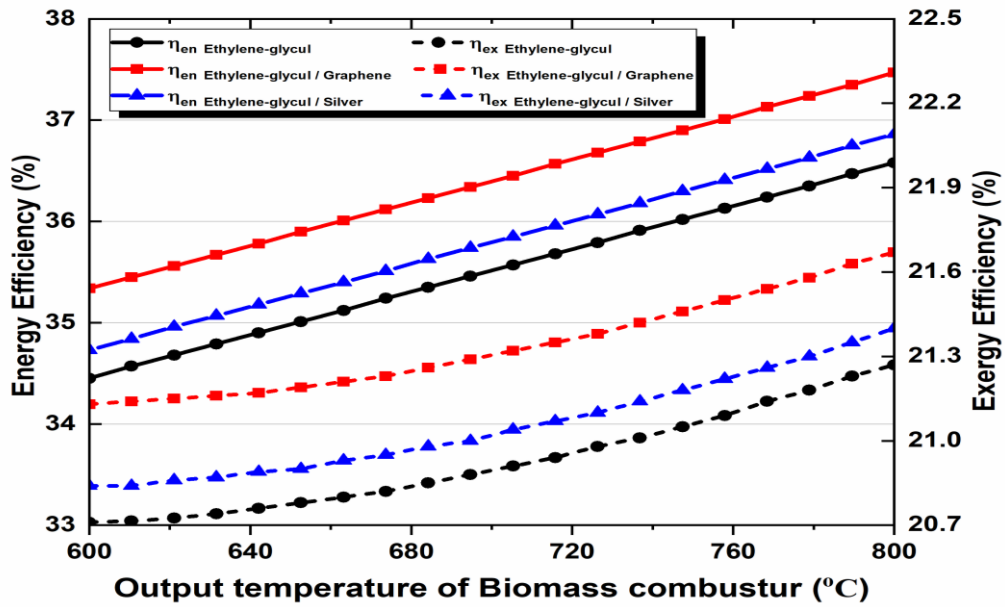
Figure 5.17. Effect of biomass combustor outlet temperature on overall energy efficiency and overall exergy efficiency of proposed system.

5.5.5. Effect of Turbine Rankine Cycles Inlet Pressure

Since the inlet pressure of SRC and ORC turbines is a key design parameter, the impact of this pressure on system efficiencies is discussed and shown in Figure 6.18. It is found that the overall energy and exergy efficiencies increase with the raise of turbines inlet pressure (P14, P36), but the growth in multigeneration energy efficiency is more notable than exergy. The relation can be justified by the fact that the increase in high pressure causes an increase in enthalpy at the turbine inlet, which in turn causes an increase in turbine power produced.

Inlet pressure of SRC turbine and ORC turbine affect the net power output; so, we studied the SRC produced power and the ORC produced power by a detailed analysis.

In this study, inlet pressure (P14, P36) ranged from 3 MPa to 15 MPa, and the effect of this increase on the ORC and SRC net power outputs are shown in Figure 5.19. It is clear that the net power of the ORC subsystem exhibited improvement with increasing turbine inlet pressure as opposed to the SRC subsystem whose power output decreased slightly with increasing inlet pressure.

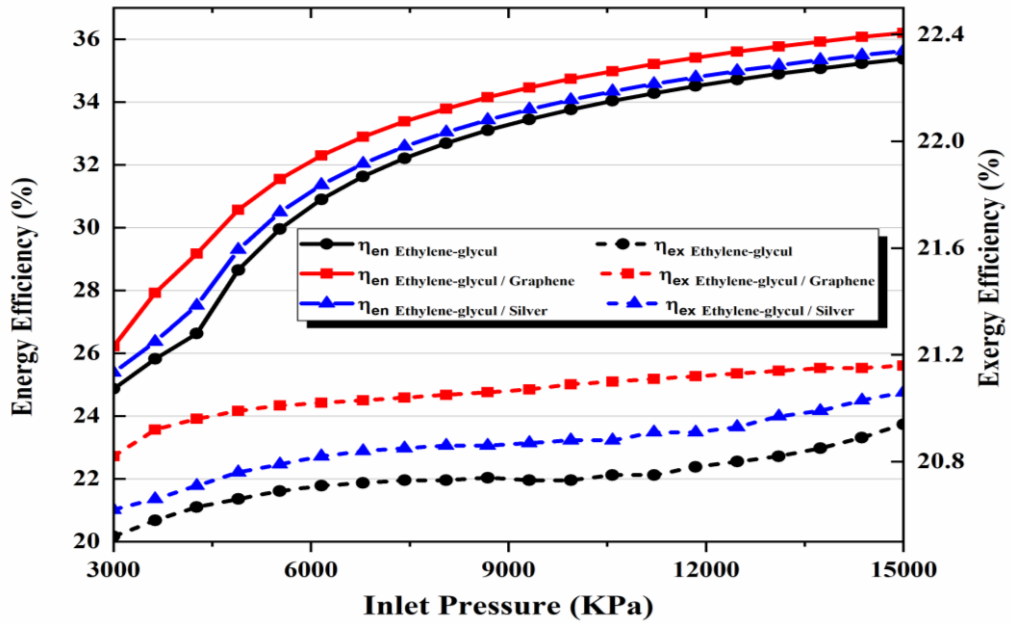

Figure 5.18. Effect of ORC and SRC turbines inlet pressure on overall energy efficiency and overall exergy efficiency of proposed system.
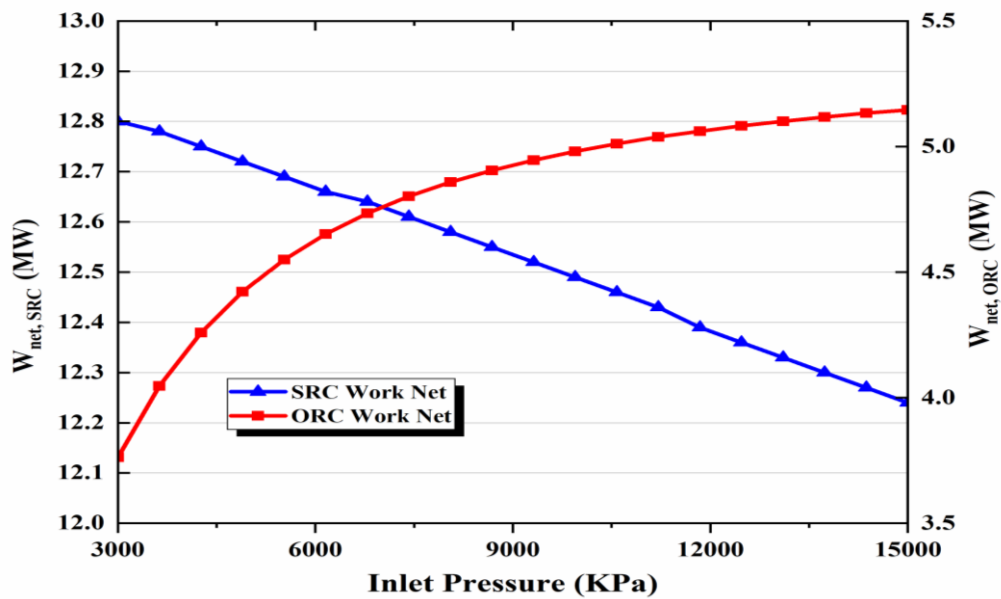

Figure 5.19. Effect of ORC and SRC turbines inlet pressure on their net power output.

5.5.6. Effect of ORC Working Fluid

To assess the impact of the used ORC working fluid on the system's performances, a comparative study was conducted considering the different fluids n-Pentane, HFE7500, Toluene, Cyclohexane and Isobutane (used as a working fluid) as shown in Figure 5.20. The thermodynamic properties of the fluids were extracted from EES software. The simulations' results show that the choice of the working fluid can impact the thermodynamic of the studied system. Indeed, the use of Isobutane as a working fluid gives the best performance values for the ORC and thus obtaining the highest energy and exergy efficiencies in the overall system.
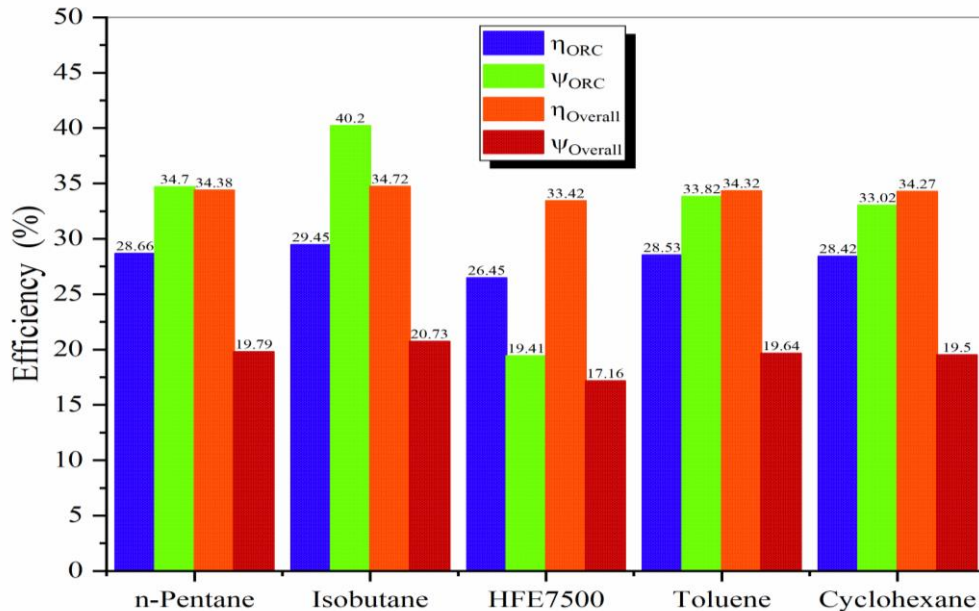
Figure 5.20. Effect of ORC working fluids on ORC energy efficiency, ORC exergy efficiency, overall energy efficiency and overall exergy efficiency.

5.5.7. Effect of Air-Biomass Flow Rate

The subsystems are operated independently using the two types of heat source, solar energy and biomass combustor. One of key parameters when considering solar-biomass based energy systems is the flow rate of air and biomass within the biomass combustion. Therefore, air-biomass flow rate impact on related subsystems energy efficiency and exergy efficiency is examined as shown in Figure 5.21. It is found that

the efficiencies of the considered subsystems have varying sensitivity to the studied range of air flow rate and biomass.

The energy efficiency and exergy efficiency of the drying and MSF sub-systems clearly decrease with an increasing air-biomass flow rate from 25 to 33 kg/s. However, for subsystems SRC, PEM, and ORC, the opposite is true as the energy and exergy efficiencies are noticed to slightly increase.
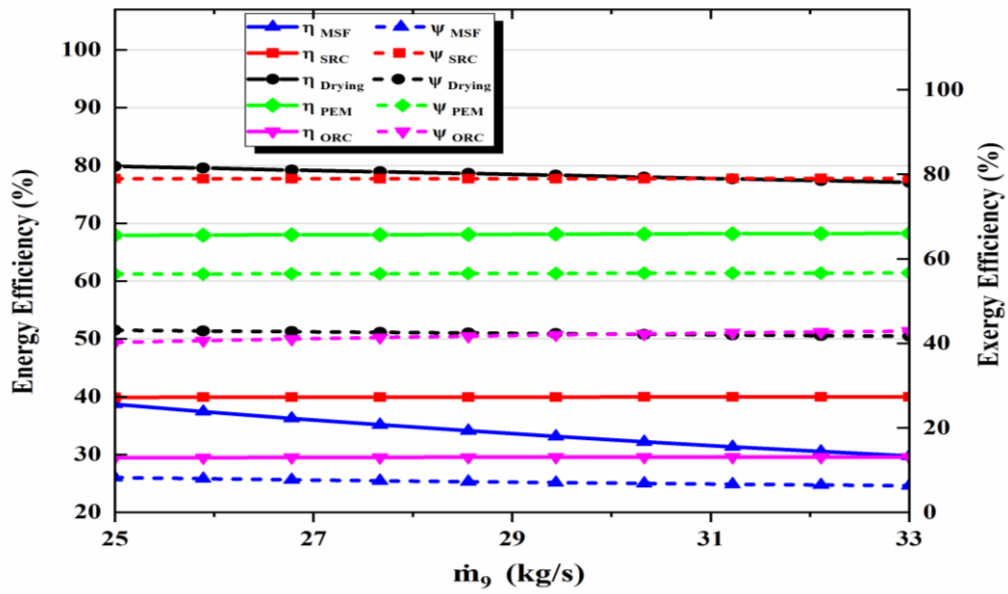
Figure 5.21. Effect of air-biomass flow rate on related subsystems energy and exergy efficiencies.
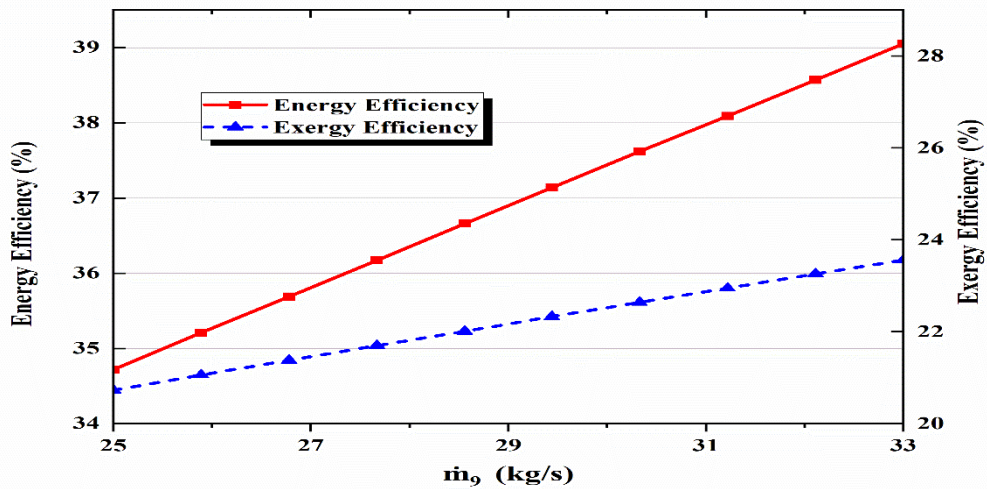
Figure 5.22. Effect of air-biomass flow rate on overall energy efficiency and overall exergy efficiency.

84

The results of the parametric analysis of air-biomass flow rate on the energetic and exergetic efficiency of the proposed system is illustrated in Figure 5.22. It can be observed that by increasing the air and biomass flow rate entering the biomass combustion, the energy efficiency increases remarkably while the exergy efficiency increases but at a slower rate. By increasing the air-biomass flow rate from 25 to 33 kg/s, the overall energetic and exergetic efficiency increases from 34.72 to 39.05% and from 20.73 to 23.56%, respectively.

5.6. Environmental Impact Assessment

To supply environmental vision, the multigeneration system environmental impact is compared to that of the other power systems as shown in Figure 5.23. It is noted that the multigeneration system has lower CO_2 emissions than the other systems, as it causes 364 kg/MWh of carbon dioxide emissions while the single, cogenerating and trigeneration systems cause respectively an estimated 1123 kg/MWh, 919.8 kg/MWh, 426.4 kg/MWh. On the other hand, the multigeneration system has highest environmental sustainable index among other generation systems. That consequence gives a great impetus to the use of multi-generation systems.

Figure 5.23 Comparison of environmental impacts for four types systems.

CHAPTER 6

CONCLUSIONS AND RECOMMENDATIONS

6.1.   CONCLUSIONS

To meet the basic human needs and to carry on with production, all societies need energy. Since 1850s, the global fossil fuel use (oil, coal, and gas) exceeded the energy supply, which led to its depletion and a global rise in greenhouse gas e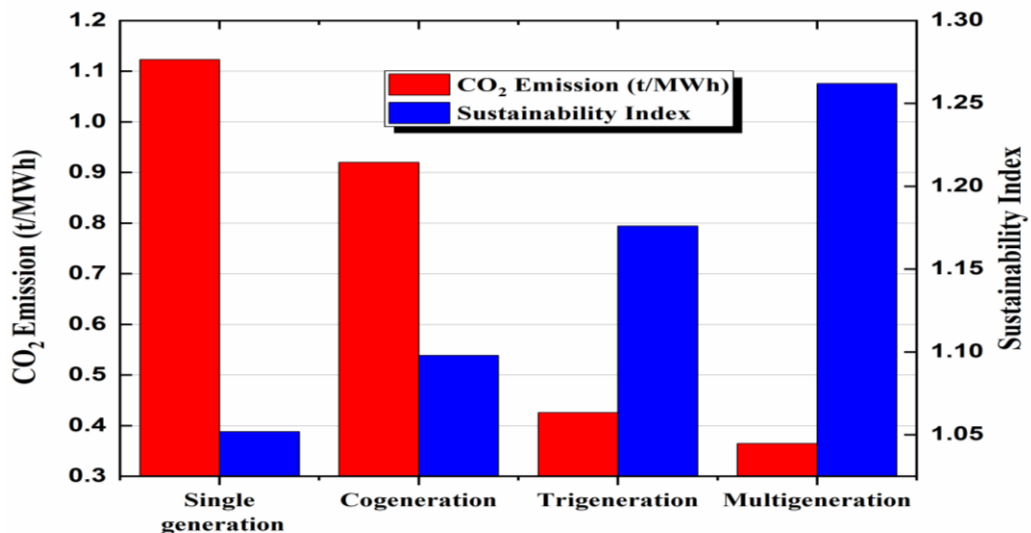missions. Many options have been presented so far for reducing greenhouse gas emissions while still meeting the global energy demand. Renewable energies such as solar and biomass energies are considered the best alternatives to fossil fuels. Biomass is an organic matter such as wood, animal waste, seaweed and crops that can be used as an energy resource. Biomass is obtained from living or dead materials that exist in the world. The hybrid biomass-solar systems is the technology that has attracted the attention of researchers for recent decades. This is mainly due to their efficiency and diminishing impacts regarding pollution and emission problems, and they can be used as the energy sources for multi-generation systems. Solar energy conversion systems solve the problem of low thermal and optical performance by using nanofluids as a working fluid in solar thermal systems. This has been viewed as an innovative approach to the improvement of thermal performance and making systems more sustainable. Nanofluids represent a new class of modern heat transfer fluids designed to disperse nanoparticles smaller than 100 nanometers in conventional heat transfer fluids.

This study is an endeavor to conduct the energy, exergy and environmental impact analyses of a new biomass-solar multi-generation system, which produces power, hydrogen, heating, cooling, drying, and fresh water. We conducted a comparative analysis to assess the nanofluids' effectiveness in the solar cycle on the integrated system performance, the impact of ambient conditions as well as some significant parameters.

86

Graphene and silver are the selected forms of nanoparticles in an ethylene glycol base fluid in the solar field. Several parameters such as solar irradiation, biomass combustor outlet temperature, ambient temperature, nanoparticle volume concentration, ORC working fluid, air-biomass flow rate, and inlet pressure of Rankine cycles turbines were also individually investigated to assess their effects on the overall system performance. The system modeling was conducted by the Engineering Equation Solver (EES) program under constant conditions. The summary of the main results is given below:

1. The system performance actually improved when nanofluids were used as working fluids in the solar collector. It was found that graphene nanoparticles performed better as compared to the silver nanoparticles.

2. The multi-generation system's overall energy and exergy efficiencies were 34.72% and 20.73%, respectively, and it has been found that these efficiencies raise by using nanofluids to reach 35.6% and 21.15%, respectively, with Graphene-EG nanofluid.

3. It has been observed that the nanofluids increase a solar collector's outlet temperature as compared to the thermal oils and this will give a positive effect on the overall system performance. The highest CPC outlet temperature was achieved with Graphene-EG at 197.6 °C, while the lowest temperature was obtained with the EG base fluid at 170 °C.

4. The highest exergy destruction rate in SRC subsystem was 15MW (49.4%) while the lowest value was approximately 0.16 MW (0.5%) in the drying system; therefore, the integrated system's overall exergy performance can be improved by working on certain subsystems, which have higher exergy destruction rates.

5. The freshwater production by the desalination subsystem is 37.93 kg/s and that amount will be increase to reach 38.47 when the air-biomass flow rate within

the biomass combustor increased to 33 kg/s, while the hydrogen production by PEM electrolyzer is 44.77 kg/h.

6. The environmental impact assessment illustrated that the transition from a single-generation system to a multigeneration system reduced CO_2 emissions of around 758 kg/MWh, which is giving a strong motivation to convert to multigeneration systems.

7. As shown by parametric studies, solar irradiation, biomass combustor outlet temperature, ambient temperature, nanoparticle volume concentration, ORC working fluid, air-biomass flow rate, and inlet pressure of both Rankine cycles turbines have a highly considerable effect on the proposed system's overall efficiency.

8. The highest efficiencies for the subsystems were achieved in the following conditions:

   - The SRC subsystem's energy and exergy efficiencies using Graphene-EG nanofluid were 40.21% and 79.08%, respectively.
   - The drying subsystem's energy and exergy efficiencies at base conditions were 71.17% and 38.57%, respectively.
   - The CPC subsystem's energy and exergy efficiencies using Graphene-EG nanofluid were 50.75% and 15.82%, respectively.
   - The DEAC subsystem's COP and exergy efficiencies using EG were 0.9922 and 24.77%, respectively.
   - The ORC subsystem's energy and exergy efficiencies were 29.45% and 40.2%, respectively, when air-biomass flow rate reached 33 kg/s. Furthermore, Isobutane was found to be the best organic fluid in comparison with the other fluids studied.
   - The MSF subsystem's energy and exergy efficiencies were 38.72% and 8.233%, respectively.
   - The PEM subsystem's energy and exergy efficiencies were 68.28% and 56.67%, respectively, when air-biomass flow rate reached 33 kg/s.

6.2. RCOMMENDATIONS

By using this thesis results, more efficient multigeneration systems can be designed and developed. The following suggestions can be very useful for optimizing multigeneration systems:

1. Incorporating more renewable energy sources such as geothermal, wind and ocean thermal energy conversion depending on the availability of local resources, and getting more diverse outputs.
2. Experimental studies with nanofluids are needed to fill the scientific gap in the literature on this area.
3. The development of heat transfer science can be harnessed and new ideas such as novel different types of nanofluids and hybrid nanofluids can be used.
4. Conducting experimental studies of similar systems in order to enhance the cognitive body.
5. Developing solar energy storage technologies because of its impact on the efficiency and costs of systems based on solar energy.
6. The study should be expanded by including more parameters that affect system performance.
7. The exergoeconomic results should be obtained by considering the total exergy and the cost of its basic components.
8. Some studies need to be done to show future cost predictions for similar systems based on market fluctuations in past decades.

REFERENCES

1. Owusu, P. A. and Asumadu-Sarkodie, S., "A review of renewable energy sources, sustainability issues and climate change mitigation", *Cogent Engineering*, 3 (1): 1–14 (2016).

2. Panwar, N. L., Kaushik, S. C., and Kothari, S., "Role of renewable energy sources in environmental protection: A review", *Renewable and Sustainable Energy Reviews*, 15 (3): 1513–1524 (2011).

3. Voitko, S., Trofymenko, O., and Pavlenco, T., "Decarbonisation of the economy through the introduction of innovative technologies into the energy sector", (2021).

4. Energy Agency, I., "Net Zero by 2050 - A Roadmap for the Global Energy Sector", (2050).

5. Lamb, W. F., Wiedmann, T., Pongratz, J., Andrew, R., Crippa, M., Olivier, J. G. J., Wiedenhofer, D., Mattioli, G., al Khourdajie, A., and House, J., "A review of trends and drivers of greenhouse gas emissions by sector from 1990 to 2018", *Environmental Research Letters*, (2021).

6. Kumar, M., "Social, Economic, and Environmental Impacts of Renewable Energy Resources", Wind Solar Hybrid Renewable Energy System, *IntechOpen*, (2020).

7. Wu, D. W. and Wang, R. Z., "Combined cooling, heating and power: A review", *Progress in Energy And Combustion Science*, 32 (5–6): 459–495 (2006).

8. McCrone, A., Ajadi, T., Boyle, R., Strahan, D., Kimmel, M., Collins, B., Cheung, A., and Becker, L., "Global Trends in Renewable Energy Investment 2019", *Bloomberg New Energy Finance*, 76 (2019).

9. Zhao, L., Zhang, Y., Deng, S., Ni, J., Xu, W., Ma, M., Lin, S., and Yu, Z., "Solar driven ORC-based CCHP: Comparative performance analysis between sequential and parallel system configurations", *Applied Thermal Engineering*, 131: 696–706 (2018).

10. Cioccolanti, L., Rajabi Hamedani, S., and Villarini, M., "Environmental and energy assessment of a small-scale solar Organic Rankine Cycle trigeneration system based on Compound Parabolic Collectors", *Energy Conversion and Management*, 198 (June): 111829 (2019).

11. Cioccolanti, L., Villarini, M., Tascioni, R., and Bocci, E., "Performance assessment of a solar trigeneration system for residential applications by means of a modelling study", *Energy Procedia*, 126: 445–452 (2017).

12. Dincer, I. and Zamfirescu, C., "Renewable-energy-based multigeneration systems", *International Journal of Energy Research*, 36 (15): 1403–1415 (2012).

13. Azhar, M. S., Rizvi, G., and Dincer, I., "Integration of renewable energy based multigeneration system with desalination", *Desalination*, 404: 72–78 (2017).

14. Bellos, E. and Tzivanidis, C., "Thermal efficiency enhancement of nanofluid-based parabolic trough collectors", *Journal of Thermal Analysis and Calorimetry*, 135 (1): 597–608 (2019).

15. Basbous, N., Taqi, M., Belouaggadia, N., and Author, C., "Numerical Study of a Parabolic Trough Collector Using a Nanofluid", *Asian Journal of Current Engineering And Maths*, 4: 40–44 (2015).

16. Farhana, K., Kadirgama, K., Rahman, M. M., Ramasamy, D., Noor, M. M., Najafi, G., Samykano, M., and Mahamude, A. S. F., "Improvement in the performance of solar collectors with nanofluids — A state-of-the-art review", *Nano-Structures And Nano-Objects*, 18 (June): (2019).

17. Moradi, A., Sani, E., Simonetti, M., Francini, F., Chiavazzo, E., Asinari, P., and Torino, P., "CFD Modeling of Solar Collector With Nano-Fluid Direct Absorption for Civil Application, National Institute of Optics, National Research Council (CNR-INO), largo E . Fermi 6", *3 Microgen*, (April 2013): (2013).

18. Chaudhari, K., Walke, P., Wankhede, U., and Shelke, R., "An Experimental Investigation of a Nanofluid ($Al_2O_3+H_2O$) Based Parabolic Trough Solar Collectors", *British Journal of Applied Science & Technology*, 9 (6): 551–557 (2015).

19. Dinçer, İ. and Zamfirescu, C., "Integrated multigeneration energy systems", Sustainable Energy Systems and Applications, *Springer*, 479–517 (2011).

20. Dinçer, İ. and Bicer, Y., "Integrated Energy Systems for Multigeneration", *Elsevier*, (2019).

21. Guo, S., Liu, Q., Sun, J., and Jin, H., "A review on the utilization of hybrid renewable energy", *Renewable and Sustainable Energy Reviews*, 91: 1121–1147 (2018).

22. Evangelisti, L., Vollaro, R. D. L., and Asdrubali, F., "Latest advances on solar thermal collectors: A comprehensive review", *Renewable and Sustainable Energy Reviews*, 114: 109318 (2019).

23. Pranesh, V., Velraj, R., Christopher, S., and Kumaresan, V., "A 50 year review of basic and applied research in compound parabolic concentrating solar thermal collector for domestic and industrial applications", *Solar Energy*, 187 (December 2018): 293–340 (2019).

24. Nasri-n, R., "A 3D Numerical Study of Thermofluid Characteristics of a Flat Plate Solar Collector using Nanofluid", 125 (2015).

25. Sabiha, M. A., Saidur, R., Mekhilef, S., and Mahian, O., "Progress and latest developments of evacuated tube solar collectors", *Renewable and Sustainable Energy Reviews*, 51: 1038–1054 (2015).

26. al Naimat, F., Ziauddin, M., Mathew, B., Darabseh, T., and Alhseinat, E., "Performance of concentrated solar collectors: Studying the absorber pipe outlet temperature variations", (2018).

27. Yılmaz, İ. H. and Mwesigye, A., "Modeling, simulation and performance analysis of parabolic trough solar collectors: A comprehensive review", *Applied Energy*, 225 (April): 135–174 (2018).

28. Hafez, A. Z., Soliman, A., El-Metwally, K. A., and Ismail, I. M., "Solar parabolic dish Stirling engine system design, simulation, and thermal analysis", *Energy Conversion and Management*, 126: 60–75 (2016).

29. Schell, S., "Design and evaluation of esolar's heliostat fields", *Solar Energy*, 85 (4): 614–619 (2011).

30. Barbier, E., "Nature and technology of geothermal energy: a review", *Renewable and Sustainable Energy Reviews*, 1 (1–2): 1–69 (1997).

31. Higman, C., "Gasification", Combustion Engineering Issues for Solid Fuel Systems, *Elsevier*, 423–468 (2008).

32. Ahmad, M., Ahmed, Z., Yang, X., Hussain, N., and Sinha, A., "Financial development and environmental degradation: Do human capital and institutional quality make a difference?", *Gondwana Research*, (2021).

33. WU, X., Zhou, H., and Huang, M., "Wind speed and generated power forecasting based on pattern recognition in wind farm [J]", *Relay*, 36 (1): 27–32 (2008).

34. Murshed, S. M. S., Leong, K. C., and Yang, C., "Thermophysical and electrokinetic properties of nanofluids–a critical review", *Applied Thermal Engineering*, 28 (17–18): 2109–2125 (2008).

35. Yu, W. and Choi, S. U. S., "The role of interfacial layers in the enhanced thermal conductivity of nanofluids: a renovated Maxwell model", *Journal of Nanoparticle Research*, 5 (1–2): 167–171 (2003).

36. Xiong, Q., Altnji, S., Tayebi, T., Izadi, M., Hajjar, A., Sundén, B., and Li, L. K. B., "A comprehensive review on the application of hybrid nanofluids in solar energy collectors", *Sustainable Energy Technologies And Assessments*, 47: 101341 (2021).

37. Stojić, D. L., Grozdić, T. D., Umićević, B., and Maksić, A. D., "A comparison of alkaline and proton exchange membrane electrolyzers", *Russian Journal of Physical Chemistry A, Focus on Chemistry*, 82 (11): 1958–1960 (2008).

38. Falcão, D. S. and Pinto, A., "A review on PEM electrolyzer modelling: Guidelines for beginners", *Journal of Cleaner Production*, 261: 121184 (2020).

39. Yosaf, S. and Ozcan, H., "Exergoeconomic investigation of flue gas driven ejector absorption power system integrated with PEM electrolyser for hydrogen generation", *Energy*, 163 (August 2018): 88–99 (2018).

40. O'Connor, E., "Water; recovery, reclamation and recycling within the Irish dairy industry", (2020).

41. Xu, B., Li, P., and Guo, P., "Solar Thermal-Driven Desalination Pursuing Products of Pure Water and Salts and Leaving Minimum Impact to Environment", *Desalination*, 143: (2017).

42. El-Ghonemy, A. M. K., "Performance test of a sea water multi-stage flash distillation plant: Case study", *Alexandria Engineering Journal*, 57 (4): 2401–2413 (2018).

43. Dincer, I. and Zamfirescu, C., "Renewable-energy-based multigeneration systems", *International Journal of Energy Research*, 36 (15): 1403–1415 (2012).

44. Yuksel, Y. E., Ozturk, M., and Dincer, I., "Performance assessment of a solar tower-based multigeneration system with thermal energy storage", *Energy Storage*, 1 (4): e71 (2019).

45. Ozturk, M. and Dincer, I., "Thermodynamic analysis of a solar-based multi-generation system with hydrogen production", *Applied Thermal Engineering*, 51 (1–2): 1235–1244 (2013).

46. Yilmaz, F., "Thermodynamic performance evaluation of a novel solar energy based multigeneration system", *Applied Thermal Engineering*, 143: 429–437 (2018).

47. Siddiqui, O. and Dincer, I., "Analysis and performance assessment of a new solar-based multigeneration system integrated with ammonia fuel cell and solid oxide fuel cell-gas turbine combined cycle", *Journal of Power Sources*, 370: 138–154 (2017).

48. Yilmaz, F., Ozturk, M., and Selbas, R., "Energy and exergy performance assessment of a novel solar-based integrated system with hydrogen production", *International Journal of Hydrogen Energy*, 44 (34): 18732–18743 (2019).

49. El-Emam, R. S. and Dincer, I., "Investigation and assessment of a novel solar-driven integrated energy system", *Energy Conversion and Management*, 158: 246–255 (2018).

50. Ahmadi, P., Dincer, I., and Rosen, M. A., "Performance Assessment of a Novel Solar and Ocean Thermal Energy Conversion Based Multigeneration System for Coastal Areas", *Journal of Solar Energy Engineering*, 137 (1): 011013 (2014).

51. Ozturk, M., "Thermodynamics Assessment of the Multi-Generation Energy Production Systems", *Clean Energy for Better Environment*, (2012).

52. Al-Ali, M. and Dincer, I., "Energetic and exergetic studies of a multigenerational solar–geothermal system", *Applied Thermal Engineering*, 71 (1): 16–23 (2014).

53. Almahdi, M., Dincer, I., and Rosen, M. A., "A new solar based multigeneration system with hot and cold thermal storages and hydrogen production", *Renewable Energy*, 91: 302–314 (2016).

54. Hassoun, A. and Dincer, I., "Analysis and performance assessment of a multigenerational system powered by Organic Rankine Cycle for a net zero energy house", *Applied Thermal Engineering*, 76: 25–36 (2015).

55. Al-Sulaiman, F. A., Dincer, I., and Hamdullahpur, F., "Energy and exergy analyses of a biomass trigeneration system using an organic Rankine cycle", *Energy*, 45 (1): 975–985 (2012).

56. Ahmadi, P., Dincer, I., and Rosen, M. A., "Development and assessment of an integrated biomass-based multi-generation energy system", *Energy*, 56: 155–166 (2013).

57. Safari, F. and Dincer, I., "Development and analysis of a novel biomass-based integrated system for multigeneration with hydrogen production", *International Journal of Hydrogen Energy*, 44 (7): 3511–3526 (2019).

58. Casas-Ledón, Y., Spaudo, F., and Arteaga-Pérez, L. E., "Exergoenvironmental analysis of a waste-based Integrated Combined Cycle (WICC) for heat and power production", *Journal of Cleaner Production*, 164: 187–197 (2017).

59. Al-Sulaiman, F. A., Hamdullahpur, F., and Dincer, I., "Greenhouse gas emission and exergy assessments of an integrated organic Rankine cycle with a biomass combustor for combined cooling, heating and power production", *Applied Thermal Engineering*, 31 (4): 439–446 (2011).

60. Gholamian, E., Mahmoudi, S. M. S., and Zare, V., "Proposal, exergy analysis and optimization of a new biomass-based cogeneration system", *Applied Thermal Engineering*, 93: 223–235 (2016).

61. Boyaghchi, F. A., Chavoshi, M., and Sabeti, V., "Multi-generation system incorporated with PEM electrolyzer and dual ORC based on biomass gasification waste heat recovery: Exergetic, economic and environmental impact optimizations", *Energy*, 145: 38–51 (2018).

62. Khalid, F., Dincer, I., and Rosen, M. A., "Energy and exergy analyses of a solar-biomass integrated cycle for multigeneration", *Solar Energy*, 112: 290–299 (2015).

63. Shahid, U. bin, Bicer, Y., Ahzi, S., and Abdala, A., "Thermodynamic assessment of an integrated renewable energy multigeneration system including ammonia as hydrogen carrier and phase change material energy storage", *Energy Conversion and Management*, 198 (August): 111809 (2019).

64. Wang, J. and Yang, Y., "Energy, exergy and environmental analysis of a hybrid combined cooling heating and power system utilizing biomass and solar energy", *Energy Conversion and Management*, 124: 566–577 (2016).

65. Bet Sarkis, R. and Zare, V., "Proposal and analysis of two novel integrated configurations for hybrid solar-biomass power generation systems: Thermodynamic and economic evaluation", *Energy Conversion and Management*, 160 (October 2017): 411–425 (2018).

66. Hashemian, N. and Noorpoor, A., "Assessment and multi-criteria optimization of a solar and biomass-based multi-generation system: Thermodynamic, exergoeconomic and exergoenvironmental aspects", *Energy Conversion and Management*, 195 (May): 788–797 (2019).

67. Karellas, S. and Braimakis, K., "Energy–exergy analysis and economic investigation of a cogeneration and trigeneration ORC–VCC hybrid system utilizing biomass fuel and solar power", *Energy Conversion and Management*, 107: 103–113 (2016).

68. Ghasemi, A., Heidarnejad, P., and Noorpoor, A., "A novel solar-biomass based multi-generation energy system including water desalination and liquefaction of natural gas system: Thermodynamic and thermoeconomic optimization", *Journal of Cleaner Production*, 196: 424–437 (2018).

69. Bai, Z., Liu, Q., Gong, L., and Lei, J., "Investigation of a solar-biomass gasification system with the production of methanol and electricity: Thermodynamic, economic and off-design operation", *Applied Energy*, 243: 91–101 (2019).

70. Cao, Y., Nikafshan Rad, H., Hamedi Jamali, D., Hashemian, N., and Ghasemi, A., "A novel multi-objective spiral optimization algorithm for an innovative

solar/biomass-based multi-generation energy system: 3E analyses, and optimization algorithms comparison", ***Energy Conversion and Management***, 219 (February): 112961 (2020).

71. Bai, Z., Liu, Q., Lei, J., Wang, X., Sun, J., and Jin, H., "Thermodynamic evaluation of a novel solar-biomass hybrid power generation system", ***Energy Conversion and Management***, 142: 296–306 (2017).

72. Sahoo, U., Kumar, R., Pant, P. C., and Chaudhary, R., "Development of an innovative polygeneration process in hybrid solar-biomass system for combined power, cooling and desalination", ***Applied Thermal Engineering***, 120: 560–567 (2017).

73. Liu, Q., Bai, Z., Wang, X., Lei, J., and Jin, H., "Investigation of thermodynamic performances for two solar-biomass hybrid combined cycle power generation systems", ***Energy Conversion and Management***, 122: 252–262 (2016).

74. Pantaleo, A. M., Camporeale, S. M., Sorrentino, A., Miliozzi, A., Shah, N., and Markides, C. N., "Solar/biomass hybrid cycles with thermal storage and bottoming ORC: System integration and economic analysis", ***Energy Procedia***, 129: 724–731 (2017).

75. Boyaghchi, F. A., Chavoshi, M., and Sabeti, V., "Optimization of a novel combined cooling, heating and power cycle driven by geothermal and solar energies using the water/CuO (copper oxide) nanofluid", ***Energy***, 91: 685–699 (2015).

76. Nasrin, R., Rahim, N. A., Fayaz, H., and Hasanuzzaman, M., "Water/MWCNT nanofluid based cooling system of PVT: Experimental and numerical research", ***Renewable Energy***, 121: 286–300 (2018).

77. Verma, S. K., Tiwari, A. K., and Chauhan, D. S., "Experimental evaluation of flat plate solar collector using nanofluids", ***Energy Conversion and Management***, 134: 103–115 (2017).

78. Toghyani, S., Baniasadi, E., and Afshari, E., "Thermodynamic analysis and optimization of an integrated Rankine power cycle and nano-fluid based parabolic trough solar collector", ***Energy Conversion and Management***, 121: 93–104 (2016).

79. Muhammad, A., Ratlamwala, T. A. H., and Ugur, A., "Comparative Energy, Exergy, and Environmental Analyses of Parabolic Trough Solar Thermal Power Plant Using Nanofluids", Exergy for A Better Environment and Improved Sustainability 1, ***Springer***, 943–967 (2018).

80. Bellos, E. and Tzivanidis, C., "Performance analysis and optimization of an absorption chiller driven by nanofluid based solar flat plate collector", ***Journal of Cleaner Production***, 174: 256–272 (2018).

81.   Abid, M., Ratlamwala, T. A. H., and Atikol, U., "Solar assisted multi-generation system using nanofluids: A comparative analysis", *International Journal of Hydrogen Energy*, 42 (33): 21429–21442 (2017).

82.   Faizal, M., Saidur, R., Mekhilef, S., and Alim, M. A., "Energy, economic and environmental analysis of metal oxides nanofluid for flat-plate solar collector", *Energy Conversion and Management*, 76: 162–168 (2013).

83.   Ibrahim, A. and Kayfeci, M., "Comparative analysis of a solar trigeneration system based on parabolic trough collectors using graphene and ferrofluid nanoparticles", *Thermal Science*, (00): 164 (2020).

84.   Lu, L., Liu, Z. H., and Xiao, H. S., "Thermal performance of an open thermosyphon using nanofluids for high-temperature evacuated tubular solar collectors. Part 1: Indoor experiment", *Solar Energy*, 85 (2): 379–387 (2011).

85.   Liu, Z. H., Hu, R. L., Lu, L., Zhao, F., and Xiao, H. S., "Thermal performance of an open thermosyphon using nanofluid for evacuated tubular high temperature air solar collector", *Energy Conversion and Management*, 73: 135–143 (2013).

86.   Alsaady, M., Fu, R., Yan, Y., Liu, Z., Wu, S., and Boukhanouf, R., "An Experimental Investigation on the Effect of Ferrofluids on the Efficiency of Novel Parabolic Trough Solar Collector Under Laminar Flow Conditions", *Heat Transfer Engineering*, 1–9 (2018).

87.   Khosravi, A., Malekan, M., and Assad, M. E. H., "Numerical analysis of magnetic field effects on the heat transfer enhancement in ferrofluids for a parabolic trough solar collector", *Renewable Energy*, 134: 54–63 (2019).

88.   Bejan, A., Tsatsaronis, G., and Moran, M. J., "Thermal Design and Optimization", *John Wiley & Sons*, (1995).

89.   Klein, S. A. and Alvarado, F. L., "Engineering equation solver, version 10.047", *F-Chart Software*, (2016).

90.   Kalogirou, S. A., "Solar Energy Engineering: Processes and Systems", *Academic Press*, (2013).

91.   Gnaifaid, H. and Ozcan, H., "Multi-objective optimization of a concentrated solar energy driven trigeneration plant with thermal energy storage: A case study for Turkey", *Case Studies in Thermal Engineering*, 20: 100642 (2020).

92.   Pak, B. C. and Cho, Y. I., "Hydrodynamic and heat transfer study of dispersed fluids with submicron metallic oxide particles", *Experimental Heat Transfer an International Journal*, 11 (2): 151–170 (1998).

93. Xuan, Y. and Roetzel, W., "Conceptions for heat transfer correlation of nanofluids", *International Journal of Heat And Mass Transfer*, 43 (19): 3701–3707 (2000).

94. Yu, W. and Choi, S. U. S., "The role of interfacial layers in the enhanced thermal conductivity of nanofluids: a renovated Maxwell model", *Journal of Nanoparticle Research*, 5 (1): 167–171 (2003).

95. Batchelor, G. K., "The effect of Brownian motion on the bulk stress in a suspension of spherical particles", *Journal of Fluid Mechanics*, 83 (1): 97–117 (1977).

96. Duangthongsuk, W. and Wongwises, S., "An experimental study on the heat transfer performance and pressure drop of TiO2-water nanofluids flowing under a turbulent flow regime", *International Journal of Heat And Mass Transfer*, 53 (1–3): 334–344 (2010).

97. Basu, P., "Combustion and Gasification in Fluidized Beds", *CRC Press*, (2006).

98. Dincer, I. and Sahin, A. Z., "A new model for thermodynamic analysis of a drying process", *International Journal of Heat And Mass Transfer*, 47 (4): 645–652 (2004).

99. Millet, P. and Grigoriev, S., "Water Electrolysis Technologies", Renewable Hydrogen Technologies: Production, Purification, Storage, Applications and Safety, *Elsevier B.V.*, 19–41 (2013).

100. Ni, M., Leung, M. K. H., and Leung, D. Y. C., "Energy and exergy analysis of hydrogen production by a proton exchange membrane (PEM) electrolyzer plant", *Energy Conversion and Management*, 49 (10): 2748–2756 (2008).

101. Yosaf, S. and Ozcan, H., "Exergoeconomic investigation of flue gas driven ejector absorption power system integrated with PEM electrolyser for hydrogen generation", *Energy*, 163: 88–99 (2018).

102. El-Dessouky, H. T. and Ettouney, H. M., "Fundamentals of Salt Water Desalination", *Elsevier*, (2002).

RESUME

Alla Ibrahim was born in Tripoli city in Libya, where he accomplished his high school, and later graduated from the Tripoli University, Engineering Faculty in 2004. Since 2005 to date, he has been working as a full-time researcher at the Applied Research and Development Council. In 2012, he completed his MSc in Mechanical Engineering at Libyan Academic. In 2014, he got an eight-months scholarship to study English language in England. He worked as a part-time lecturer at Kara buli University in academic year 2014-2015. In 2015, he was awarded a scholarship to continue his PhD education in Turkey. In fall 2016, He started his PhD academic program in Mechanical Engineering Department at Karabuk University, at which he completed the courses, passed the qualification exam and started his PhD thesis research. His research area focuses on renewable energy systems.